PhD Thesis

Rotating Droplet - a new system for electrochemical measurements of neurotransmitters

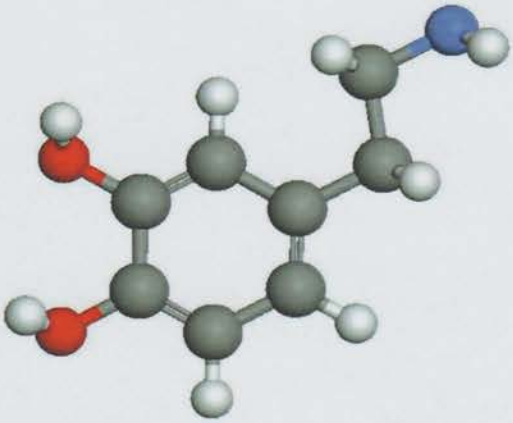

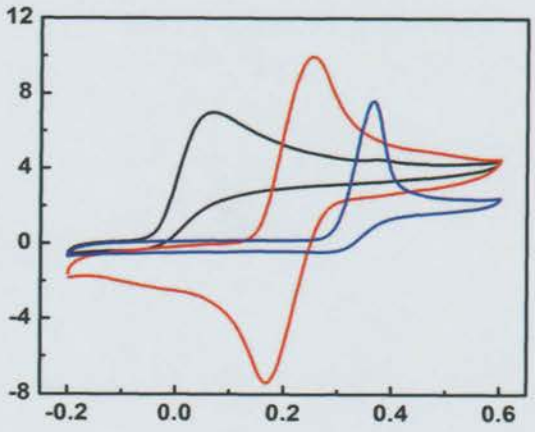

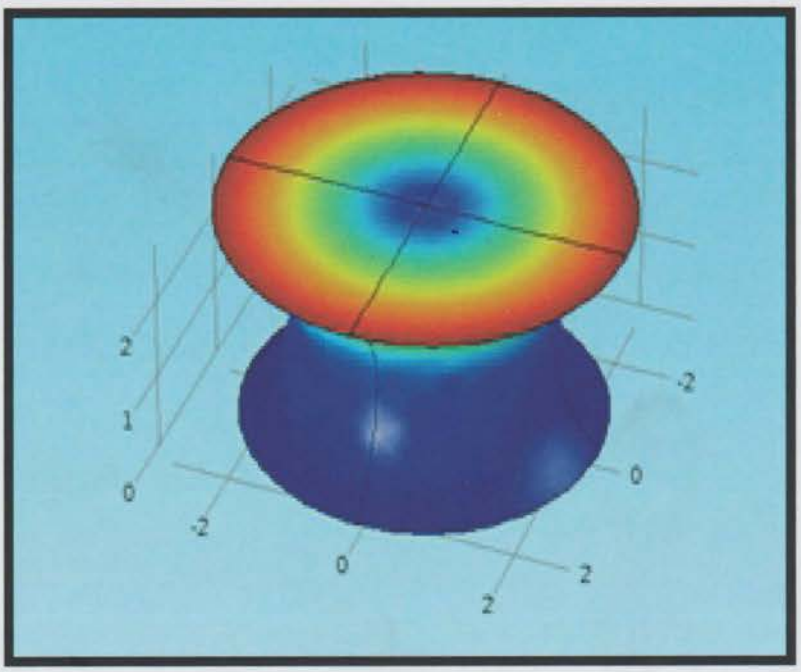

Magdalena Kundys-Siedlecka

Rotating droplet – a new system for electrochemical measurements of neurotransmitters

Magdalena Kundys-Siedlecka

Supervisor:

Ph.D., DSc. Martin Jönsson-Niedziółka, Prof. IPC PAS

This dissertation was prepared within
the International Doctoral Studies at the
Institute of Physical Chemistry Polish Academy of Sciences
Kasprzaka 44/52, 01-224 Warsaw

November 2019

Acknowledgements

First of all, I would like to acknowledge the supervisor of my thesis, Prof. Martin Jönsson-Niedziółka for directing my scientific curiosity and invaluable guidance.

I would also like to thank Prof. Marcin Opałło and Dr. Katarzyna Szot-Karpińska for their help in my first steps in electrochemistry.

I appreciate help and scientific advice from Dr. Adrianna Svensson, Dr. Wojciech Adamiak, Dr. Justyna Jędraszko, Dr. Emilia Witkowska Nery.

I am grateful to Prof. Marcus Raffel for the great opportunity to learn PIV in Göttingen, Germany, and to Dr. Micheál Scanlon hosting me for an internship at the Univerisity of Limerick, Ireland.

I would like to thank Paulina Jeleń, Dr. Magdalena Wiloch, all my colleagues from Department of Electrode Processes IPC PAS for great atmosphere at work.

Last but not least, I would like to thank all my family and friends for their constant support and understanding. And I thank Paweł for everything.

The research in this thesis was financially supported by the Polish National Science Centre, NCN, through the grants:

PRELUDIUM “Simultaneous determination of chosen neurotransmitters in 1hydrodynamic conditions” no. 2016/23/N/ST4/02702

SONATA “Generation-Collection Electrochemistry in Hydrodynamic Systems” no. 2014/15/D/ST4/03003

OPUS “Capturing the flow: 3D-electrodes for enzymatic redox reactions in microfluidic channels” no. 2014/15/B/ST4/04646

Abstract

In this dissertation I present my research on characterization and optimization of a new electrochemical setup called the Rotating Droplet (RD). The goal of my research was to apply the RD system to detection of neurotransmitters and determine their concentration in the samples containing interferents.

Detection of neurotransmitters with electrochemical methods is a complicated issue. The electrochemical activity of different neurotransmitters comes from the possibility of oxidation or reduction of their functional groups. Oxidation or reduction signals for neurotransmitters are measured within a small potential range. Signals from interferents, coexisting in the sample with the neurotransmitters, are often measured in the same potential range. To selectively detect neurotransmitters a number of different electrode modifications are used. In this dissertation I present a modification of the electrode surface with carbon materials. Application of negatively charged carbon nanoparticles allowed for separation of the electrochemical signals from several neurotransmitters and the most common interferents. Usually, the electrochemical analysis is done under static conditions, where diffusion controls the mass transport. However, application of hydrodynamic methods, where forced convection controls the mass transfer, can significantly improve the limits of detection. Use of the innovative Rotating Droplet hydrodynamic system allowed for smaller limit of detection for neurotransmitters such as dopamine and serotonin in the presence of common interferents as ascorbic and uric acids. Application of the Rotating Droplet to neurotransmitter detection was preceded by its optimization. I performed a number of experiments for different redox probes, geometries and rotation velocities. In this thesis I have shown application of the RD setup in enzymatic oxygen reduction and in the generation-collection experiments. For better understanding of the flow profile of RD, I have performed computer simulations using the COMSOL Multiphysics software. The results of the numerical computations are also presented in this thesis and compared with experimental data.

Streszczenie

W niniejszej rozprawie opisuję badania dotyczące optymalizacji i charakteryzacji nowego układu pomiarowego jakim jest metoda wirującej kropli (*ang. Rotating Droplet)*. Celem moich badań było zastosowanie metody wirującej kropli do wykrywania i oznaczania stężeń neuroprzekaźników w próbkach biologicznych, zawierających substancje przeszkadzające.

Wykrywanie neuroprzekaźników metodami elektrochemicznymi jest skomplikowanym zagadnieniem. Aktywność elektrochemiczna różnych neuroprzekaźników wynika z możliwości ich utleniania lub redukcji. Sygnały utlenienia lub redukcji w małym, charakterystycznym dla neuroprzekaźników zakresie, często pokrywają się z sygnałami red-oks innych substancji obecnych w próbce. Aby móc selektywnie wskazać sygnał od danego neuroprzekaźnika stosuje się modyfikacje powierzchni elektrodowych. W rozprawie doktorskiej przedstawiam modyfikacje powierzchni elektrod materiałami węglowymi. Modyfikacja elektrod ujemnie naładowanymi nanocząstkami węgla umożliwiła odseparowanie sygnałów od neuroprzekaźników oraz substancji przeszkadzających. Zwykle pomiary elektrochemiczne prowadzone są w warunkach stacjonarnych, gdzie transport masy kontrolowany jest dyfuzyjnie. Jednak zastosowanie metod hydrodynamicznych, z transportem masy kontrolowanym poprzez wymuszoną konwekcję, znacząco poprawia limity detekcji metod elektrochemicznych. Wykorzystanie innowacyjnego układu wirującej kropli pozwoliło na obniżenie możliwych do oznaczenia stężeń neuroprzekaźników takich jak dopamina i serotonina w obecności interferentów, takich jak kwas moczowy i askorbinowy. Zastosowanie układu wirującej kropli wymagało uprzedniego jego zoptymalizowania. W tym celu przeprowadziłam szereg pomiarów dla różnych układów redoks, na różnych powierzchniach elektrodowych. W wyników tych pomiarów ustalono optymalną geometrię układu oraz możliwe prędkości wirowania. Pokazałam zastosowanie układu w enzymatycznej redukcji tlenu oraz pomiarach typu generator-kolektor. W pracy przedstawiam także przykłady symulacji komputerowych z wykorzystaniem programu COMSOL Multiphysics w celu lepszego zrozumienia profilu przepływu wewnątrz układu wirującej kropli.

Contents

List of abbreviations 1

Published papers 2

Introduction and Goal of the Dissertation 4

Chapter 1. Hydrodynamic methods in electrochemistry 7

1.1 Introduction 7

1.2 Rotating Disc Electrode 9

1.3 Fluidic systems 13

1.4 Rotating droplet 17

Bibliography 18

Chapter 2. Detection of Neurotransmitters 23

2.1 Introduction 23

2.2 Neurotransmitters 23

2.3 Chemical sensors and biosensors 29

2.4 Electrochemical sensors for neurotransmitters detection 33

2.5 Future trends in electrochemical neurotransmitters detection 37

Bibliography 38

Chapter 3. Computer simulations in electrochemistry 41

3.1 Introduction 41

3.2 The need for calculations 44

3.3 Software for electrochemical simulations 45

3.4 Calculation with COMSOL Multiphysics 46

3.5 Drawbacks of computations 51

Bibliography 51

Chapter 4. Methods 55

4.1 Introduction 55

4.2 Cyclic voltammetry 55

4.3 Chronoamperometry 57

4.4 Square wave voltammetry 58

4.5 Scanning electron microscopy 59

4.6 Particle Image Velocimetry 60

Bibliography 62

Chapter 5. Optimization and testing of the Rotating Droplet setup 63

5.1 Introduction 63

5.2 Setup configurations 64

5.3 Electrode modification 65

5.4 Results 69

Conclusions 83

Bibliography 84

Chapter 6. Generation-collection experiments in a Rotating Droplet system 85

6.1 Introduction 85

6.2 Electrode surface modification 88

6.3 Results 90

Conclusions 98

Bibliography 99

Chapter 7. Simultaneous neurotransmitters detection in the Rotating Droplet system 101

7.1 Introduction 101

7.2 Rotating Droplet setup configuration 102

7.3 System characterization 103

7.4 Results 105

Conclusions 114

Bibliography 115

Chapter 8. COMSOL calculations for electrochemistry and description of the flow inside the RD system 117

8.1 Introduction 117

8.2 COMSOL Multiphysics for electrochemistry 117

8.3 Calculations of the concentration profile and efficiency of the electrochemical reaction in posts based microchannel device. 119

8.4 Calculation of the electrochemical depletion zone in a microfluidic channel 122

8.5 COMSOL calculations results for the RD system 124

8.6 Particle Image Velocimetry 126

8.7 Results of COMSOL calculations on Rotating Droplet system 132

Conclusions 138

Bibliography 139

Summary 140

List of abbreviations

5-HT	serotonin (5-hydroxytryptamine)
AA	ascorbic acid
ABTS	2,2′-azino-bis(3-ethylbenzthiazoline-6-sulfonate)
BOx	Bilirubin Oxidase
CA	chronoamperometry or chronoamperogram
CE	counter electrode
CNPs	carbon nanoparticles
CNTs	carbon nanotubes
CV	cyclic voltammetry or cyclic voltammogram
DA	dopamine
DET	direct electron transfer
EP	epinephrine
Et-OH	ethanol
GCE	glassy carbon electrode
ITO	indium-tin oxide (electrode)
LbL	layer by layer
MET	mediated electron transfer
Met-OH	methanol
MTMOS	methyltrimethoxysilane
MWCNTs	multiwall carbon nanotubes
NEP	norepinephrine
ORR	oxygen reduction reaction
PIV	particle image velocimetry
RDE	rotating disc electrode
RE	reference electrode
RRDE	rotating ring-disc electrode
SEM	scanning electron microscopy
SWV	square wave voltammetry or square wave voltammogram
TMA	(Trimethoxysilyl)propyl)-N,N,N-trimethylammonium chloride
TEOS	tetraethoxysilane
TMOS	tetramethoxysilane
UA	uric acid
WE	working electrode

Published papers

The results presented in this thesis are partially published in following papers. These are referred to in the text with Roman numerals.

I. M. Kundys, K. Szot, E. Rozniecka, M. Jönsson-Niedziółka, R. Lawrence, S. D. Bull, F. Marken and M. Opallo
Electrochemical determination of selected neurotransmitters at electrodes modified with oppositely charged carbon nanoparticles, Anal. Methods 6, 7532 – 7539 (2014).

II. M. Kundys, W. Adamiak, M. Jönsson-Niedziółka
Rotating droplet as a new alternative for small volume electrochemical measurements, Electrochem. Commun. 72, 46-49 (2016)

III. M. Kundys, M. Nejbauer, M. Jönsson-Niedziolka , W. Adamiak
Generation–Collection Electrochemistry Inside a Rotating Droplet, Anal. Chem. 89, 8057–8063 (2017)

IV. E. Witkowska Nery, M. Kundys-Siedlecka, Y. Furuya, M. Jönsson-Niedziółka
Pencil Lead as a Material for Microfluidic 3D-Electrode Assemblies, Sensors 18(11), 4037 (2018)

V. M. Kundys-Siedlecka, E. Bączyńska, M. Jönsson-Niedziółka
Electrochemical Detection of Dopamine and Serotonin in the Presence of Interferences in a Rotating Droplet System, Anal. Chem. (2019)

Other publications not related to the thesis

1. E. Witkowska Nery, M. Kundys, P. S. Jeleń, M. Jönsson-Niedziółka Electrochemical glucose sensing – is there still room for improvement?, Anal. Chem. 88, 11271–11282 (2016)

2. M. Podrażka, E. Bączyńska, M. Kundys, P. S. Jeleń, E. Witkowska Nery Electronic Tongue—A Tool for All Tastes?, Biosensors 8, 3 (2018)

Introduction and Goal of the Dissertation

The scientific goal of the work behind this dissertation is to create and optimize a new hydrodynamic system called the Rotating Droplet (RD) system and utilize it in detection of multiple neurotransmitters in physiological fluids. The RD system is based on principles of a rotating disc electrode. However, RD exceeds the better-known method by using much smaller volume samples and giving more possibilities for choosing the working electrode material than the standard method does. Moreover, the unique construction of the RD system provides previously unexplored possibilities for detection of electrochemically active molecules.

This dissertation is divided into 8 chapters and is concluded with a short summary. Chapter 1 gives a general overview and basic information on hydrodynamic methods used in electrochemistry. In Chapter 2 I present a literature overview on neurotransmitters, their role in the human body, electrochemical properties and present state of art in terms of neurotransmitters detection. Chapter 3 contains basic information on the computer simulation in electrochemistry. Chapter 4 shows techniques and methods used in this dissertation. The scientific analysis of the performed experiments is presented in Chapters 5-8.

Chapter 5 is devoted to a thorough description of the RD system, its construction and preparation of electrodes surfaces. I describe the optimization of the system with usage of common redox probes and application of the RD system in enzymatic oxygen reduction. Data presented in this chapter were partially published in paper II.

In Chapter 6 I show how to utilize the RD system to perform electrochemical generation-collection experiments. I describe the preparation of the system and the set of electrodes. Chapter 6 contains the results of generation-collection measurements with a redox probe, which lead to outstanding results of collection efficiency in the RD system. The last part of this chapter describes application of the generation-collection phenomenon to filtering interferents' signal from the mixture of neurotransmitters and interferents. Results presented in this chapter were partially published in paper III.

Chapter 7 is a summary of the research on the utilization of the RD system for neurotransmitters detection. I describe a simultaneous detection of two neurotransmitters in a solution containing interferents. Data presented in Chapter 7 shows possible application of the RD system for detection of serotonin and dopamine in the presence of uric and ascorbic acids in a buffer solution. The system can be used for the determination of serotonin concentration in a biological sample. Results presented in this chapter were partially published in paper V.

In Chapter 8 I present the results obtained with the help of a computer simulation (COMSOL Multiphysics) and with Particle Image Velocimetry (PIV). The performed analysis was aimed at determination of the flow profile inside the RD system and simulation of electrochemical experiments performed with the use of the RD system. Moreover, in this chapter, I also briefly present simulations which I performed for other electrochemical hydrodynamic systems.

The summary contains a collection of the most important results presented on the pages of this dissertation.

Chapter 1.
Hydrodynamic methods in electrochemistry

1.1 Introduction

Electrochemical experiments are govern by three types of transport of electroactive species to the working electrode surface, i.e. migration, convection and diffusion. Migration is the movement of charged species in an electric field. In a typical electrochemical measurements supporting electrolyte is applied, which shields the field in the bulk of the liquid. Therefore, migration is limited to the distances very close to the electrode surface. For this reason the migration effects can generally be neglected. Convection is the movement of species driven by the thermal movements or stirring of the solution. Most of electrochemical experiments are carried out under static conditions and with a constant surrounding temperature, which eliminates the convection. Thus, in standard experiments the diffusion, spontaneous movement of molecules from higher to lower concentration regions, is the leading way of transporting the electroactive species. However, diffusion is considered as a rate limiting factor for many reactions [1]. These are reactions where the slow transport to the electrode surface as well as the removal of the products to the bulk solution impairs the efficacy of the reaction. In one dimension the flux J_i of a species i is described by the Nernst-Plank equation 1.1.1. [2]

$$\mathrm{J}_i(x) = -D\frac{\partial C_i(x)}{\partial x} - \frac{z_i F}{RT} D_i C_i \frac{\partial \Phi(x)}{\partial x} + C_i v(x), \qquad \text{Eq (1.1.1)}$$

where x is the distance from the surface, D_i is the diffusion coefficient, $\partial C_i(x)/dx$ is the concentration gradient, z_i is the charge, and C_i the concentration of species i. $\partial\Phi(x)/\partial x$ is the potential gradient and $\upsilon(x)$ is the velocity of the liquid motion along the x axis.

In order to avoid limitations imposed by diffusion in electrochemical systems, hydrodynamic methods were implemented. The forced convection methods in electrochemistry are those where either the fluid is in movement against a stationary electrode surface, or where the electrode enforces the movement of the fluid. Even though uncontrolled convection is considered as being problematic, the forced convection delivers fast and controlled mass transfer to the system. Rates of mass transfer at the electrode surface in hydrodynamic methods are often larger than the rates governed only by the diffusion. The biggest advantage of hydrodynamic methods is that steady state is attained quickly and the measurement can be made with a high precision. Both the production of reproducible measurements conditions and the theoretical/computational approach to the hydrodynamic methods problems are much more difficult than for experiments in stationary systems. However, the number of possible alterations in the system for creating the best tool in electroanalytical analysis suited to a given problem balances that effort. There is one general condition for the theoretical treatment of hydrodynamic methods - that the flow in the system is laminar. This condition is often described with the help of the Reynolds number (Re). The Reynolds number is a dimensionless parameter which helps to illustrate the flow behavior in different systems, by using the ratio of the inertial forces to the viscous forces. Usage of Re enables scaling between the systems and prediction the laminar-turbulent transition. Both prognosis of scaling of the system and the transition between laminar and turbulent flow applies widely for industrial purposes. Re depends on the characteristic flow rate v_{ch} and the characteristic length l for the system, and the kinematic viscosity of the fluid ν:

$$Re = \frac{v_{ch} l}{\nu}. \qquad \text{Eq 1.1.2}$$

Laminar flow is characterized by a smooth and constant fluid motion, which occurs when the viscous forces are predominant. Contrary to the laminar flow the turbulent flow is instable, often with co-existing vortices and chaotic eddies (known as swirling motion which can reverse the original flow direction). One can determine whether the flow is laminar or turbulent by comparing the Reynolds number of a given system to the Critical Reynolds number (Re_{cr}) for the system. In laminar flow the Re is always smaller than Re_{cr}. Typically for Re < 2100 flow is laminar, for 2100 < Re < 3000 is a transition state - the flow can be laminar or turbulent - and for Re > 3000 the flow is always turbulent. Due to the unpredictable behavior of the flow in turbulent systems only laminar flow can be used in hydrodynamic electrochemistry.

The obvious benefits of using hydrodynamic methods and not only being dependent on diffusion was a starting point for investigations of many kinds of systems exploiting this phenomena. The oldest and the most common is the Rotating Disc Electrode (RDE).

1.2 Rotating Disc Electrode

Rotating disc electrode (RDE) is a commonly used hydrodynamic method. In the RDE systems the electrode material is typically a rod of platinum or another electrode material sealed within an insulating material, so that only the front end is exposed. Rotation of the electrode enforces movement of the fluid in the closest surrounding of the working electrode surface. Far away from the electrode the fluid is moving perpendicularly to the electrode surface and for close distances the movement is centrifugal.

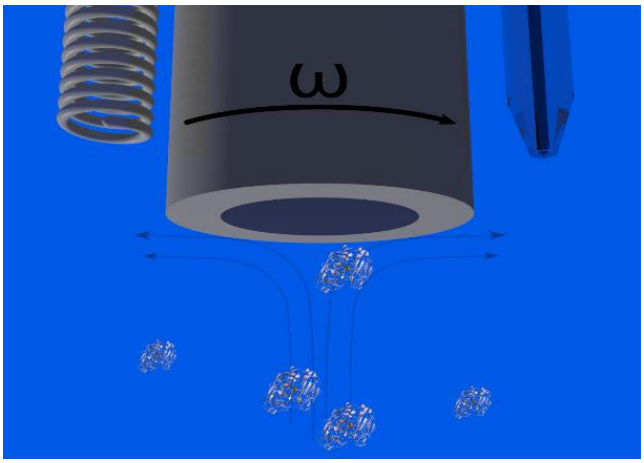

Fig 1.2.1 The fluid flow profiles, the perpendicular movement for far distances from the electrode surface and schematic flow of molecules reaching the working electrode surface.

In 1962 the Russian scientist Veniamin Grigorievich Levich , formulated an equation, describing the limiting current at the RDE, which has since been named after him. The Levich equation works under certain condition. According to these assumptions, if the electrochemical reaction is fast enough and the reaction is therefore limited only by the mass-transfer conditions, the limiting current, I_l, for a given rotation rate is proportional to the concentration of the electroactive species in the bulk solution (C_0), the area of the electrode (A), the diffusion coefficient (D) to the power of 2/3 and the square root of the rotation rate (ω), and viscosity (ν) to the power of (-1/6):

$$I_l = 0.620\, nFAD^{2/3}\nu^{-1/6}\omega^{1/2}C_0. \qquad \text{Eq. 1.2.1}$$

In principle, a fast enough electrochemical reaction registered at an RDE rotating with the infinite velocity should result in infinite current, and only kinetic limitations of the reaction itself will

control the maximum current. However, in practice, there will always be some maximum reaction rate, which is lower than infinity.

In the absence of any mass-transfer effects, the current would flow under kinetic limitations. Kinetic current is then described by the equation

$$I_k = FA\, k_f(E) C \qquad \text{Eq 1.2.2}$$

and is independent on the flow rate. Here $k_f(E)$ is the reaction rate for a given potential, which describes the kinetics of the electrochemical reaction.

Considering the contribution of the Levich (I_l) and kinetic current (I_k) to the total current (I) in the electrochemical reaction, an equation for the total current can be defined. In fact both current inputs can be treated as separate resistors which determine the total current value. For that reason the influence from both of them can be taken as the resistance of resistor connected in parallel and the total current can be derived from equation 1.2.3 called the Koutecký – Levich[1] equation:

$$\frac{1}{I} = \frac{1}{I_k} + \frac{1}{I_l} \qquad \text{Eq 1.2.3}$$

The kinetic current is strongly dependent on the reaction constant (k_f), and because of that RDE is often used for the determination of k_f. Separation of the input from Levich current and kinetic current is based on of plotting the reciprocal of the total value of the current vs the reciprocal of the square root of rotation rate. The extrapolation of the response towards infinite ω (i.e. to $1/\omega^{1/2} \rightarrow 0$) gives the value of the reciprocal of the current limited by the reaction kinetics. As presented in the Fig. 1.2.2 the total current values are different for different potentials, at which the current values were taken.

[1] Koutecký, the name of the co-author of the Koutecký-Levich equation in the original publications is presented as a Я. Коутецкий and later transliterated as Ya. Koutetskii in English publications. After a few iteration this became Koutecký, which seems to be far from the Russian original.

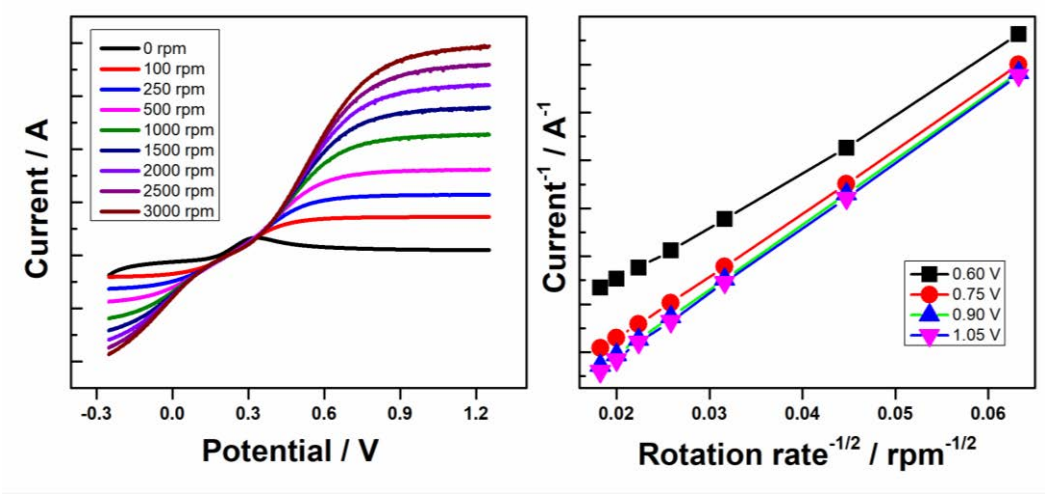

Figure 1.2.2 RDE oxidation of 20 mM K4Fe(CN)6 and 10 mM K3Fe(CN)6 in 0.1 M KCl together with Koutecký – Levich plots at potentials 0.60, 0.75, 0.90, 1.05 V

Due to these useful properties of the RDE, such as elimination of the diffusion limitations, possibility for determination of certain electrochemical reactions parameters, it has become a very popular method among electrochemists.

1.2.1 RDE applications

The Rotating disc electrode is a well-known and developed hydrodynamic method that has been used in variety of applications. Most of applications of RDE focus on studying of reaction kinetics of especially sluggish reaction such as oxygen reduction reaction (ORR). RDE is frequently used for determination of the diffusion coefficient [3]–[5] and kinetic parameters of the electrochemical reactions [6]–[8]. Due to its industrial importance in the field of fuel cells and corrosion, ORR is a very often studied reaction [9]. There are many reports on application of the RDE for studying kinetics of corrosion[10], its inhibition[11] and protection from corrosion[12].

Because RDE can be used to overcome mass-transport limitations due to slow diffusion it is very often used as a sensor. The fast kinetics of electrochemical reactions encourages the applications of RDE for improving of the efficiency of reactions, as well as for analytical purposes[13]–[15].

1.2.2 RRDE

One of the alterations of the RDE is a system where an electrode ring surrounds the disc. Such a system is called Rotating Ring Disc Electrode (RRDE) and it was described in 1959 in [16] where the authors proved its utility for the detection of the intermediate of the oxygen reduction in alkaline solution. In general, the fluid flow is such that after being exposed to the disc electrode the reaction fluid is transported to the downstream placed ring electrode and can take part in the reaction therein. This type of reaction is often used for the study of the multi-electron processes

[17], kinetics of slow electron transfer, adsorption/desorption steps[18], [19], and electrochemical reaction mechanisms [20]. The most often studied multielectron reaction is oxygen reduction (ORR). The importance of that particular reaction was mentioned above. ORR is a 4-electron reaction, and its mechanism is different depending on the pH of the solution, the electrode material, the presence of external catalysts etc. The most desired path, which is also very difficult to obtain, is a one step 4-electron reduction. Most often ORR is performed on platinum electrodes and consist of two steps of 2-electron reactions. The verification of the mechanism is often performed on the platinum-platinum ring disc electrode, where the first 2-electron reduction occurs on the disc, and the by-product (hydrogen peroxide) is moved downstream to the ring electrode where the second 2-electron reduction can occur:

Disc reaction: $O_2 + 2\,H^+ + 2\,e^- \rightarrow H_2O_2$ Eq. 1.2.2.1a

Ring reaction: $H_2O_2 + 2\,H^+ + 2\,e^- \rightarrow 2H_2O$ Eq. 1.2.2.1b

In the RRDE system is very often generation–collection experiments [21]. The most often used parameter describing the generation-collection results is the collection efficiency. Collection efficiency is a ratio between the total current value on the collector and the total current value on the generator. Depending on the system collection efficiency can vary. The width of the generator and collector electrodes and the distance between them are the most important variables for generation-collection system. For the standard RRDE tip the collection efficiency reaches up to 32% [22].

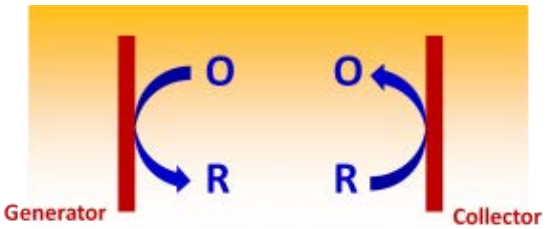

$$Collection\ efficiency = \frac{Current\ on\ collector}{Current\ on\ generator}$$

Fig. 1.2.2.1 Schematic generation-collection system, together with the definition of collection efficiency. Adapted from publication III.

Along with RRDE a variety of different generation-collection systems exist such as: double flow-channel electrodes, interdigitated electrode arrays, dual disc systems, dual hemisphere systems, ring-recessed disc systems. In this thesis data obtained in a generation-collection rotating droplet

system will be presented. The Ring Disc Electrode tip is a base for the Rotating Droplet system, which will be described in details later, where the disc acts as a reference electrode and the ring as a counter electrode.

1.3 Fluidic systems

The other well-established field concerning hydrodynamic methods is microfluidics. Its origin can be traced to the need for continuous supply of reaction substrates, such as flow injection analysis (FIA) systems, where on a macroscopic scale the sample is injected into the flowing system, and later is transported to an external detector device. FIA is an analytical technique, where reagents are mixed before reaching the detector. This technique was developed into a wide range of applications depending on the detectors used, e.g. mass-spectrometry, spectrophotometry and fluorescence spectroscopy. Despite many advantages of these systems miniaturization was needed. In 1983 Ruzicka proposed a miniaturized fluidic system [23] , where dimensions of the reaction chip were established to use no more than 20 µL of the sample volume.

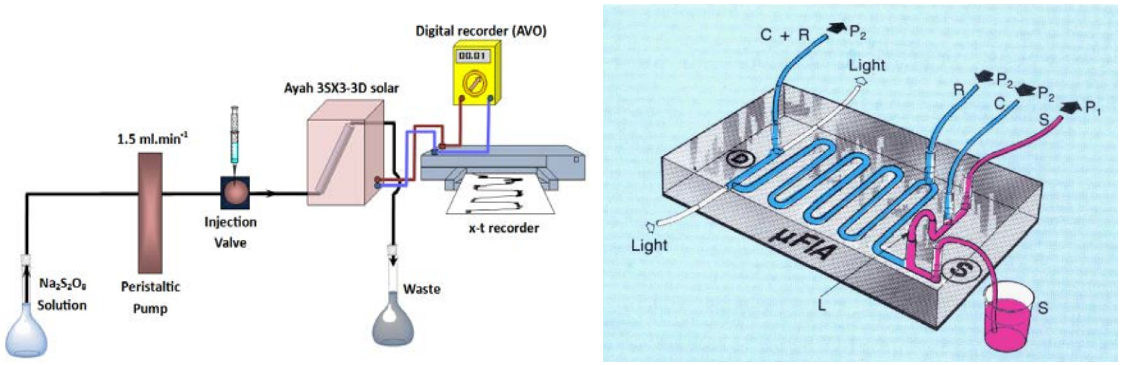

Fig. 1.3.1 Schematic diagram of Flow Injection Analysis system. Adapted from [24] *and Integrated microconduit for FIA. Adapted from* [23].

Microfluidic systems have specific dimensions from tens to hundreds of micrometers. First microfluidic systems were created for one purpose–mixing of reagents, before reaching the detector [25]. Later microfluidics were integrated with several kinds of detectors and engineered to act as independent devices [26]. The idea of miniaturization of the fluidic systems was developed for many years and nowadays even nanofluidic devices are created [27].

1.3.1 Microfluidics

There are many different microfluidic families which purpose is to mix or separate reagents, such as designed for elecrowetting, centrifugal, paper devices or microdroplets formation [28]. In most cases channels are prepared either with laser cutting or using photolithography methods[29]. In scientific research the most often used method is soft lithography, based on the fabrication of

channels in slabs of the polymer polidimethylosiloxane (PDMS). An outline of this procedure is presented in figure 1.3.1.2. Creation of the channel in PDMS block requires designing and printing a 2D negative pattern of the channel, preparation of the substrate wafer master covered with photoresist 1.3.1.2 (a), UV exposure 1.3.1.2 (b), and development of the photoresist 1.3.1.2 (c). A chip prepared in such a way is used as a master for PDMS molding 1.3.1.2 (d). If further treated at a temperature of 70˚C for 2 h, the channels are grooved into the polymer block 1.3.1.2 (e). The PDMS surface is usually activated with O_3 treatment and can be later attached to a glass surface because of the creation of the van der Waals interaction between functional groups of the PDMS and glass.

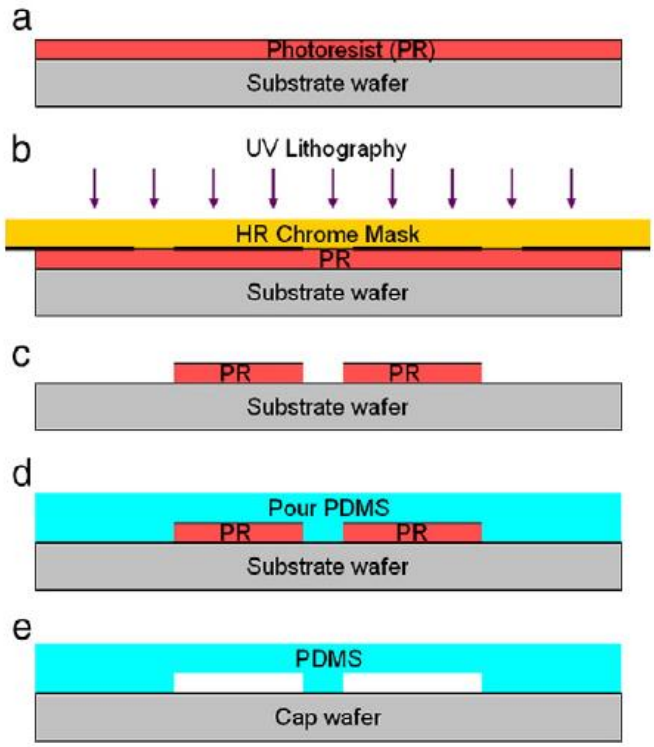

Figure 1.3.1.2 Fabrication process of PDMS devices by soft-lithography. Adapted from [30].

Such a procedure allows for preparation of custom-designed microchannel patterns, which can be used for standard microchannel chips as well as for new types of fluidic systems. Usually the fluid containing the electroactive substance, in the case of electrochemistry, is pumped into the fluidic channel with the help of a peristaltic pump, controlled by the operator. However, several other techniques are in use. One of the most common alternatives for conventional pumping is usage of gravitational force. In such a system the difference in height between the source of the fluid and the reactive platform create the difference of potential energy, which drives the movement of the fluid through the channel. Depending on application, the microfluidic channels can be equipped with different reagents and sensors. One of the examples is the addition of band-electrodes on the bottom of the microchannel. Recently this approach has evolved into application

of multiple electrodes inside the channel, or application of many mixing reservoirs. This concept is known as a lab on a chip. The need for both integration of many different sensors and fast mixing was a driving force for creation of centrifugal microfluidics on CD discs [31]. In this type of systems, fluids on disc can be pumped by the centrifugal force controlled by the rotational speed of the CD. The spinning disc equipped with the channels and reservoirs enforces the movement of the fluid through the desired pathways.

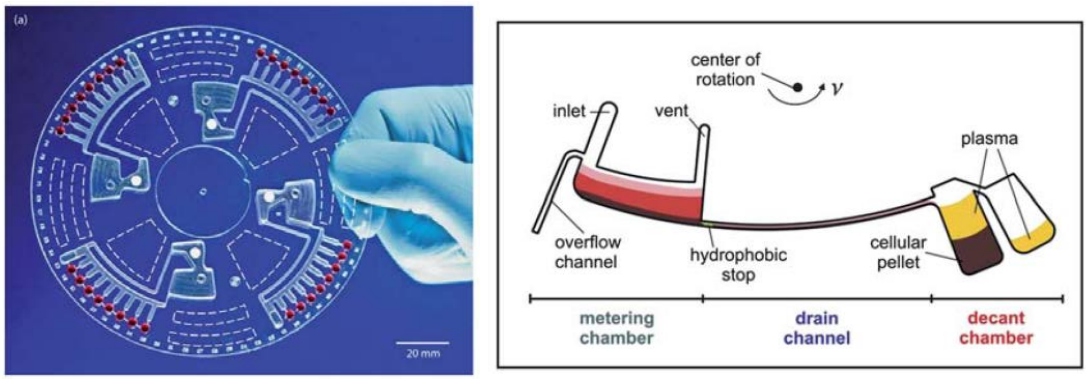

Fig. 1.3.2 Design of the foil cartridge (A) Photograph of a foil disk (B). Adapted from [32]. *Flow scheme in the separation structure of the blood serum. Adapted from* [33].

1.3.2 Electrochemical sensing in microfluidics

Well described fluid transport through the channel enabled an easier implementation of the detector inside the channel, such as electrodes, which can act an electrochemical sensor. The characteristics of a useful fluidic system for electrochemical purposes are both a laminar flow inside a channel and a known fluid flow profile above the electrode surface. By the approximation that microfluidic systems are ruled by laminar flow, the Levich-like equation for electrochemical experiments in microfluidic channels describes the limiting current *(I_{lim})*:

$$I_{lim} = 0.925\, n\, F\, c\, D^{2/3}\, (h^2 d)^{-1/3}\, w\, x^{2/3}\, V_f^{1/3} \quad ,$$

where *h* is the half of the height of the channel, *d* is the width of the microchannel, *w* is the width of the band-electrode, *x* is the electrode length, and V_f is the flow rate value. The main difference between the Levich equation and Levich-like equation for microfluidic channel is the flow rate power. For RDE system flow rate exponent is 1/2, whereas for microfluidic channel it is 1/3, the difference indicate that the flow rate in microfluidic channel has smaller impact on the total current value. An interesting point is that the current is not directly proportional to the length of the electrode, since the downstream end of the electrode sees a lower concentration of analyte than the upstream end. Specifics of the microfluidic system are the small dimensions which assure

the laminar flow inside the system and provide the repeatable conditions for electrochemical purposes.

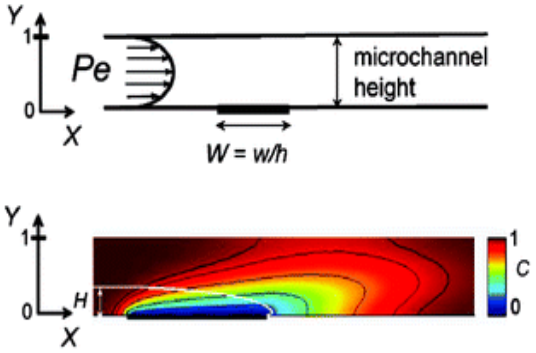

Figure 1.3.2.1 Flow profile inside a microfluidic channel over the working band electrode. Steady-state concentration profiles developing over the working electrode. Adapted from [34] *and* [35]

The first reports on electrochemical experiments performed in microfluidic systems are mostly patent applications. This amount of commercial interest in microfluidics electrochemistry can indicate how promising the method was from the very beginning. However, from the beginning of the 21st century also the number of scientific research publications on the microfluidic application in the electrochemistry field had grown.

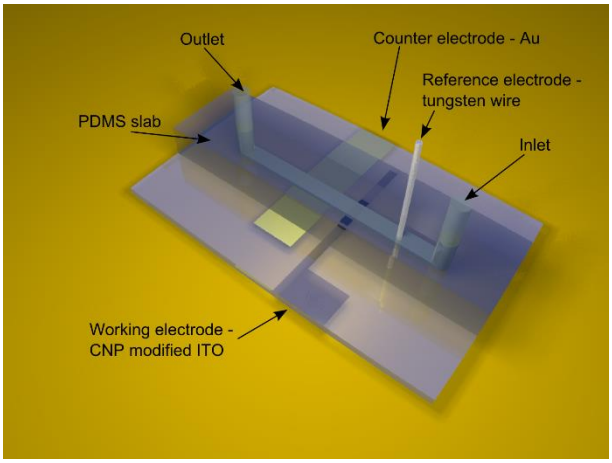

Fig. 1.3.2.2 Scheme of microfluidic channel, where the working and counter electrode are placed on the glassy plate, reference electrode is placed inside the PDMS channel slab.

Nowadays, electrochemical microfluidic devices are often used for multiple purposes. In most cases the fluid is pumped inside the channel with a peristaltic or a syringe pump. There are other approaches, i.e. where the flow is dependent on a driven voltage [36], where the high voltage changes was used to enforce the sample movement. Usability of such system was proven for the

detection of very small concentrations such as 2 pM of trinitrotoluene which is competitive compared with alternative detection methods. Other examples of sensors in fluidic condition are those based on the gravitational forces [37]. Paper based microfluidic devices create a separate field of microfluidic devices. Due to the multiple advantages of paper based systems, such as inexpensive materials, light weight and easy disposability, their possible usage has grown in last years. In those systems the fluid is transported passively because of wicking by the hydrophilic fibers of the material [38], [39]. Even though microfluidic systems are considered as low volume usage the problem of dead volume still exist. In order to minimize the sample volume an innovative configuration of fluidic method was needed. To fill this niche, a rotating droplet system was suggested.

1.4 Rotating droplet

In terms of miniaturization of fluidic systems the "mother method" RDE has been altered to different systems. The first approach for minimizing the sample of a small hydrodynamic droplet was proposed by Cserey et al.[40]. The system was designed so that the nitrogen was pumped through the pipe, which end was close to the walls of droplet. The gas flow enforced the movement of the solution inside the droplet. The other examples with preservation of the typical hydrodynamic flow borrowed from the RDE was the kinetic rotating droplet developed by Kuramitz for of the electrochemical genotoxicity test shown in the figure 1.4.1 [41] and later the slightly alternated of the system for the evaluating soil enzyme activity [42].

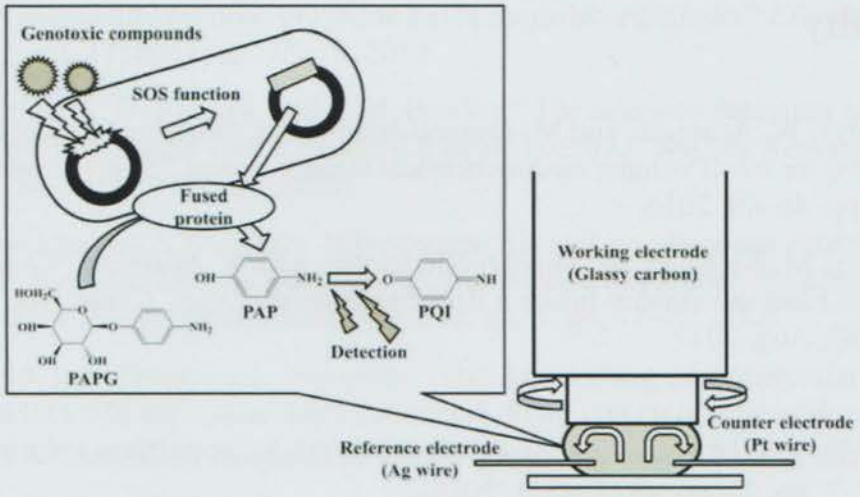

Figure 1.4.1. The schematic diagram for genotoxicity test with hydrodynamic electrochemical detection using the rotating disc electrode in a microdroplet. Adapted from [41].

The other approaches to the creation new techniques which use a small rotating volume is the biological study of chemical oxidative deprotection of a boronic ester by H_2O_2, a biomolecular binding recognition between a small target molecule and an aptamer, and the inhibition of the redox-mediated catalytic cycle of horseradish peroxidase where the hydrodynamic conditions turned out to be essential for the fast transport of reagents inside small reactor volume Figure 1.4.2 [43].

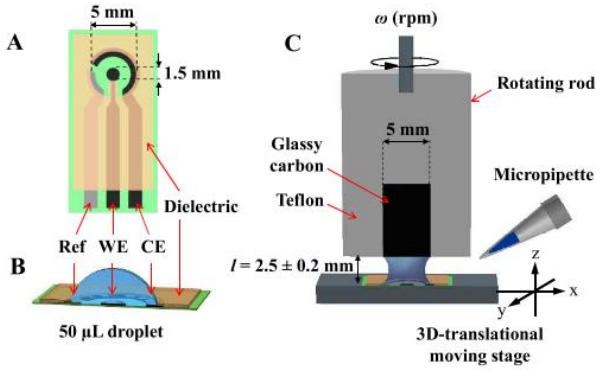

Figure 1.4.2. (A) Graphical representation of the screen-printed three-electrode electrochemical microcell, (B) cross- sectional view of a 50 µL droplet deposited over the electrochemical microcell, (C) cross-sectional view of the rotating droplet system. Adapted from [43].

These presented examples form the origin for the Rotating Droplet (RD) system described later in this thesis, chapter 5, and in the publications II and III.

Bibliography

II M. Kundys, W. Adamiak, and M. Jönsson-Niedziółka, "Rotating droplet as a new alternative for small volume electrochemical measurements," *Electrochem. commun.*, vol. 72, pp. 46–49, 2016.

III M. Kundys, M. Nejbauer, M. Jönsson-Niedziolka, and W. Adamiak, "Generation–Collection Electrochemistry Inside a Rotating Droplet," *Anal. Chem.*, vol. 89, no. 15, pp. 8057–8063, Aug. 2017.

[1] S. Eloul and R. G. Compton, "General Model of Hindered Diffusion," *J. Phys. Chem. Lett.*, vol. 7, no. 21, pp. 4317–4321, 2016.

[2] A. J. Bard and L. R. Faulkner, *ELECTROCHEMICAL METHODS Fundamentals and Applications Allen*. 1985.

[3] F. M. Everaerts, L. J. J. Janssen, and R. A. Tacken, "Diffusion coefficients of oxygen, hydrogen peroxide and glucose in a hydrogel," *Anal. Chim. Acta*, vol. 273, no. 2, pp. 553–560, 1993.

[4] H. Tian and C. E. Reece, “Evaluation of the diffusion coefficient of fluorine during the electropolishing of niobium,” *Phys. Rev. Spec. Top. - Accel. Beams*, vol. 13, no. 8, pp. 1–7, 2010.

[5] R. G. Compton and R. G. Harland, “Rotating-disc Electrodes and the Theory of CE Processes,” vol. 85, no. 3, pp. 761–771, 1989.

[6] D. A. Finkelstein, N. Da Mota, J. L. Cohen, and H. D. Abruña, “Rotating disk electrode (RDE) investigation of BH4- and BH3OH-electro-oxidation at Pt and Au: Implications for BH 4- fuel cells,” *J. Phys. Chem. C*, vol. 113, no. 45, pp. 19700–19712, 2009.

[7] R. Vargas, C. Borrás, J. Mostany, and B. R. Scharifker, “Kinetics of surface reactions on rotating disk electrodes,” *Electrochim. Acta*, vol. 80, pp. 326–333, 2012.

[8] J. Masa, C. Batchelor-McAuley, W. Schuhmann, and R. G. Compton, “Koutecky-Levich analysis applied to nanoparticle modified rotating disk electrodes: Electrocatalysis or misinterpretation,” *Nano Res.*, vol. 7, no. 1, pp. 71–78, 2014.

[9] J. K. Nørskov *et al.*, “Origin of the overpotential for oxygen reduction at a fuel-cell cathode,” *J. Phys. Chem. B*, vol. 108, no. 46, pp. 17886–17892, 2004.

[10] F. C. Walsh, L. F. Arenas, and G. Kear, *The Electrode Kinetics of Oxygen Reduction: A Case Study. The Corrosion of Copper and its Alloys in Aqueous Chloride Solution at a Smooth Rotating Disk Electrode*. Elsevier, 2017.

[11] E. Asghari, H. Ashassi-Sorkhabi, and M. Gholizadeh-Khajeh, “Synergism between Tartaric acid and Zinc ions under hydrodynamic conditions for corrosion inhibition of steel in cooling water solution-electrochemical impedance and morphological studies,” *Prot. Met. Phys. Chem. Surfaces*, vol. 52, no. 6, pp. 1070–1078, 2016.

[12] F. C. Walsh, G. Kear, A. H. Nahlé, J. A. Wharton, and L. F. Arenas, “The rotating cylinder electrode for studies of corrosion engineering and protection of metals—An illustrated review,” *Corros. Sci.*, vol. 123, no. November 2016, pp. 1–20, 2017.

[13] V. Mani, A. P. Periasamy, and S. M. Chen, “Highly selective amperometric nitrite sensor based on chemically reduced graphene oxide modified electrode,” *Electrochem. commun.*, vol. 17, no. 1, pp. 75–78, 2012.

[14] C. C. Harley, A. D. Rooney, and C. B. Breslin, “The selective detection of dopamine at a polypyrrole film doped with sulfonated β-cyclodextrins,” *Sensors Actuators, B Chem.*, vol. 150, no. 2, pp. 498–504, 2010.

[15] V. S. Vasantha and S. M. Chen, “Electrocatalysis and simultaneous detection of dopamine and ascorbic acid using poly(3,4-ethylenedioxy)thiophene film modified electrodes,” *J. Electroanal. Chem.*, vol. 592, no. 1, pp. 77–87, 2006.

[16] B. L. and J. I. A. Frumkin, L. Nekrasov, “Die Anwendung der rotierenden scheibenelektrode mit einem ringe zuruntersuchung von zwishenprodukten elektromischer reaktionen,” *J. Electroanal. Chem.*, vol. 1, pp. 84–90, 1959.

[17] Y. C. Lu, Q. He, and H. A. Gasteiger, “Probing the lithium-sulfur redox reactions: A rotating-ring disk electrode study,” *J. Phys. Chem. C*, vol. 118, no. 11, pp. 5733–5741, 2014.

[18] S. Sankarasubramanian, J. Seo, F. Mizuno, N. Singh, and J. Prakash, “Rotating Ring-Disc Electrode Investigation of the Aprotic Superoxide Radical Electrochemistry on Multi-Crystalline Surfaces and Correlation with Density Functional Theory Modeling: Implications for Lithium-Air Cells,” *J. Electrochem. Soc.*, vol. 163, no. 10, pp. A2377–

A2384, 2016.

[19] F. R. Shu and G. S. Wilson, “Rotating Ring-Disk Enzyme Electrode for Surface Catalysis Studies,” *Anal. Chem.*, vol. 48, no. 12, pp. 1679–1686, 1976.

[20] C. Ma, N. M. Contento, L. R. Gibson, and P. W. Bohn, “Redox cycling in nanoscale-recessed ring-disk electrode arrays for enhanced electrochemical sensitivity,” *ACS Nano*, vol. 7, no. 6, pp. 5483–5490, 2013.

[21] E. O. Barnes, G. E. M. Lewis, S. E. C. Dale, F. Marken, and R. G. Compton, “Generator-collector double electrode systems: A review,” *Analyst*, vol. 137, no. 5, pp. 1068–1081, 2012.

[22] E. Verney, J. R. Martin, and P. Clechet, “Experimental Determination of the Collection Efficiency of a Metal/n-Type Semiconductor Rotating Ring-Disk Electrode,” *J. Electrochem. Soc.*, vol. 132, no. 9, p. 2178, 1985.

[23] J. Ruzicka, “Flow Injection Analysis From Test Tube to Integrated Microconduits,” vol. 55, no. 11, 1983.

[24] I. M. A. Shakir and N. S. Turkey, “Flow injection analysis for the photometric determination of promethazine-HCl in pure and pharmaceutical preparation via oxidation by persulphate using Ayah 3SX3-3D solar micro photometer Abstract : Introduction : Materials and Methods :,” *Bagdad Sci. J.*, vol. 10, no. 4, 2013.

[25] A. Manz, N. Graber, and H. M. Widmer, “Miniaturized Total Chemical Analysis Systems : a Novel Concept for Chemical Sensing,” *Sensors and Actuators*, pp. 244–248, 1990.

[26] S. Shoji, M. Esashi, and T. Matsuo, “Prototype miniature blood gas analyser fabricated on a silicon wafer,” *Sensors and Actuators*, vol. 14, no. 14, pp. 101–107, 1988.

[27] Q. Xie *et al.*, “Fast water transport in graphene nanofluidic channels,” *Nat. Nanotechnol.*, vol. 13, no. March, 2018.

[28] P. Garstecki, M. J. Fuerstman, A. Stone, and G. M. Whitesides, “Formation of droplets and bubbles in a microfluidic T-junction — scaling and mechanism of break-up {,” pp. 437–446, 2006.

[29] M. J. Cooper and G. M. Whitesides, “Poly (dimethylsiloxane) as a Material for Fabricating Microfluidic Devices,” *Acc. Chem. Res.*, vol. 35, no. July, pp. 491–499, 2002.

[30] B. Prabhakarpandian, M. C. Shen, K. Pant, and M. F. Kiani, “Microfluidic devices for modeling cell-cell and particle-cell interactions in the microvasculature,” *Microvasc. Res.*, vol. 82, no. 3, pp. 210–220, 2011.

[31] R. Burger, L. Amato, and A. Boisen, “Detection methods for centrifugal microfluidic platforms,” *Biosens. Bioelectron.*, vol. 76, pp. 54–67, 2016.

[32] M. Focke *et al.*, “Microstructuring of polymer films for sensitive genotyping by real-time PCR on a centrifugal microfluidic platform,” *Lab Chip*, vol. 10, no. 19, pp. 2519–2526, 2010.

[33] J. Ducr, S. Haeberle, S. Lutz, S. Pausch, F. Von Stetten, and R. Zengerle, “The centrifugal microfluidic Bio-Disk platform,” *J. Micromechanics Microengineering*, vol. 17, pp. 103–115, 2007.

[34] C. Amatore, N. Da Mota, C. Lemmer, C. Pebay, C. Sella, and L. Thouin, “Theory and

Experiments of Transport at Channel Microband Electrodes under Laminar Flows. 2. Electrochemical Regimes at Double Microband Assemblies under Steady State," *Anal. Chem.*, vol. 80, no. 24, pp. 9483–9490, 2008.

[35] C. Amatore, C. Lemmer, P. Perrodin, C. Sella, and L. Thouin, "Theory and experiments of microelectrodes performing as concentration probes within microfluidic channels with high temporal resolution," *Electrochem. commun.*, vol. 13, no. 12, pp. 1459–1461, 2011.

[36] J. Wang, R. Polsky, B. Tian, and M. P. Chatrathi, "Voltammetry on Microfluidic Chip Platforms," *Anal. Chem.*, vol. 72, no. 21, pp. 5285–5289, 2000.

[37] X. Zhang *et al.*, "Gravitational Sedimentation Induced Blood Delamination for Continuous Plasma Separation on a Microfluidics Chip," 2012.

[38] W. Dungchai, O. Chailapakul, and C. S. Henry, "Electrochemical detection for paper-based microfluidics.," *Anal. Chem.*, vol. 81, no. 14, pp. 5821–6, Jul. 2009.

[39] X. Liu, O. Akbulut, and G. M. Whitesides, "Integration of paper-based microfluidic devices with commercial electrochemical readers †," no. C, pp. 3163–3169, 2010.

[40] A. Cserey and M. Gratzl, "Rotating sample system: an equivalent of a rotating electrode for microliter samples.," *Anal. Chem.*, vol. 69, no. 18, pp. 3687–3692, 1997.

[41] H. Kuramitz *et al.*, "Electrochemical Genotoxicity Assay Based on a SOS/umu Test Using Hydrodynamic Voltammetry in a Droplet," *Sensors*, vol. 12, no. 12, pp. 17414–17432, Dec. 2012.

[42] K. Sazawa and H. Kuramitz, "Hydrodynamic Voltammetry as a Rapid and Simple Method for Evaluating Soil Enzyme Activities," *Sensors*, vol. 15, no. 3, pp. 5331–5343, 2015.

[43] L. Challier, R. Miranda-Castro, D. Marchal, V. Noel, F. Mavre, and B. Limoges, "Kinetic Rotating Droplet Electrochemistry: a Simple and Versatile Method for Reaction Progress Kinetic Analysis in Microliter Volumes.," *J. Am. Chem. Soc.*, Aug. 2013.

Chapter 2.

Detection of Neurotransmitters

2.1 Introduction

In the following chapter the main concepts standing behind neurotransmitters detection will be described. I would like to introduce neurotransmitters themselves, their properties and a justification for a necessity of looking for an appropriate method for their detection. In the second part of the chapter I would like to give an overview on the state of art in neurotransmitters sensing and present the direction which I followed during my research towards biosensing.

2.2 Neurotransmitters

Neurotransmitters are biologically active molecules responsible for transmission of nervous impulses. Neurotransmission itself was discovered in 1921 by Otto Loewi, who observed the chemically originated connection between the two frogs hearts[2], described later. In his experiments Loewi proved that nerve impulses are based on chemical reaction, in contrast to previously believed electrical impulses. During his studies he observed that electrical stimulation of the first frog heart (placed in the first chamber) slowed down its beats. The fluid from surroundings of the first heart was injected into the second chamber (where the second frog heart was located), which caused the reaction of the second heart: it has slowed down its beats too. The reaction of the second heart was ascribed to the molecules released by neurons of the first heart, later found to be the molecules of acetylcholine [1]. The reaction of that neurotransmitters was

[2] Otto Loewi is known from the way, he came up with the idea of the experiment with frog hearts. In the middle of the night he woke up, and scribed down the notes about experiment, which he dreamed about. However, in the morning he couldn't read he's bad handwriting. Fortunately, the next night he had the same dream, he woke up and taught by experience immediately performed the experiment.

confirmed in later studies [2]. Otto Loewi together with Elliott Dale in 1936 were awarded with a Nobel Prize in Physiology or Medicine for studies and discoveries related to neurotransmission [3].

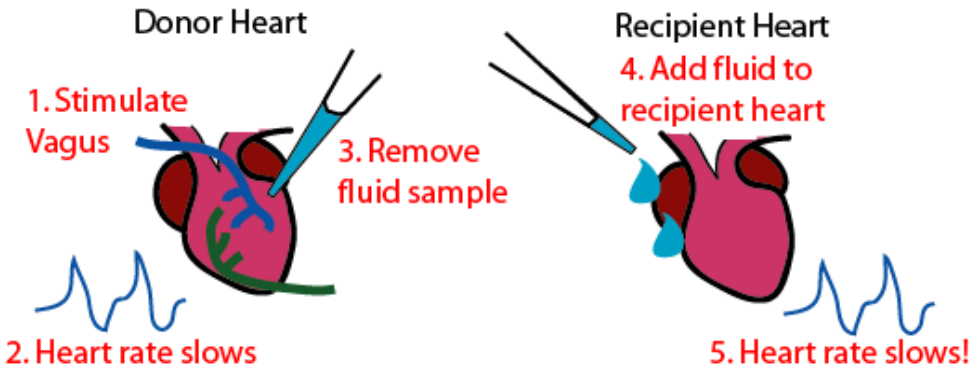

Figure 2.2.1 Schematic of Loewi's experiment on neurotransmission. Adapted from [4].

Function of a given neurotransmitter varies depending on the place of secretion and is very often interconnected with other neurotransmitters. Neurotransmitters are secreted by the presynaptic part of the dendrite to the synaptic cleft, where they can be captured by the postsynaptic receptors, and then initiate the nerve impulse and the organism reaction. One of the most often referred to examples of the transmission of nerve impulses is the scalding of the skin. In that process nerves have to transport the information from the place in the body where scalding have occurred to the decision making organ – brain. The decision on the action is also transported from the brain to muscles, in order to move the hand away. Inside the axons, the nerve impulses are electrical signals. However, the connection between nerves is accomplished by transport of neurotransmitters across the synapse and reception by a specialized site of the following nerve called receptor. Transmission between nerve cells is done through the chemical transmission. The typical neuron resting potential is around -60 to -70 mV across the membrane. The action of the receptor can be driven by the depolarisation potential, which is the increase of the potential usually the threshold value is -55 mV (excitatory postsynaptic potential), and the hyperpolarisation potential, which is considered the same as inhibitory postsynaptic potential. Neurotransmitters are enclosed in the vesicles, and released simultaneously after the depolarisation of the neuron. Neurotransmitters are released into the synaptic cleft reach the proteins on the other side of the synapse, where they are specifically bonded to the receptors.

There are certain criteria which must be fulfilled by a chemical to be a neurotransmitter. Those are e.g. that it has to be produced by a neuron after a stimulation (depolarisation), it supposed to be found by a neuronal postsynaptic receptor and cause the biological reaction.

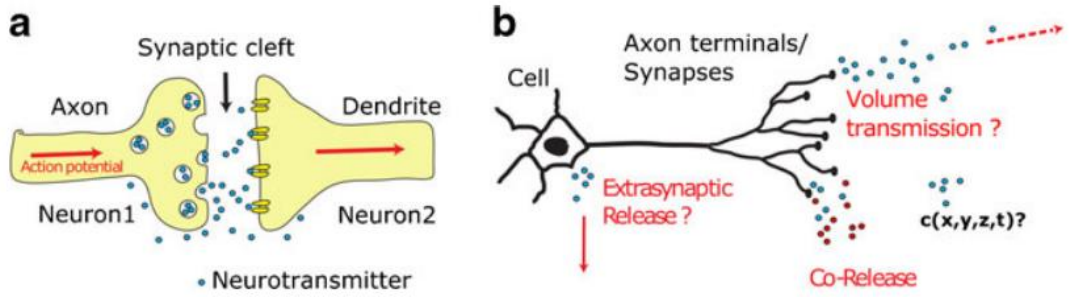

Figure 2.2.2 Neurotransmitters release and analytical challenges. (a) Schematic of a synapse that connects two neurons. (b) Modes of neurotransmitter release beyond the simplified synapse picture. Adapted from [5].

An additional criterion for the neurotransmitters is that after the stimulation the release of the chemical molecule should be inactivated either by the reuptake mechanism or through enzymatic reaction, which stops the neurotransmitters action. The action of the neurotransmitter can be stopped by four different mechanisms:

- diffusion, where neurotransmitters diffuse away from the synaptic cleft, and cannot be specifically bonded to the receptor any more
- enzymatic deactivation, where a specific enzyme changes the structure of a given neurotransmitter, causing its inactivity due to the nonspecific binding with the receptor
- glial cells, where the astrocytes remove the neurotransmitters from the synaptic cleft, preventing the specific binding to the receptor
- reuptake, where the neurotransmitter molecule is taken back inside through the presynaptic membrane to the axon terminal. In both cases the glial cells and reuptake mechanisms the neurotransmitters molecules are removed from the synaptic cleft and cannot be specifically bonded to the receptor molecule and the neuron reaction is being stopped [6].

Neurotransmitters are divided into many different groups, depending on the chemical origin, reaction mechanism, target group of stimulation. The most often used division is:

- Monoamines; Serotonin (5-HT), Histamine, Acetylcholine, Dopamine (DA), Epinephrine (EP), Norepinephrine (NEP)
- Amino Acids; Gamma-aminobutyric acid (GABA), Aspartame, Glutamate, Glycine
- Neuroactive peptides; e.g. insulin, glucagon, oxytocin, prolactin, bradykinin, thyrotropin, gonadotropin
- Soluble gases (Gasotransmitters); carbon monoxide, nitric oxide.

Each of the neurotransmitters is believed to be responsible for a certain body reaction. However, it is known that a given reaction is complex and dependant on a simultaneous secretion of many neurotransmitters.

The group of neurotransmitters belonging to the family of catecholamines (DA, NEP, EP) is synthesized in step-by-step reaction, where one neurotransmitter after the enzymatic influence is transformed into another. These are mainly synthesized in the cytoplasm of the cell body and transported inside the vesicles to the axon terminals. The fusion of the vesicles occurs together with spilling of the molecules to the synaptic cleft. In fact, neurotransmitters are not excreted to the synaptic cleft but rather spilled outside of the synapse and diffuse to many other neuronal receptors. This phenomena is so called volume transmission [5], shown schematically on Fig. 2.2.2 (b). Moreover, more than one neurotransmitter can be released which is called co-release [7]. Besides, neurons possess an unique property of switching between neurotransmitters, in order to adjust to the behavioural changes, such as dopamine-somatostatin changes in the rat brain, induced by exposure to different photoperiods[8]. The recognition of neurotransmitters can be performed only with the specific postsynaptic receptor on the postsynaptic membrane, where the neurotransmitter can be bonded and initiate the body action.

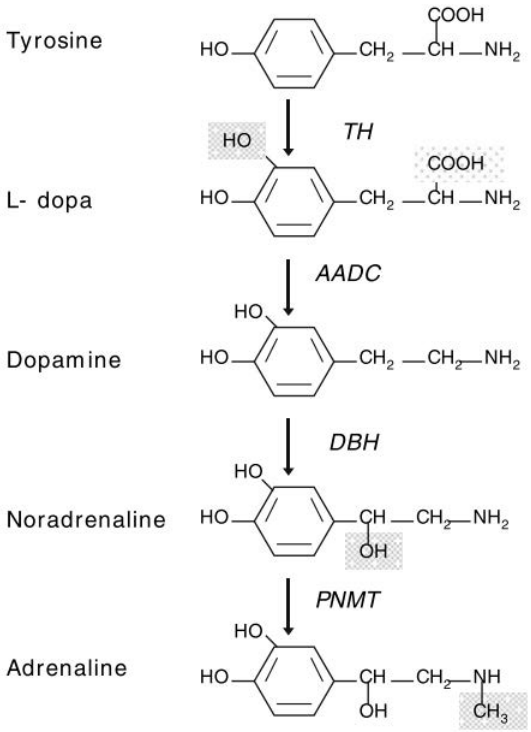

Figure 2.2.3 Biosynthesis of catecholamines. Enzyme abbreviations: TH, tyrosine hydroxylase; AADC: amino acid decarboxylase; DBH, dopamine-β-hydroxylase; PNMT: phenylethanolamine-N-methyl transferase

Examples of neurotransmitters

Below some of the most common neurotransmitters, their properties and specific functions will be presented. The detection of these is the main topic of the experimental section of this thesis of chapter 7.

Dopamine

Dopamine (DA; 3,4-dihydroxyphenethylamine) is a neurotransmitter which belongs to the catecholamine family together with epinephrine and norepinephrine. DA plays important roles in living organisms. It is synthesized and released by dopaminergic neurons of the central nervous system but also locally in different organs in the body. Dopamine is responsible for different body actions depending on a place of appearance:

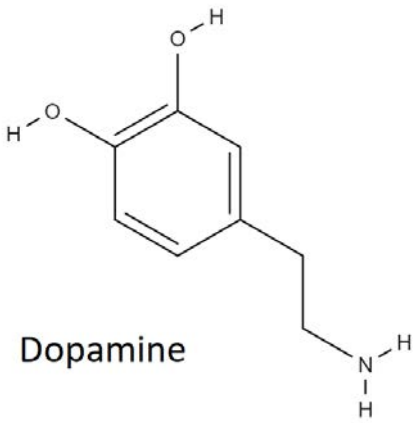

- in the extrapyramidal system it is responsible for movement, coordination and muscles tension
- in the limbic system dopamine plays a role in controlling emotional processes
- and in the hypothalamus, it controls the secretion of hormones.

Dopamine can be released in the brain, but also in the kidneys, where it increases sodium excretion; in the pancreas, where it reduces insulin production; in the immune system, where it controls the activity of lymphocytes. The dysfunction of the dopamine system is associated with multiple disorders and diseases, e.g. Alzheimer's disease; Parkinson's disease which is caused by a limited number of dopamine secreting neurons; Attention Deficit Hyperactivity Disorder (ADHD), increasingly diagnosed among children and teenagers over the last decades. Due to the increase of dopamine's impact on many different medical and scientific arenas, the possibility for determination of dopamine concentration in living organisms is indispensable.

Epinephrine

Epinephrine (EP), also commonly known as adrenaline, is a monoamine catecholamine synthesized in a step-by-step reaction in the tyrosine, L-dopa, Dopamine and Norepinephrine chain (see Figure 2.2.3). EP is responsible for different organism actions, such as known fight-or-flight reaction, and is connected with an increase of blood pressure, pupil dilatation response, blood sugar level. Release of epinephrine is often associated with fast and aggressive body reactions.

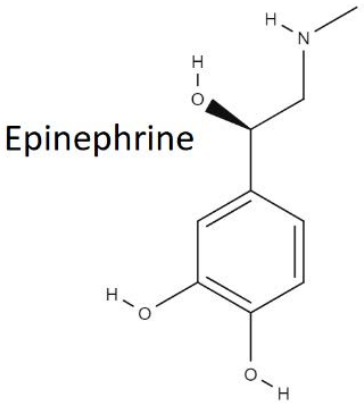

Serotonin

Serotonin (5-HT; 5-hydroxytryptamine) is a monoamine neurotransmitter, which is a derivative from tryptophan. 5-HT similarly to DA, interacts with other neurotransmitters but is mostly associated with physiological processes in the organism. Serotonin is produced mostly in the autonomic nervous system of the stomach and intestine where it controls the intestinal movement. The other source of serotonin is located in serotonergic neurons in the central nervous system, where it is responsible for numerous functions. 5-HT is linked to the regulation of sleep, appetite and mood, and some cognitive functions, learning and memory, or even wound healing. Serotonin levels in the brain are connected to the sexual needs of the organism and impulsive behavior. Abnormal concentrations of 5-HT can lead to aggressiveness and fatigue or increased sensitivity to pain. The serotonergic action is usually terminated by the reuptake of 5-HT from the synapse. The main mechanism of prevention from the serotonin loss from the synaptic cleft is application of the MAOIs inhibitors (monoamine oxidase inhibitors), which prevents the monoamine breakthrough and SSRI (selective serotonin reuptake inhibitors). Serotonin together with other neurotransmitters, controls several actions of the organism and in order to understand its function more research is needed.

Many mechanisms governing the nervous impulses transmission are not yet understood and thus require further investigation. In many cases the nervous impulses are governed by multiple

neurotransmitters and the combination of a number of different receptors can spark the organism reaction [5]. The study of the transmission of the nerve information is a very active topic of scientific investigation. There are methods based on the neuron cells imaging, where different aspects of the cell morphism can be determined. The other approach is based on measurement of the neurotransmitters concentration in the synaptic cleft, where probing fluid from brain tissue is necessary. However, for living patients some non-invasive method would be better. Such non-invasive techniques already exist; positron emission tomography (PET) or functional magnetic resonance (fMRI). Despite great possibilities of analysis with the usage of these methods the temporal, spatial and chemical resolution is limited, which makes them insufficient for detection of neurotransmitters around the cells that secrete neurotransmitters. The last approach is based on the measurement of the neurotransmitters concentration extracellularly. This analysis can be performed with variety of different methods. However, in many cases a big volume sample is necessary. Body fluids available in bigger volumes such as urine, blood, blood serum, saliva, have much lower concentration of neurotransmitters. The insufficient concentration results in no possible quantification of the neurotransmitters in those fluids. The other problem is caused by different content of the neurotransmitters in the inter-synaptic fluid and already metabolized or oxidized neurotransmitters in the body fluid. For that reason it would be best to determine the neurotransmitters concentration in the place of origin – the brain. That is the reason for multiple studies where the appropriate method for neurotransmitters detection can be created [9].

2.3 Chemical sensors and biosensors

In order to determine the concentration of certain compounds, such as neurotransmitters, some more information about typical sensors, their properties and recent trends in their creation must be mentioned more specifically. Chemical sensors are devices which collect chemical information and converts it into analytically useful signals [10]. Measured properties can be taken as an output from chemical reactions or the physicochemical properties of the measurement. The sensor is composed of two main elements; a receptor and a transducer. The receptor assures selectivity of the measurement whereas the transducer is capable of a transformation of the signal from the receptor to a form readable for the user. Selective sensors enable the detection of a single component of a mixed sample or the whole composition of the sample.

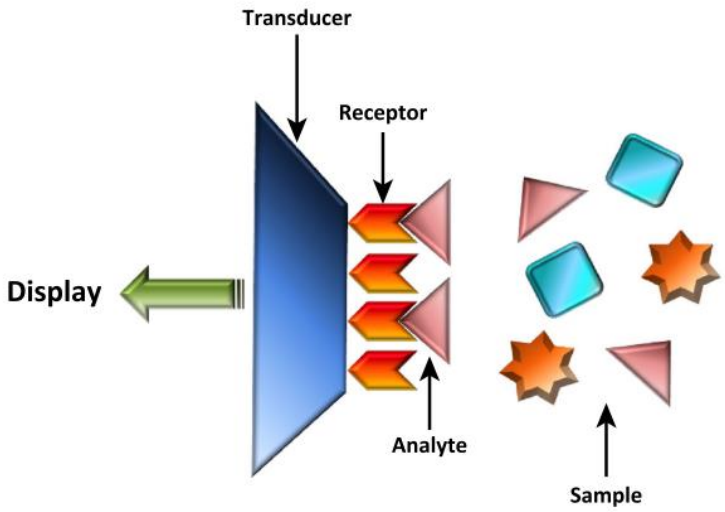

Figure 2.3.1.1 Schematic showing important parts of a typical sensor, adapted from [10].

Biosensors are a group of sensors, in which a biomolecule has been used as a part of receptor. In such cases receptor is composed of enzymes, antibodies, microorganisms or even DNA molecules. However, in some terminologies biosensors are also sensors which are used for detection of biomolecules.

For practical use of biosensors some important features have to be considered:

- lifetime
- sensor stability
- reproducibility of sensor readout [11].

Generally, sensors are divided into groups on the basis of the signal which is recorded and later transformed into an analytical information. Possibility of creation the non-invasive sensors has attracted attention of multiple scientific groups creating sensors. Some of the suggested solution for detection of a certain metabolites have been already implemented to the market. Most commonly known are glucose-meters from blood sample [12] or detection of different metabolites in urine [13], those can indicate serious health problems. The ease of use and common access to sensors can be useful for early self-diagnosis and help with starting proper treatment on time. Compatibility of the sensors with the human body or skin is especially important for the neonatal and elderly patients, in which cases blood sampling can be challenging. Continuous monitoring of some metabolites could alert the patients and prevent from common diseases such as stroke, infarct etc. Sensors that could perform continuous sensing allow to design implantable or wearable chemical sensors for detection of certain analytes inside the human body or excretion on the human skin. One of the suggested chemical sensors group are electrochemical sensors. They offer high sensitivity, ease of miniaturization and low cost solutions. One of the biggest

advantages of electrochemical sensors is possibility of creation of non-toxic and wearable devices [10].

2.3.1 Electrochemical sensing

Electrochemical detection methods can be based on coulometry, potentiometry or amperommetry. The only condition for the electrochemical methods, which has to be met is the sensitivity to the exact analyte. The electrochemical concepts stand out with a very good time resolution. The ubiquitous trend for miniaturization would not interfere with the electrochemical analysis thanks to the ease of creation smaller and smaller electrochemical devices. The electrochemical measurements are based on different approaches to measure one of the electrochemical properties of the analyte. Moreover sensors can be assembled into integrated systems with various designs with a number of different electrodes. There are known solutions called electrochemical tongues, which detect several components in fluid samples [14] or electrochemical noses, dedicated to the gaseous samples [15].

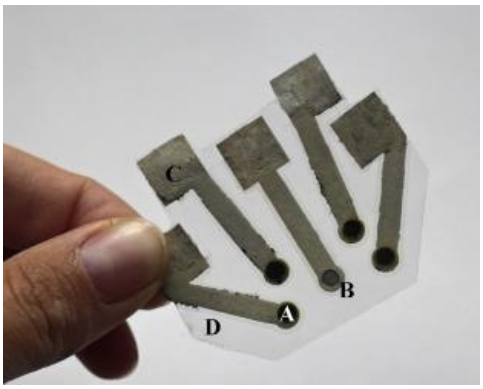

Figure 2.3.1.1 Electronic tongue with an integrated reference: A. working electrodes, B. Ag/AgCl reference electrode, C. electrical contacts, D. lamination foil. Adapted from [16]

Usage of such integrated systems provides a spatiotemporal imaging of a region of interest. In coulometric methods amount of electricity which was produced or consumed is measured over time, which allows to create sensors where coulometry and HPLC are combined [17].

There are known potentiometric methods for detection neurotransmitters. However, most measurements are based on registration of current in a cell, while their potential is altered actively. These techniques allow for the determination of a multiple components in the sample. The distinction is based on different oxidation / reduction potentials of the analytes. Even though amperommetric methods are highly valuable, they have some limitations such as coexistence of the electroactive molecules characterized by similar or the same redox potential in the same test sample. This phenomenon occurs when the same functional groups belonging to a different

molecules participate in the same redox reactions. In such case the experimenter observe the redox peaks in the same position in the voltammogram, which prevents from the differentiation between analyzed substances. Coexistence of peaks causes a lot of difficulties in order to distinguish between the components of the sample, but it is not entirely impossible. To ascribe the signal to a certain reaction in a given molecular composition various complementary techniques can be used. Often used are combination of electrochemical techniques with other analytical methods such as HPLC [18], where the screening of the electroactive substrate with electrode reaction is used, products are read by the liquid chromatography. The other sensing method can be a combination of many methods to lower the detection limit to a nanomolar range [19], where sample taken via microdialysis are measured with UPLC-MS/MS. An application of such combination allows for a minimization of the measured sample. Another often found solution is application of the internal addition method, which is useful for the detection of molecules which give signal slightly overlapping with signals from the other molecule. However, the most often used and most prominent method is application of working electrode surface modification. Several modifications of the electrode surface has been shown already [20]. Many of the modifications are taking advantage of the porosity and catalytic properties of nanomaterials [21]. One of the examples is an application of carbon nanohorn-modified carbon fiber microelectrodes used for dopamine detection (Fig. 2.3.1.2)

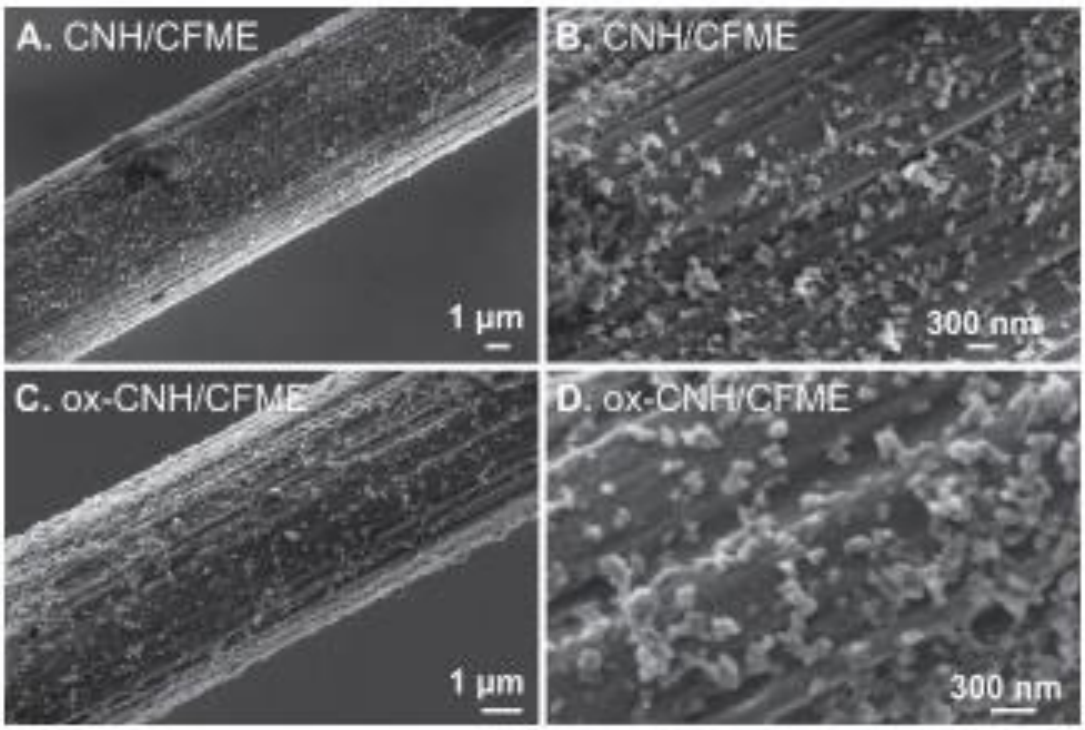

Figure 2.3.1.2 SEM images with the electrodeposited carbon nanohorn on the carbon fiber microelectrodes, used for detection of dopamine.[23]

Nanomaterials are known from their excellent properties for expanding the active electrode surface. Application of the certain nanomaterials allows for a separation of the peaks originated from different components of the sample. The other of the solution already implemented was the usage of graphene quantum dots based fluorescence sensor, which loses its fluorescence in presence of DA [24].

2.4 Electrochemical sensors for neurotransmitters detection

A growing interest in both early detection of diseases caused by abnormal neurotransmitters concentration and a desire for precise knowledge about the signaling pathways in the brain has resulted in a large number of new ideas in the neurotransmitters detection area.

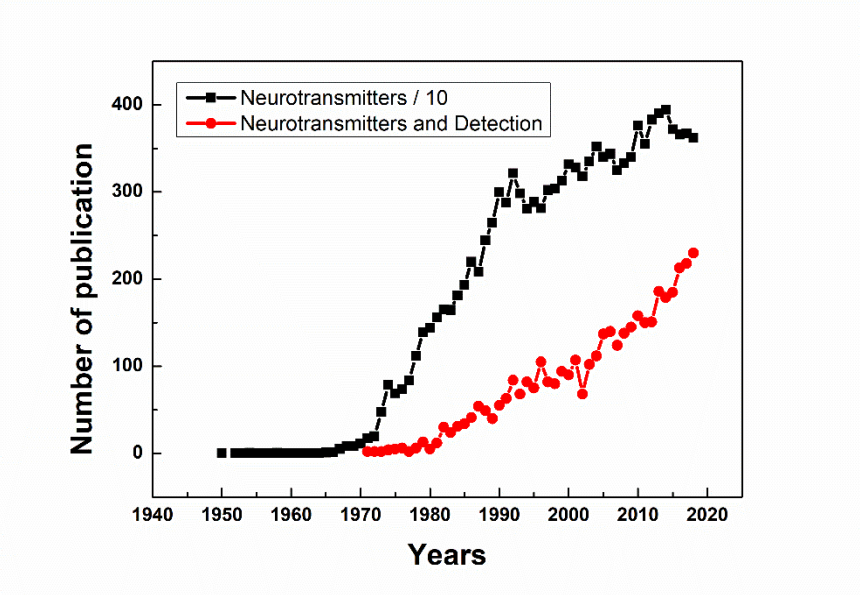

Figure 2.4.1 Growing number of publication containing words "neurotransmitter" and "neurotransmitters detection" as an Article title, Abstract or Keyword according to the Scopus.

The two challenging section of the useful detection has to be fulfilled, those are diagnostic purposes and understanding of signaling pathways. From patients treatment point of view, the detection of the neurotransmitter deficiency has to be detected early enough to start the treatment. In order to detect starting point of the disease the measurement could be performed near the synapses which release the neurotransmitters, where concentration of secreted neurotransmitters is high. Unfortunately such regions are hidden deep in the brain structures. The other approach is to detect either neurotransmitters or their metabolites in the body fluids. Their concentration is much lower than in the place of excretion. As a consequence very tiny fluctuations of concentration of neurotransmitters have to be measured in body fluids such as blood, serum, urine etc. The possibility of a simultaneous detection of multiple neurotransmitters is considered as a

second task in area of neurotransmitters detection. Neuronal co-release of neurotransmitters was already mentioned. In order to differentiate between different neurotransmitters, the perfect method should be able to register their local and global concentration. Sensors for neurotransmitters detection should be characterized by:

- possibility and specificity of detection of a certain compound,
- its limits of detection and quantification,
- repeatability of the measurement,
- linearity of response.

In terms of using the electrochemical method for detection and determination of neurotransmitter concentration the following three methods seems to be useful Direct Current (DC) amperommetry, Differential Pulse Voltammetry (DPV) and Fast Scan Cyclic Voltammetry (FSCV). DC amperommetry has been successfully applied for determination of dynamic changes of catecholamines concentration in brain slices [25] and monitoring of single vesicle dopamine release with nanoelectrodes [26]. Much more selective and sensitive technique is Differential Pulse Voltammetry, its usage allows for differencing between neurotransmitters composition in an analyzed sample. DPV served as an analytical tool for in vivo dopamine detection with usage boron-doped diamond microelectrodes [27]. Registered peak heights correspond to the determined analyte inside. The most frequently used technique for determination of neurotransmitters concentration in vivo measurement is Fast Scan Cyclic Voltammetry. In this measurement the voltage is cycled with rates higher than 100 V/s in triangular fashion. Using FSCV allows for determination of multiple components in vivo measurement [11]. Only electroactive compounds can be detected with amperometric sensors. Some neurotransmitters, especially the catecholamines (DA, EP, NEP) and 5-HT, contain a hydroxylic group bonded to a carbon ring. This group can be oxidised at a relatively small overpotential and measurement of the oxidation current serves as a basis for electrochemical detection of the neurotransmitters. The presence of the same hydroxylic group in many different neurotransmitters causes difficulties for exact distinction between them. However, chemical surrounding differs in different neurotransmitters. Differences in chemical surrounding can be captured with a proper electrode surface modification. An application of materials which specifically react with groups other than hydroxylic group in the neurotransmitter molecule assist in specific detection of neurotransmitters.

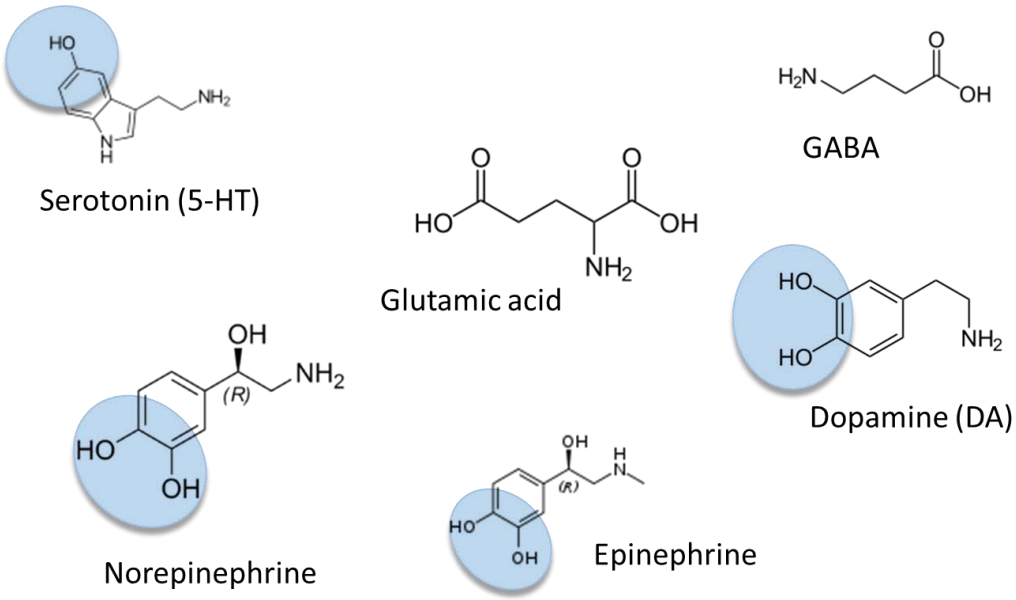

Figure 2.4.2 Schematic representation of different neurotransmitters with marked hydroxylic groups oxidized in direct electrochemical detection.

There are known other examples of neurotransmitters such as a Gamma-aminobutyric acid (GABA), which can be detected indirectly, with application of an additional modification e.g. the use of a liquid-liquid interface in the nanopipet with octanoic acid in one phase [28]. The other well-known example is an enzymatic detection of glutamate on electrodes modified with different supporting material and glutamate oxidase, which is a key recognition element[29].

Common interferents coexisting with neurotransmitters in body fluids have the same hydroxylic reacting group. Oxidation potential of the interferents is similar to the oxidation potential of the neurotransmitters of interest. Electrochemical detection methods offer a great advantage over the analytical methods, which is the low detection limit. Unfortunately, the specificity of those analysis is limited. In the modern analysis the main goal would be to detect the neurotransmitters in the sample without a pre-treatment. In such a sample many different interferents exist in different concentrations depending on the organism condition. The most disturbing are the interferents with the same oxidation potential as the catecholamines specific group, which are: Ascorbic Acid (AA), Uric Acid (UA) and Acetaminophen (AC). For the measurements in the presence of these interferents the specific electrode modifications can be applied in order to shift the oxidation potential of certain groups.

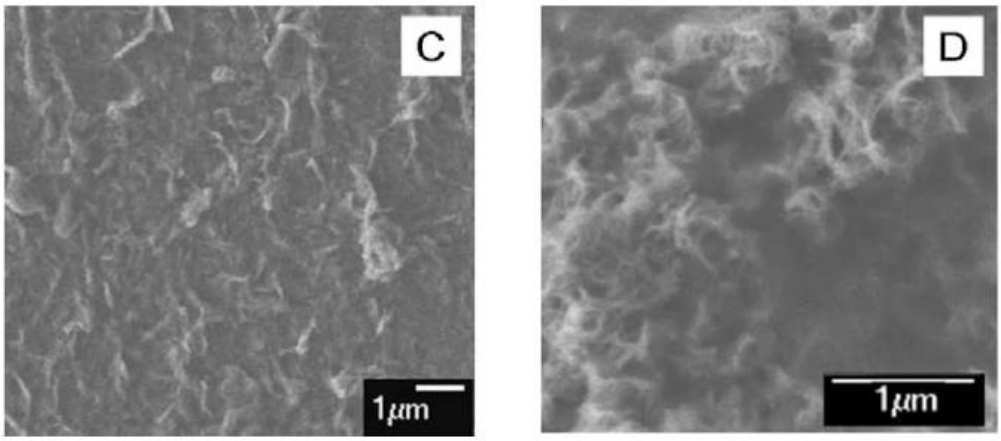

Figure 2.4.3 SEM images of graphene–CS (C) and MWNTs-CS (D) on the glassy carbon. Adapted from [30].

Neurotransmitters detection due to its difficulty can be classified into three types according to used methodologies. The separation of the signals from neurotransmitters and interferents is often done with using ionic liquids modification. The other approach can be made with modification of the surface of working electrode with enzymes (tirosinase, glucose oxides etc.) which catalases the neurotransmitters oxidation. However, the most popular among the electrochemists seems to be the electrode modification with graphene and semiconductors/metallic nanoparticles, which poses electrocatalytic properties [30]. In order to enlarge the signal from a single detection event some enzymatic modification are often applied [31]. One of the already reported enzymatic enhancements was the application of Glucose oxidase. It enlarged the neurotransmitters signal by 10 times. Another enzymatic based enhancement of neurotransmitters detection was the application of tirosinase-single walled carbon nanotubes-polypyrrole modification of the working electrode surface [32]. In this case authors managed to separate signals of dopamine and ascorbic acid in the same sample. Even though, the miniaturized detection issue seems to be difficult and complicated, some approaches to create a compact and portable electrochemical sensors are made. One of the reported examples is the integrated handheld system [33], or already created i-Stat portable analyzer [34] and Sandia's MicroChemLab biotoxin [35]. Nowadays reported method are mostly performed ex vivo. The best from therapeutic point of view would be to detect and measure exact concentration of secreted neurotransmitters, at a place of secretion. The closest to this idea is the measurement where the sample is taken via microdialysis [36]. In this experiment a cannula is inserted to a certain brain region and, within a few minutes fluid is probed and ready for further analysis.

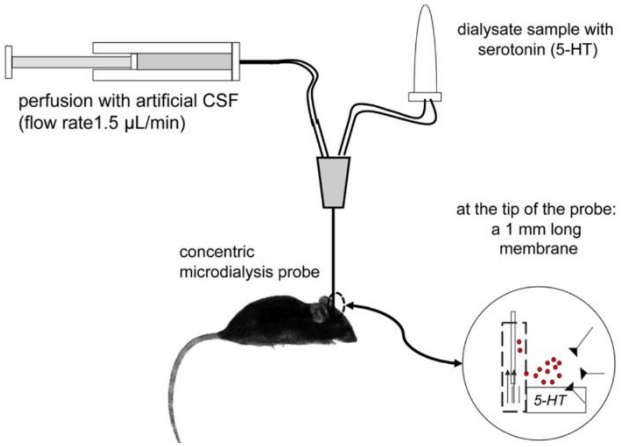

Figure 2.4.4 Principle of intracerebral microdialysis in awake, freely moving mice. Adapted from [36].

The temporal resolution is poor due to the longtime probing of the fluid. For some application the time needed to probe the brain tissue is too long for meaningful experiments, and the necessity of in-vivo measurement is considered. The very effective technique for detection of neurotransmitters are those based on FSCV with using microelectrodes inserted in a brain tissues. Microelectrodes are much smaller than cell bodies, for that reason they cause a minimal tissue damage. Such microelectrodes can be chronically fixed for long-term experiments. In case of dopamine detection the use of of microelectrodes improves signal-to noise ratio, response is much faster because of small capacitance of double layer charging, and i-R drop is much smaller than for macro electrodes. In Fast Scanning Cyclic Voltammetry the microelectrode can be inserted into the place of interest, and there can detect the secreted neurotransmitters. There are some approaches where microelectrodes are modified with nanostructures with combination of enzymes enhances the sensory properties. One of those examples is creation of microelectrodes decorated with gold nanoparticles, later modified with acetylcholinesterase and choline oxidase, which improved the sensing abilities toward acetylcholine [37]. However, even though microelectrodes were created to be inserted into the synapse, and measure directly excreted neurotransmitters, their sizes were too big to be fitted into the synaptic cleft (20 – 100 nm). Effectively, the acetylcholine concentration was measured in the extracellular space [38].

2.5 Future trends in electrochemical neurotransmitters detection

Nowadays used electrode for neurochemistry experiments are able to provide information about extrasynaptic concentration of neurotransmitters. It is possible to control position of an microelectrode array in order to obtain simultaneous information from multiple synapses.

However most of currently used microelectrodes are too large to fit into a synapse, where the concentration of neurotransmitters is much higher than in the extracellular space. Future trends should focus on minimization of the electrodes diameter to fit into the synapse, e.g. carbon fiber microelectrodes (CFMEs) or platinum nanoelectrodes. The second idea is to create the addressable nanoarrays for multinalyte and multisynapse monitoring, but also coupling electrochemical methods with other analytical methods for better understanding of chemical changes inside the synapse [38].

Bibliography

[1] O. Loewi, "Weiteres über Humorale Übertragbarkeit der Herznervenwirkung," *Klin. Wochenschr.*, vol. 3, no. 16, pp. 680–681, 1924.

[2] B. Y. R. Fischmeister and H. C. Hartzell, "Mechanism of Action of Acetylcholine on Calcium," *J. Physiol.*, vol. 376, pp. 183–202, 1986.

[3] A. N. McCoy and S. Y. on. Tan, "Otto Loewi (1873-1961): Dreamer and Nobel laureate," *Singapore Med. J.*, vol. 55, no. 1, pp. 3–4, 2014.

[4] "Part 2 of Loewi's experiment describing the existence of Vagusstoff." [Online]. Available: https://commons.wikimedia.org/w/index.php?curid=2385256. [Accessed: 13-May-2019].

[5] E. Polo and S. Kruss, "Nanosensors for neurotransmitters," *Anal. Bioanal. Chem.*, vol. 408, no. 11, pp. 2727–2741, 2015.

[6] S. Paudel, N. Sun, D. B. Khadka, G. Yoon, K. M. Kim, and S. H. Cheon, "Design, synthesis and docking study of 4-arylpiperazine carboxamides as monoamine neurotransmitters reuptake inhibitors," *Bioorganic Med. Chem.*, vol. 26, no. 14, pp. 4127–4135, 2018.

[7] C. E. John and S. R. Jones, "Chapter 4 Fast Scan Cyclic Voltammetry of Dopamine and Serotonin in Mouse Brain Slices Advantages of the Use of Mouse Brain Slices Methodology for Fast Scan Cyclic Voltammetry in Mouse Brain Slices," *Brain*, pp. 1–15, 2007.

[8] D. Dulcis, P. Jamashidi, S. Leutgeb, and N. C. Spitzer, "Neurotransmitter Switching in the Developing and Adult Brain Regulates Behavior," *Annu. Rev. Neurosci.*, vol. 340, pp. 449–453, 2013.

[9] E. S. Bucher and R. M. Wightman, "Electrochemical Analysis of Neurotransmitters," *Annu. Rev. Anal. Chem.*, vol. 8, no. 1, pp. 239–261, 2015.

[10] A. J. Bandodkar and J. Wang, "Non-invasive wearable electrochemical sensors: a review," *Trends Biotechnol.*, vol. 32, no. 7, pp. 363–371, 2014.

[11] K. Jackowska and P. Krysinski, "New trends in the electrochemical sensing of dopamine," *Anal. Bioanal. Chem.*, vol. 405, no. 11, pp. 3753–3771, 2013.

[12] V. Beni, D. Nilsson, P. Arven, P. Norberg, G. Gustafsson, and A. P. F. Turner, "Printed Electrochemical Instruments for Biosensors," *ECS J. Solid State Sci. Technol.*, vol. 4, no. 10, pp. S3001–S3005, 2015.

[13] I. Sarosiek, R. Schicho, P. Blandon, and M. Bashashati, “Urinary metabolites as noninvasive biomarkers of gastrointestinal diseases: A clinical review,” *World J. Gastrointest. Oncol.*, vol. 8, no. 5, p. 459, 2016.

[14] I. Marques, G. Magalhâes-Mota, F. Pires, S. Sério, P. A. Ribeiro, and M. Raposo, “Detection of traces of triclosan in water,” *Appl. Surf. Sci.*, vol. 421, pp. 142–147, 2017.

[15] M. Śliwińska, P. Wiśniewska, T. Dymerski, W. Wardencki, and J. Namieśnik, “Advances in Electronic Noses and Tongues for Food Authenticity Testing,” *Adv. Food Authent. Test.*, pp. 201–225, 2016.

[16] E. W. Nery and L. T. Kubota, “Integrated, paper-based potentiometric electronic tongue for the analysis of beer and wine,” *Anal. Chim. Acta*, vol. 918, pp. 60–68, 2016.

[17] B. A. Donzanti and B. K. Yamamoto, “An improved and rapid HPLC-EC method for the isocratic separation of amino acid neurotransmitters from brain tissue and microdialysis perfusates,” *Life Sci.*, vol. 43, no. 11, pp. 913–922, 1988.

[18] W. R. Matson, P. Langlais, L. Volicer, P. H. Gamache, E. Bird, and K. A. Mark, “n-Electrode three-dimensional liquid chromatography with electrochemical detection for determination of neurotransmitters,” *Clin. Chem.*, vol. 30, no. 9, pp. 1477–1488, 1984.

[19] T. Suominen *et al.*, “Determination of Serotonin and Dopamine Metabolites in Human Brain Microdialysis and Cerebrospinal Fluid Samples by UPLC-MS/MS: Discovery of Intact Glucuronide and Sulfate Conjugates,” *PLoS One*, vol. 8, no. 6, pp. 2–10, 2013.

[20] M. Sajid, M. K. Nazal, M. Mansha, A. Alsharaa, S. M. S. Jillani, and C. Basheer, *Chemically modified electrodes for electrochemical detection of dopamine in the presence of uric acid and ascorbic acid: A review*, vol. 76. Elsevier B.V., 2016.

[21] C. Yang, M. E. Denno, P. Pyakurel, and B. J. Venton, “Recent trends in carbon nanomaterial-based electrochemical sensors for biomolecules: A review,” *Anal. Chim. Acta*, vol. 887, pp. 17–37, 2015.

[22] B. Dembinska and P. J. Kulesza, “Electrochimica Acta Multi-walled carbon nanotube-supported tungsten oxide-containing multifunctional hybrid electrocatalytic system for oxygen reduction in acid medium,” vol. 54, pp. 4682–4687, 2009.

[23] P. Puthongkham, C. Yang, and B. J. Venton, “Carbon Nanohorn-modified Carbon Fiber Microelectrodes for Dopamine Detection,” *Electroanalysis*, vol. 30, no. 6, pp. 1073–1081, 2018.

[24] S. Baluta, J. Cabaj, and K. Malecha, “Neurotransmitters detection using a fluorescence-based sensor with graphene quantum dots,” *Opt. Appl.*, vol. Vol. 47, no. nr 2, 2017.

[25] B. J. Venton, K. P. Troyer, and R. M. Wightman, “Response times of carbon fiber microelectrodes to dynamic changes in catecholamine concentration,” *Anal. Chem.*, vol. 74, no. 3, pp. 539–546, 2002.

[26] W. Z. Wu *et al.*, “Monitoring dopamine release from single living vesicles with nanoelectrodes,” *J. Am. Chem. Soc.*, vol. 127, no. 25, pp. 8914–8915, 2005.

[27] A. Suzuki *et al.*, “Fabrication, characterization, and application of boron-doped diamond microelectrodes for in vivo dopamine detection,” *Anal. Chem.*, vol. 79, no. 22, pp. 8608–8615, 2007.

[28] N. T. Iwai, M. Kramaric, D. Crabbe, Y. Wei, R. Chen, and M. Shen, “GABA Detection with Nano-ITIES Pipet Electrode: A New Mechanism, Water/DCE-Octanoic Acid

Interface," *Anal. Chem.*, vol. 90, no. 5, pp. 3067–3072, 2018.

[29] G. Hughes, R. M. Pemberton, P. R. Fielden, and J. P. Hart, "The design, development and application of electrochemical glutamate biosensors," *TrAC - Trends Anal. Chem.*, vol. 79, pp. 106–113, 2016.

[30] Y. Wang, Y. Li, L. Tang, J. Lu, and J. Li, "Application of graphene-modified electrode for selective detection of dopamine," *Electrochem. commun.*, vol. 11, no. 4, pp. 889–892, 2009.

[31] M. A. Schwarz, "Enzyme-catalyzed amperometric oxidation of neurotransmitters in chip-capillary electrophoresis," *Electrophoresis*, vol. 25, no. 12, pp. 1916–1922, 2004.

[32] K. Min and Y. J. Yoo, "Amperometric detection of dopamine based on tyrosinase-SWNTs-Ppy composite electrode," *Talanta*, vol. 80, no. 2, pp. 1007–1011, 2009.

[33] S. Kwakye and A. Baeumner, "An embedded system for portable electrochemical detection," *Sensors Actuators, B Chem.*, vol. 123, no. 1, pp. 336–343, 2007.

[34] C. Papadea *et al.*, "Evaluation of the i-STAT Portable Clinical Analyzer for point-of-care blood testing in the intensive care units of a University Children's Hospital," *Ann. Clin. Lab. Sci.*, vol. 32, no. 3, pp. 231–243, 2002.

[35] J. A. Fruetel *et al.*, "Microchip separations of protein biotoxins using an integrated hand-held device," *Electrophoresis*, vol. 26, no. 6, pp. 1144–1154, 2005.

[36] A. M. Gardier, "Antidepressant activity: Contribution of brain microdialysis in knock-out mice to the understanding of BDNF/5-HT transporter/5-HT autoreceptor interactions," *Front. Pharmacol.*, vol. 4 AUG, no. August, pp. 1–12, 2013.

[37] J. D. Keighron, J. Wigström, M. E. Kurczy, J. Bergman, Y. Wang, and A. S. Cans, "Amperometric detection of single vesicle acetylcholine release events from an artificial cell," *ACS Chem. Neurosci.*, vol. 6, no. 1, pp. 181–188, 2015.

[38] M. Shin, Y. Wang, J. R. Borgus, and B. J. Venton, "Electrochemistry at the Synapse," *Annu. Rev. Anal. Chem.*, vol. 12, no. 1, pp. 1–25, 2019.

Chapter 3.

Computer simulations in electrochemistry

3.1 Introduction

In electrochemistry the interplay between experiment and theory is significant [1]. The electrochemical processes can be seen as a superposition of two separate events. The first is the electrode reaction, where an electron from the molecule is exchanged with the electrode surface, and the second the way which the molecule takes to reach the electrode surface.

3.1.1 Electrode reaction

The rate at which an electron can be transported from electron donor to the electron acceptor is theoretically described by Marcus theory. Marcus theory is appropriate for a one outer-sphere electron transfer reaction, where the chemical species exchange the electron but do not undergo large structural changes [2]. The theory was later extended to inner-sphere electron transfer to consider both solvation and coordination shells of chemicals exchanging the electron. The classical Marcus theory treats the electron transfer with the quantum mechanical understanding of the charge exchange. It leads to calculation of the Gibbs free energy of activation for reactants and products which is needed for a redox reaction to start. According to the Marcus theory the temperature dependency in reaction rate formula allows for determination of the activation energy.

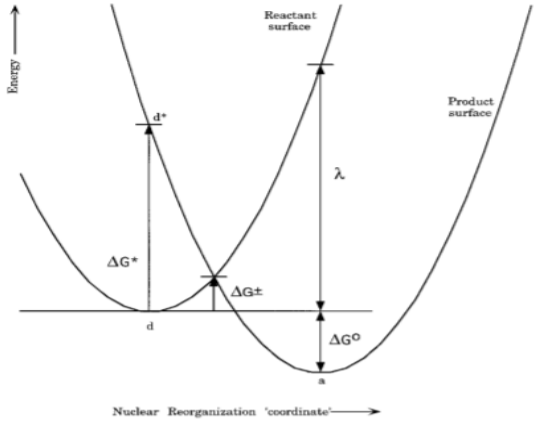

Figure 3.1.1.1 Marcus diagram for electron transfer. Adapted from [3].

The Marcus diagram (see Figure 3.1.1.1) represents the energy of both reactant and product as a function of the nuclear reorganization coordinate. In the diagram λ is the reorganization energy, which is the energy needed for the molecules in the solvation shells around the electrochemically active species to rearrange themselves to "make space" for the newly created species. Reorganization energy needs to be provided for electron transfer to occur. Marcus theory is believed to be the most appropriate theoretical calculation of the electron transfer reaction. It is widely appreciated by chemists and biologists, as a tool for better understanding of the electron transfer phenomenon in a wide range of problems, e.g. classical electrochemistry, corrosion, photosynthesis, chemiluminescence etc. Application of Marcus theory enables comparison of the electron transfer rates in different systems. However, the computational results obtained with application of Marcus theory are not satisfactory for nowadays experimentalists, because it delivers only theoretical value of reorganization energy, based on probabilistic calculations.

Instead of using the fully theoretical treatment of electrochemical problems, which is too difficult to carry out to obtain useful parameters for experimentalists, phenomenological methods were introduced. In order to solve the standard electron transfer problems between the chemical species and the electrode surface the Butler-Volmer equation (Eq. 3.1.4) was proposed. Let's consider the Butler-Volmer equation in case of the one electron transfer reaction presented in (Eq. 3.1.1),

$$O + ne^{-} \rightleftarrows R \qquad \text{(Eq. 3.1.1)}$$

as a simplified equation for oxidation-reduction reaction in contact with electrode surface, where: O is oxidized species, and R is reduced species. The Butler-Volmer equation for a kinetic rate constants are given by equations for forward and backward fluxes,

$$k_f = k_0 \exp[-\frac{\alpha_f nF\left(E-E^{\phi'}\right)}{RT}] , \qquad \text{(Eq. 3.1.1.2)}$$

$$k_b = k_0 \exp[\frac{\alpha_b nF\left(E-E^{\phi'}\right)}{RT}] , \qquad \text{(Eq. 3.1.1.3)}$$

where: k_f and k_b are respectively forward and backward kinetic rates, k_0 is a standard kinetic rate constant, α is a charge transfer coefficient, n is a number of electrons, F is the Faraday constant, E is the electrode potential, $E^{\phi'}$ is the equilibrium potential, R is the universal gas constant and T is the absolute temperature. The Butler-Volmer equation takes the form:

$$i = FAk_0[C_0 exp^{-\alpha_f\left(E-E^{\phi'}\right)} - C_R exp^{(1-\alpha_f)\left(E-E^{\phi'}\right)}] , \qquad \text{(Eq. 3.1.1.4)}$$

where C_0 and C_R are concentrations at the electrode surface of the oxidized and reduced species respectively. Due to the exponential function, Butler-Volmer equation can be used only for very slow reaction rates. For fast reactions, the flux of oxidized and reduced species on the electrode surface is a difference between forward and backward reaction rates multiplied with concentration of species, which are involved in the reaction:

$$\phi = k_f[C_R] - k_b[C_O], \qquad \text{(Eq. 3.1.1.5)}$$

The current is given by:

$$i = \phi\, nFA \qquad \text{(Eq. 3.1.1.6)}$$

In general, finding the C_o and C_R for a specific system are the most challenging tasks. In cases where the overpotential is large, the current in the reaction is growing exponentially with the electrode polarization, and the current is given by Tafel equation (Eq. 3.1.7):

$$i = i_0 \frac{nF}{RT} \Delta V, \qquad \text{(Eq. 3.1.1.7)}$$

where: ΔV is overpotential, i is a measured current density, and i_0 is a current density exchanged on the electrode. The phenomenological description of the electron transfer phenomena can be presented with other equations, which consider the influence of diffusion of the substrates to the electrode surface, such as the Cottrell equation - typical for chronoamperommetric measurements, Randles-Sevcik equation – describing the peak current of results from cyclic voltammetry measurement, and those are described in the next chapter. However, application of the Butler-Volmer equation is believed to be the most faithful description of electron transfer process between electroactive species and the electrode surface.

3.1.2 Mass transfer calculation

The reasoning presented above explains how the electron transfer takes place, but still there is a question of how species are travelling to the electrode surface. It was shown in the first chapter

of this thesis with the Fick's law, that the mass transport (transport of the electrochemical species) can be done on the way of diffusion, migration or convection. In the simplest case, when the experiment is performed in stationary conditions (no convection) and the migration is eliminated with application of an electrolyte solution of sufficient ionic strength, mass transport is ruled by diffusion only. Those problems, where mass transfer is limited only to diffusion can be solved analytically. One of the most often used software which is able to compute the simple 1dimensional (1D) with various electrochemical reactions is DigiSim, which applications are described in more details in the next subchapter. However, a wealth of new hydrodynamic measurement methods, where different and complex convection phenomena governs the mass transport, need some more detailed analysis in order to understand and predict the electrochemical output of the experiment. The more detailed analysis should take into account the way of mass transport. In order to describe the mass transport where both diffusion and convection occur, the Navier-Stokes equations are used. Navier-Stokes equations is a set of equations which describes the conservation of momentum for fluid in motion. They are useful in many scientific and engineering fields. They can be used for modeling the weather, water flow in a pipe or air flow around the aircraft wings. According to the Navier-Stokes equations the changes in momentum of the fluid depend only on the mass forces, external pressure and viscous forces in the fluid. Navier-Stokes equations can be solved analytically only for simple problems, such as for low Reynolds number – non turbulent flow. Some more complicated systems can be solved numerically. However, there is a class of problems which is considered as unsolvable with application of Navier-Stokes equations[3].

Mass transfer equation either from Fick's law or from the Navier-Stokes equations defines the Partial Differential Equations (PDEs) which can solve the mass flux in the system. Application of the Butler-Volmer equation as boundary conditions for the PDEs allows for a complete description of the electron transfer process in the system.

3.2 The need for calculations

Theoretical models for electrochemical experiments support a number of applications of the electrochemistry in both science and real-life problems. A number of different parameters, such as: a small change in the system structure, electrode material, differences in the flow rate affect the results in electrochemical experiments. The flow experiments are susceptible to turbulences, which often result in significant changes in the obtained experimental results. All of the above

[3] In 2000 the Clay Mathematics Institute announced seven millennium mathematical problems, one of them is to find Solution of Navier-Stokes equation for complicated systems or to give a counter-example.

mentioned factors can be taken into consideration simultaneously while performing the computer simulation. This method saves the time needed for systematic tests. In 1964 McLeod suggested usage of the mathematical simulation for description of the cardiovascular system. In his publication one can find an inspiring work, where such complicated biological system as a heart was the subject of mathematical description [4]. Even though there is a great number of parameters which have to be taken into consideration, the author combines the performed studies and encourages to further investigation. One of the examples, where the application of computational model is the most prominent seems to be the commercial use of a given hydrodynamic system [5]. Shevkunov et al show the importance of the simulation for manufacturing of a big scale replica of the hitherto used and optimized micro-scale systems.

3.3 Software for electrochemical simulations

Historically, self-coded programs were used for the first trials of predictions of the electrochemical systems behavior [7]. Later DigiSim (1 D) was introduced for the simple 1 dimensional problems, where cyclic voltammetry for various mechanistic types (EC, ECE, CE, etc.) can be solved [8]. Utilization of the DigiSim is divided into four basic stages, such as:

- Selection of experimental data files which will be fitted
- Entering of the mechanism of reaction
- Entering of estimated values of the chemical and electrochemical parameters and selection of those which are to be fitted
- Running of the DigiSim fitting

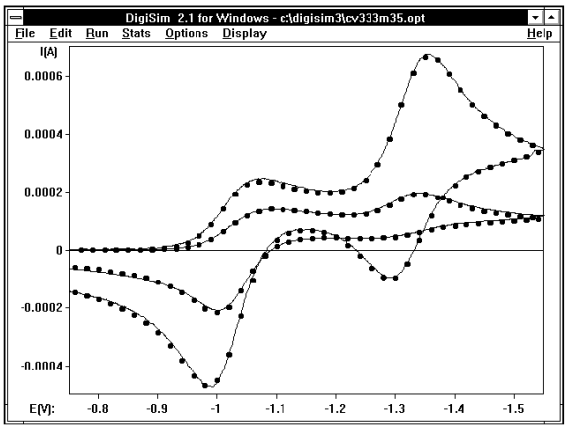

Figure 3.3.1 Comparison of experimental (lines) and simulated (circles) data for a nickel(II) complex in the presence of bipyridine at scan rates of 40 and 333 V/s. Adapted from [9].

The simplicity of the interface contributed to the popularity of the DigiSim software. DigiSim is considered as a very helpful tool among electrochemists, capable of solving and fitting simple electrochemical reactions governed by diffusion only. However, more complex and hydrodynamic measurements had to be self-coded. Over the last decades new software capable of solving the complicated Multiphysics problems has been presented, such as COMSOL Multiphysics or ANSYS FLUENT. In [10] authors show the importance of a calculation of the velocity inside a channel Fig. 3.3.2, for the leakage in an oil pipelines. The presented manuscript show a range of problems like the location of leakage, flow rates and pressure which affect the flow inside a channel.

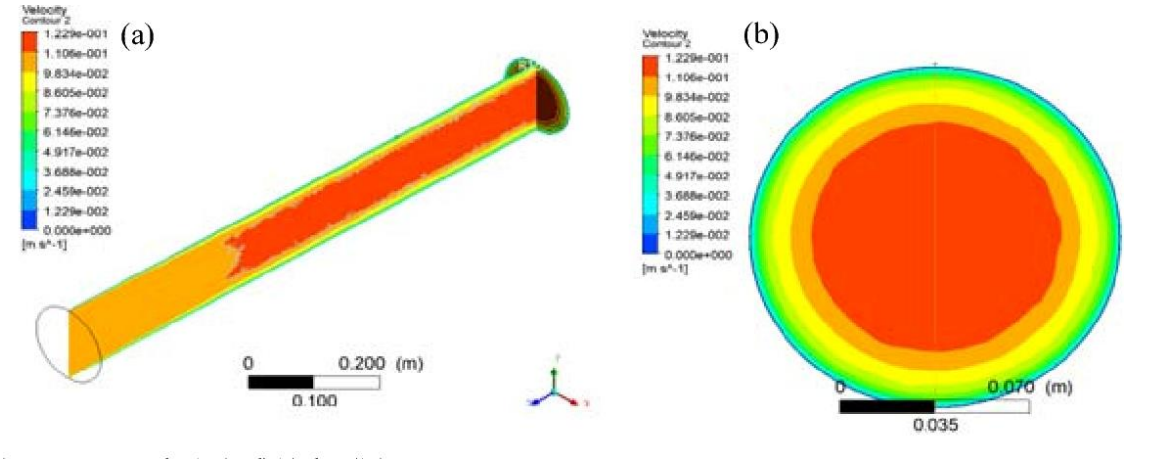

Figure 3.3.2 Pattern of velocity field calculated with ANSYS FLUENT. Adapted from [10]

In both COMSOL Multiphysics and in ANSYS FLUENT the considered issues are expressed as partial differential equations (PDEs) to be solved computationally.

3.4 Calculation with COMSOL Multiphysics

Results obtained with the use of COMSOL Multiphysics are described in the experimental part of this thesis. Thus I decided to write more about how the computations for electrochemical purposes are performed in practice, focusing on this particular program.

COMSOL Multiphysics is a modeling software capable of multiphysics simulation through utilization of the Finite Element Method (FEM). FEM provides a formalism for approximate solutions of partial differential equations (PDEs). Problem solving is based on the subdivision of the large system into many simpler, smaller parts called finite elements. The typical areas of FEM applications are: mass and heat transfer, fluid flow and structural analysis [11]. The solution to those problems is based on the solution to the boundary value problems for PDEs. COMSOL Multiphysics solves the differential equations with the set of constrains, called boundary

conditions. Application of systems which use the Finite Element algorithm gives a major advantage of ability to realize complex models [12]. Using COMSOL Multiphysics, electrical, structural and acoustics, fluidic, heat transfer, chemical and other problems can be treated. Its unique property is the possibility of combinations of multiple physical phenomena where equations can be solved simultaneously. For example an ohmic heater where the temperature affects the resistance, which in turn affects the current and the heating, or separately, as in the case of the electrochemical flow calculations presented below in the figure 3.4.1.

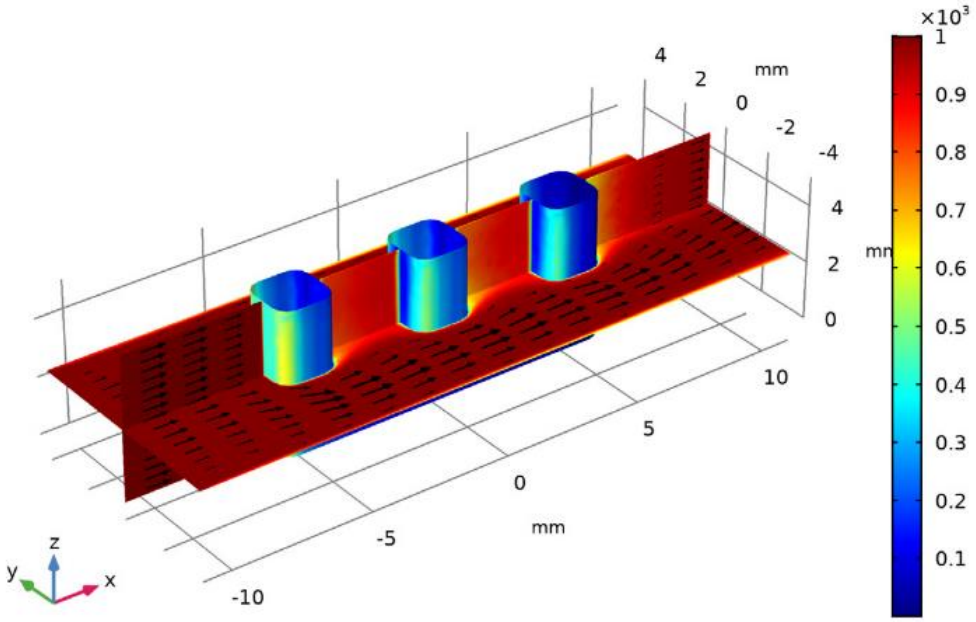

Figure 3.4.1 Flow field (top: slice plot, right: arrows) and concentration profile (bottom: slices and anode surface) at a certain potential. Adapted from the Model Library, COMSOL Multiphysics 5. [13]

3.4.1 COMSOL Multiphysics models and applications

Simulation with COMSOL Multiphysics gives the possibility to work in 1D, 2D and 3-dimensional configurations. There is also the possibility to transform the solution from smaller to bigger number of dimensions, however it is not trivial. All computations with COMSOL Multiphysics are based on the same actions:

- Creation or downloading of the geometry of the problem
- Choosing the parameters
- Defining the study which is supposed to be used in a given problem solution
- Defining the variables and functions which govern the whole reaction
- Creating a mesh, which allows to obtain accurate results in the section of interest

- Choosing the internal solver, which leads the whole computation.

Computational support often addresses a range of physical phenomena. Utilization of COMSOL Multiphysics has been proven in a large number of scientific publications [14]–[18], and since powerful computers, which are demanded for complicated calculations, are more and more common, the number of people performing simulations using COMSOL Multiphysics is still growing. The published articles concern the chemistry of the system with combination of some useful features, e.g. chemistry of phenol in presence of enzyme horseradish peroxidase with detailed analysis of battery cell, its design improvement, charging, discharging optimization. However, some engineering problems such as the operational life-time of batteries [17], deformation in corrosion systems [16] are also solved with application COMSOL Multiphysics. In 2015 R. Plascencia-Jatomea et al. presented work with the combination of simulation of the geometry, hydrodynamic properties such as velocity field and mass transport properties for membrane-aerated biofilm reactor [15] (Fig. 3.4.1.1.)

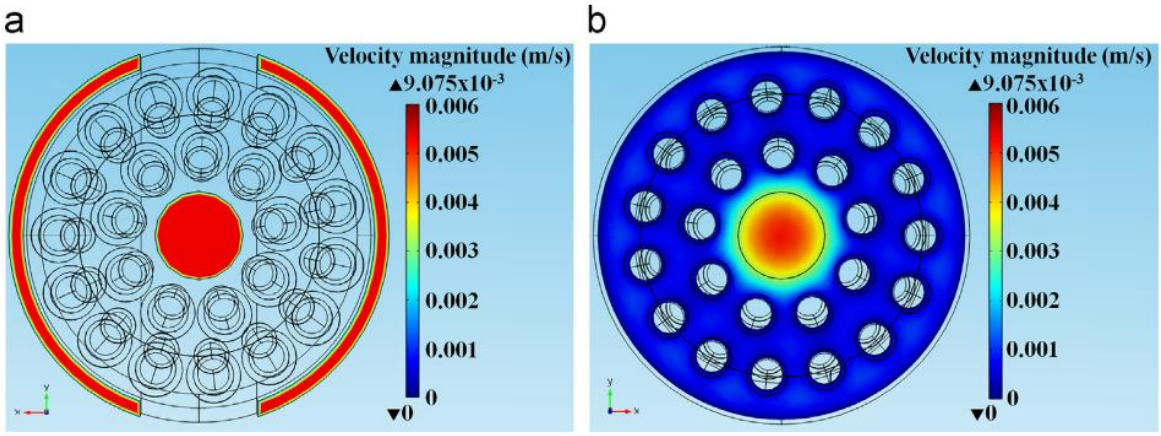

Figure 3.4.1.1 Velocity field in m/s in cross-section at the inlet (a) and outlet (b) of the membrane aerated biofilm reactor. Adapted from [15].

Moreover, the work have been supported by a thorough particle tracing analysis, which showed the great power of the COMSOL Multiphysics software.

3.4.2 COMSOL Multiphysics for electrochemical purposes

Electrochemical processes are coupling the current and charge conservation in electrodes and electrolyte, but also conservation of the mass of solute species. For the purpose of electrochemical calculations, the description of the mass and charge transport properties in the infinitely diluted electrolyte solution is given by the Nernst-Planck-Poisson equations, which extend Fick's law for the cases where not only diffusion, but also electrostatic forces between particles and fluid are considered. The particular electrode reaction and adsorption of the chemical species at the

electrode surfaces can be treated as boundary conditions. Due to the high complexity of the non-linear and multiple length- and timescales represented by the Nernst-Planck-Poisson equations, they are often approximated by the assumption of the electroneutrality. In the presence of supporting electrolyte, it is assumed that migration doesn't occur and mass transfer is only governed by diffusion and convection [19]. A literature review over the last years suggests that COMSOL Multiphysics used in analytical electrochemistry involves solutions of complex or non-standard geometries, hydrodynamic electrochemistry and complex or multiple reaction chemistry, difficult for standard methods [19]. COMSOL Multiphysics is helpful for predicting of electrochemical reactions outputs but also for a preparation of a proper design, such as an electrode arrays, meshing, and kinetic parameters [1]. Undeniable advantages of the FEMs utilized in COMSOL Multiphysics are adaptive algorithms for increasing granularity, highly useful for the reduction of the simulation time. Its advantages are possibility of usage user-specified meshing tolerance with unknown parameters which leads to saving both the computational time and memory [20].

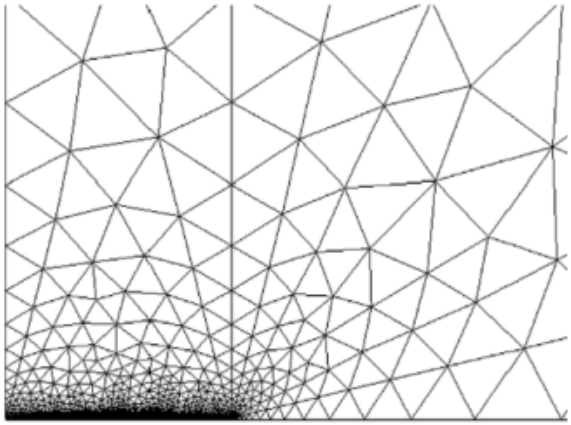

Figure 3.4.2.1 *2 Dimensional optimized mesh for the electrode surface Adapted from [1].*

The application of COMSOL Multiphysics to the optimization of the experiments parameters was shown by Kuss et.al. Authors studied the hydrodynamic effects caused by the SECM (scanning electrochemical microscopy) displacement [21] and proved that the velocity of the tip changes the electrochemical signal. In their research authors implemented COMSOL Multiphysics to the verification of the best conductive substrate geometry.

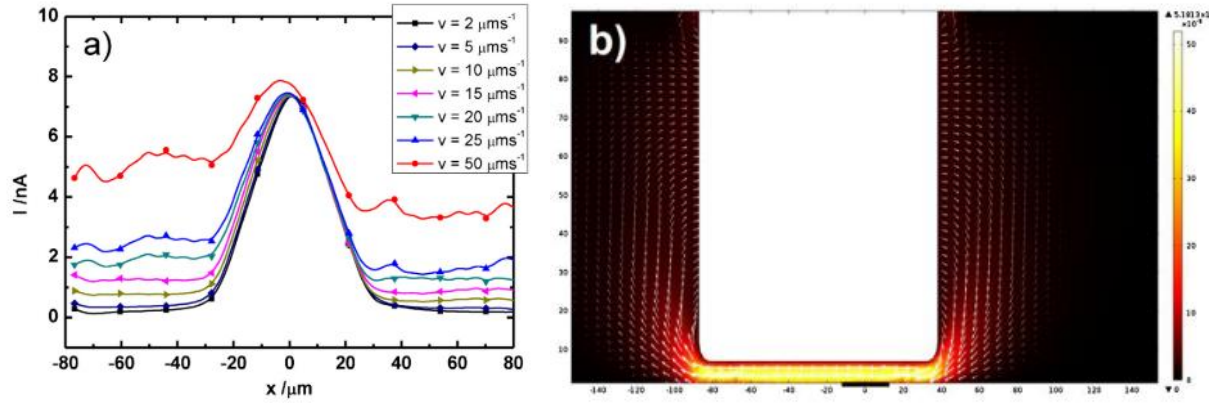

Fig 3.4.2.3 Tip current profile simulation results (a) and velocity magnitude m/s and velocity field, when the tip was scanned over a flat conductive substrate, scanning velocity 25 µm/s. Adapted from [21].

Our group have shown the possibility of the utilization of COMSOL Multiphysics for calculation of the electrochemical behavior during complicated enzymatically catalyzed electron transfer reactions (Fig. 3.4.2.2).

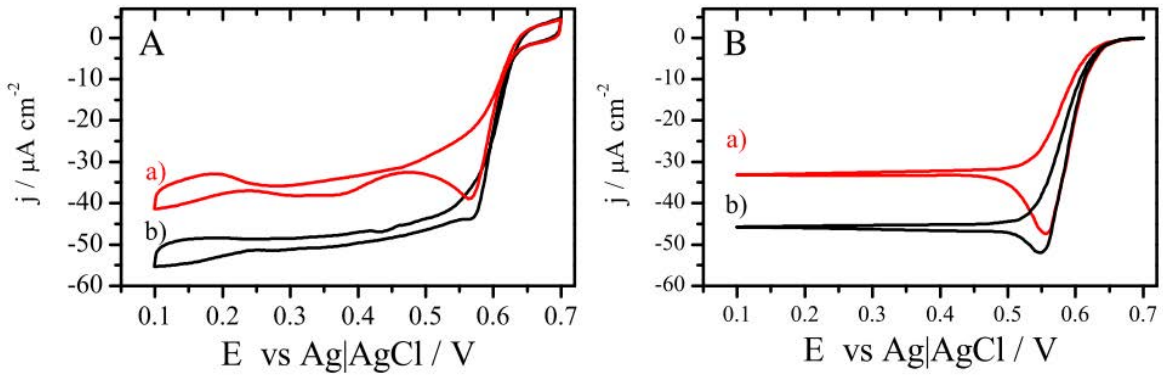

Figure 3.4.2.2 *(A) experimental and (B) calculated cyclic voltammetry curves of oxygen reduction at Bilirubin Oxidase, red curve are under nominally quiescent conditions and black curves are with a gas flow of 50 sccm over the cell surface. Adapted from* [22]

COMSOL Multiphysics has been applied to the investigation of dopamine chemical kinetics with the respect to the motion, while probing the brain structure with usage of the microelectrode inserted into a brain structures with FSCV. Various mechanical frequencies and bonding parameters could be introduced as parameter values to the COMSOL model. As a result authors have shown that the alteration of the probing changes significantly the chemical kinetics, and influences the experimental results. Thus, the micro motion of the brain structures have to be taken into consideration when creating the analytical method [23].

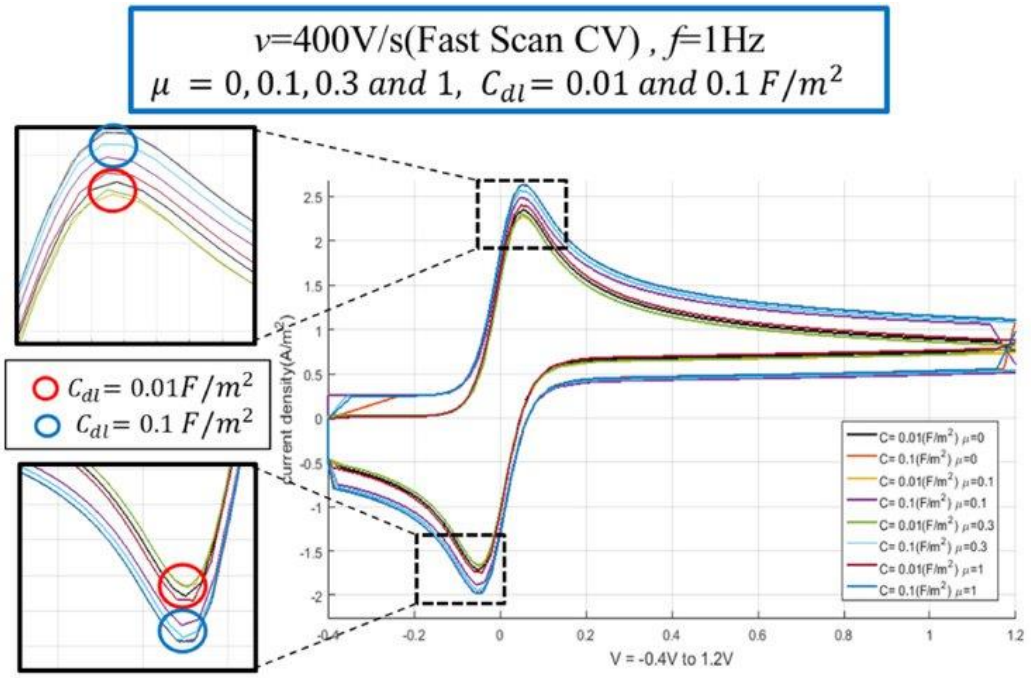

Figure 3.4.1.4 Dopamine redox reaction simulation by fast scanning cyclic voltammetry under given mechanical frequency, as a function of capacitance *Adapted from* [23].

3.5 Drawbacks of computations

Despite undeniable advantages of usage of the computer simulation for different purposes, there are some drawbacks of the method too. The results from the computation are highly dependent on the used parameters, and used parameters are often introduced manually. For that reason the computations are sensitive to the manual error. The researcher has to pay attention to the input data, to avoid false results and unnecessary errors, such as negative concentration, length, time etc. [8], [19].

Bibliography

[1] I. J. Cutress, E. J. F. Dickinson, and R. G. Compton, "Analysis of commercial general engineering finite element software in electrochemical simulations," *J. Electroanal. Chem.*, vol. 638, no. 1, pp. 76–83, 2010.

[2] R. A. Marcus, "On the theory of oxidation-reduction reactions involving electron transfer. I," *J. Chem. Phys.*, vol. 24, no. 5, pp. 966–978, 1956.

[3] K. A. Sharp, "Calculation of electron transfer reorganization energies using the finite difference Poisson-Boltzmann model," *Biophys. J.*, vol. 74, no. 3, pp. 1241–1250, 1998.

[4] J. McLeod, "Computer Simulation of the Hydrodynamics of the Cardiovascular System," *Simulation*, vol. 2, no. 3, pp. 33–41, 1964.

[5] S. V. Shevkunov, “Computer simulation of dissociative equilibrium in aqueous NaCl electrolyte with account for polarization and ion recharging. Ionization mechanism,” *Russ. J. Electrochem.*, vol. 49, no. 3, pp. 238–251, 2013.

[6] D. Mourtzis, N. Papakostas, D. Mavrikios, S. Makris, and K. Alexopoulos, “The role of simulation in digital manufacturing: Applications and outlook,” *Int. J. Comput. Integr. Manuf.*, vol. 28, no. 1, pp. 3–24, 2015.

[7] J. Britz, Dieter, Strutwolf, *Digital Simulation in Electrochemistry*, 4th ed. Springer International Publishing, 2016.

[8] M. Rudolph, “Digital simulations with the fast implicit finite difference (FIFD) algorithm. Part II. An improved treatment of electrochemical mechanisms with second-order reactions,” *J. Electroanal. Chem.*, vol. 338, no. 1–2, pp. 85–98, 1992.

[9] E. G. Jäger and M. Rudolph, “Cyclic voltammetric and impedance spectrometric investigations on addition/elimination reactions of Lewis bases accompanying the electrode reactions of a nickel chelate complex with a structural resemblance to the coenzyme F430,” *J. Electroanal. Chem.*, vol. 434, no. 1–2, pp. 1–18, 1997.

[10] C. A. De Sousa and O. J. Romero, “Influence of oil leakage in the pressure and flow rate behaviors in pipeline,” *Lat. Am. J. Energy Res.*, vol. 4, no. 1, p. 17, 2017.

[11] T. Nann and J. Heinze, “Simulation in electrochemistry using the finite element method Part 1. The algorithm,” *Electrochem. commun.*, vol. 1, pp. 289–294, 1999.

[12] T. Nann and J. Heinze, “Simulation in electrochemistry using the finite element method part 2: scanning electrochemical microscopy,” *Electrochim. Acta*, vol. 48, no. 27, pp. 3975–3980, 2003.

[13] C. Multiphysics, “Wire Electrode Library COMSOL Multiphysics,” pp. 1–32, 2019.

[14] A. Kaffash, K. Rostami, and H. R. Zare, “Modeling of an electrochemical nanobiosensor in COMSOL Multiphysics to determine phenol in the presence of horseradish peroxidase enzyme,” *Enzyme Microb. Technol.*, vol. 121, no. November 2018, pp. 23–28, 2019.

[15] R. Plascencia-Jatomea, F. J. Almazán-Ruiz, J. Gómez, E. P. Rivero, O. Monroy, and I. González, “Hydrodynamic study of a novel membrane aerated biofilm reactor (MABR): Tracer experiments and CFD simulation,” *Chem. Eng. Sci.*, vol. 138, pp. 324–332, 2015.

[16] D. Boukhlef, D. Boughrara, and H. Mohellebi, “Simulation of Border Deformation in Corrosion System by Coupling Analytical Solution and Finite Element Method,” vol. 5, pp. 267–277, 2018.

[17] M. Sarshar, M. Zarei-jelyani, I. Space, M. Babaiee, and I. Space, “Application of semi empirical and multiphysics models in simulating lithium ion battery operation,” *10thInternational Chem. Eng. Congr. &Exhibition*, no. May, 2018.

[18] T. J. Stockmann, L. Angelé, V. Brasiliense, C. Combellas, and F. Kanoufi, “Platinum Nanoparticle Impacts at a Liquid|Liquid Interface,” *Angew. Chemie - Int. Ed.*, vol. 56, no. 43, pp. 13493–13497, 2017.

[19] E. J. F. Dickinson, H. Ekström, and E. Fontes, “COMSOL Multiphysics®: Finite element software for electrochemical analysis. A mini-review,” *Electrochem. commun.*, vol. 40, pp. 71–74, 2014.

[20] D. J. Gavaghan, K. Gillow, and E. Süli, “Adaptive finite element methods in electrochemistry,” *Langmuir*, vol. 22, no. 25, pp. 10666–10682, 2006.

[21] S. Kuss, C. Kuss, D. Trinh, S. B. Schougaard, and J. Mauzeroll, “Forced convection during scanning electrochemical microscopy imaging over living cells: Effect of topographies and kinetics on the microelectrode current,” *Electrochim. Acta*, vol. 110, pp. 42–48, 2013.

[22] J. Urban, A. Zloczewska, W. Stryczniewicz, and M. Jönsson-niedziolka, “Electrochemistry Communications Enzymatic oxygen reduction under quiescent conditions — the importance of convection,” *Electrochem. commun.*, vol. 34, pp. 94–97, 2013.

[23] S. Han, M. Polanco, H. Yoon, and S. Bawab, “Simulation of Neurotransmitter Sensing by Cyclic Voltammetry under Mechanical Motion of a Neural Electrode,” pp. 6–12, 2017.

Chapter 4.
Methods

4.1 Introduction

The object of our study, rotating droplet system, was tested with usage of several methods to determine its properties and powers. The majority of work have been done with the use of electrochemical measurements. Optimization of the system was performed mainly with cyclic voltammetry. Determination of the materials used for electrode modification for detection purposes such as detection of redox probes and neurotransmitters, was obtained with chronoamperometry, square wave voltammetry, scanning electron microscopy. Flow pattern was determined with particle image velocimetry.

4.2 Cyclic voltammetry

Cyclic voltammetry (CV) is a commonly used electrochemical method. CV provides information about thermodynamics, kinetics and mechanism of redox processes. The result of the measurement (cyclic voltammogram) allows for determination of the number of electrons which take part in the electrochemical reaction, redox potential and reversibility of the process. Moreover, on the basis of cyclic voltammograms one can measure if the process occur only because of diffusion or it is proceeded by the adsorption of the electroactive species on the electroactive surface. All of those factors are affecting the shape of the cyclic voltammograms. The peak shape of the voltammogram comes from the exponential growth of the current, when potential applied to the electrode reaches the standard potential for a given reaction, and decay of the current proportional to the square root of time, given by Cottrell equation. The typical cyclic

voltammetry measurement is performed in a three electrode cell. The voltage is applied between the working electrode (WE) with respect to a non-polarizable reference electrode (RE). The current flows through the WE and a counter electrode (CE). A voltage is applied to the CE to generate a current of the same magnitude, but with a sign opposite to the one flowing through the WE. However, the voltage on the CE and the specific reaction is usually not explicitly controlled.

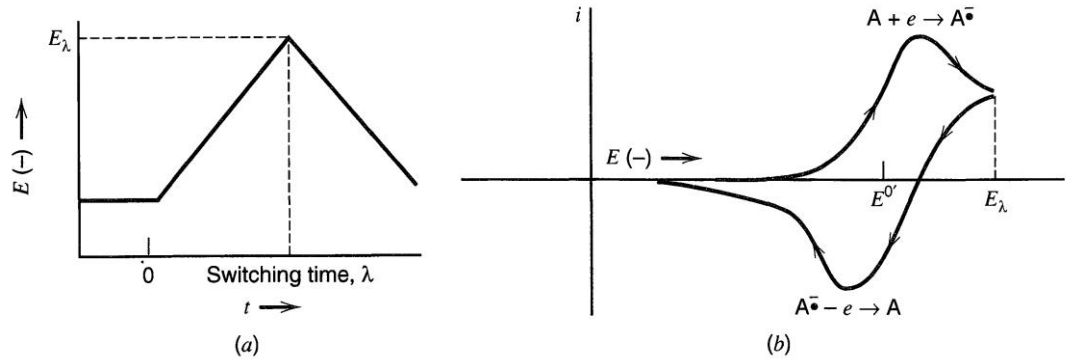

Figure 4.2.1 (A) Cyclic potential sweep, (B) resulting cyclic voltammogram, Adapted from [1].

In CV the potential of WE is linearly varied with the constant rate, called scan rate (Fig. 4.2.1). The current is registered from potential $E_{t=0}$ where no reaction occur and only capacitive current is measured, to switching potential $E_{\lambda,}$ and back to $E_{t=0}$. For the diffusion controlled processes one can distinguish three types of reactions: reversible, quasi-reversible and irreversible[4]. If the oxidation (E_{pa}) and reduction (E_{pc}) peak potentials are following the rule:

$$\left(E_{pc} - E_{pa}\right) = \frac{59\text{mV}}{\text{n}}, \qquad \text{Eq (4.2.1)}$$

where n is the number of electrons participating in the electrochemical reaction, then the reaction is reversible. In case of semi-reversible reaction the difference is larger than 57 mV but smaller than 112 mV, and for the irreversible reactions the difference between the peak potentials is higher than 112 mV or one of the peaks does not exist at all. The peak current i_p observed in a cyclic voltammogram under quiescent conditions is proportional to the concentration of the electroactive species in the bulk solution and is given by the Randles-Sevcik equation:

$$i_p = 2{,}69 \cdot 10^5 n^{3/2} A D^{1/2} C^o v^{1/2}\,, \qquad \text{Eq (4.2.2)}$$

[4] Electrochemical reversibility has different meaning than the chemical reversibility. In reaction Ox + ne^- -> Red, where Ox are oxidized species, Red are reduced species and n is a number of electrons which take part in the reaction. Electrochemical reversibility refers to the rate at which the electron transfer between the working electrode and the solution redox species occurs. The fast electron transfer is called electrochemically reversible. The slow electron transfer are electrochemically irreversible, and the intermediate rate is called quasi-reversible. Contrary to the electrochemical reversibility the chemical reversibility, means that the substrates of the reaction (Ox in the schematic reaction) can be regenerated.

where *A* is an electrode surface, *D* is the diffusion coefficient of the electroactive species C^0 is the concentration of redox species in the bulk solution and *v* is the scan rate. For the adsorption controlled processes the i_p is proportional to *v*. However, the Randles-Sevcik equation is valid only for experiments governed by diffusion only. For hydrodynamic conditions the equations appropriate for the system should be applied.

In this work I have used CV for general characterisation and optimization of the RD system and for generation-collection experiments.

4.3 Chronoamperometry

Chronoamperometry (CA) is one of several step methods, where the current is measured as a function of time after application of a perturbation of the potential. When a double step potential is applied to the working electrode the potential program follows the pattern (Figure 4.3.1). In the first step the initial potential (E_1) is applied to the WE, and redox active species doesn't undergo any reaction, the measured current equals zero. If the potential is switched to a potential above the redox potential the reaction rate is mass transfer limited. With continuation of the electrochemical reaction the concentration of redox active species at the electrode surface if decreasing resulting a current that is decreasing over time.

The changes of the measured current as a function of time are given by the the Cottrell equation,

$$i(t) = \frac{z_i F A D^{1/2} C_{ox}^*}{\pi^{1/2} t^{1/2}} \qquad \text{Eq (4.3.1)}$$

where z_i is the charge number, C_{ox}^* is the bulk concentration of species C_{ox}. When the mass transfer is diffusion-controlled in fast reactions the measured current is proportional to $t^{-1/2}$ [1].

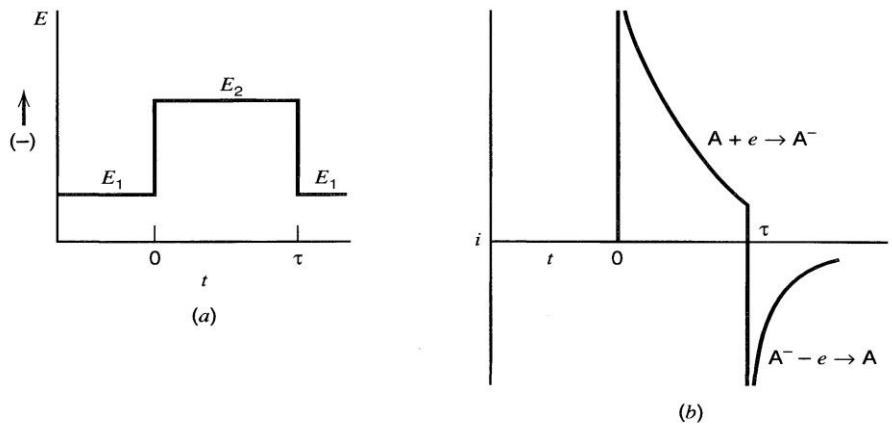

Figure 4.3.1 (A) Double potential step chronoamperometry and (B) Typical waveform current response. Adapted from [1]

Chronoamperometry is a method usually applied for investigation of the active electrode surface area such as nucleation and growth processes or the diffusion coefficient of electroactive species. CA can be combined with different electrochemical methods. In this work I present the data from combination of the chronoamperometry with cyclic voltammetry in generation-collection experiments, where the CV was performed on generator and CA was performed on collector electrode.

4.4 Square wave voltammetry

Square wave voltammetry (SWV) belongs to the family of step potential techniques, where current is measured with the constant potential kept on WE. The main advantage of that method is elimination of capacitive current.

In SWV a series of potential pulses is applied to the working electrode, where the waveform is a bipolar square wave superimposed on a staircase. The resulting potential waveform is presented in figure 4.4.1. The base potential is changing between pulses, but the amplitude and the pulse width remain constant. For each measurement the current is sampled twice, at the end of the forward pulse (Forward sample dot on the Fig. 4.4.1) and at the end of the reverse pulse (Reverse sample dot Fig. 4.4.1). The difference between forward sample and reverse sample are calculated and later considered as a single point in SWV. The main difference between the cyclic voltammetry and the pulse methods such as SWV is the decay rates of the charging and faradaic currents. The capacitive current, as an exponential function decays much more rapidly than the faradaic current, where the decay is inversely proportional to the square root of time[2].

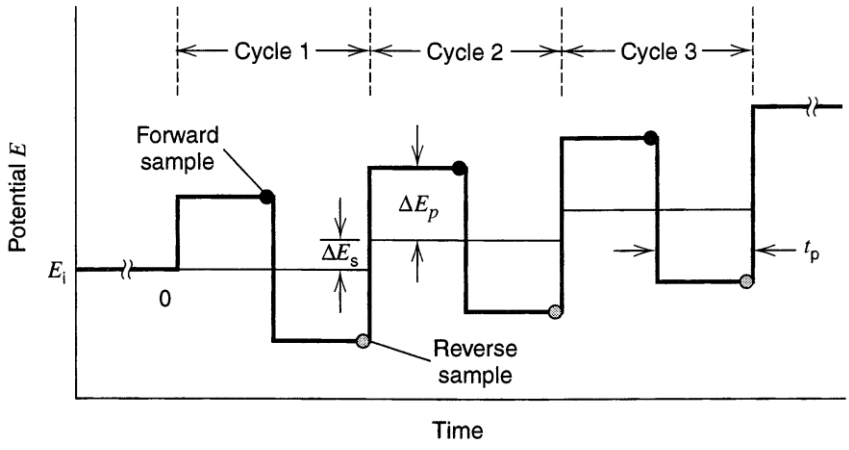

Figure 4.4.1 Waveform and measurement scheme for square wave voltammetry. A forward current sample is taken at the time indicated by the solid dot, and a reverse current sample is taken at the time marked by the shaded dot. Adapted from [1].

Plots presented on a figure 4.4.2 show the great advantage of the SWV over a CV. The current registered with square wave voltammetry is characterized with much higher peak height and no charging current is observed.

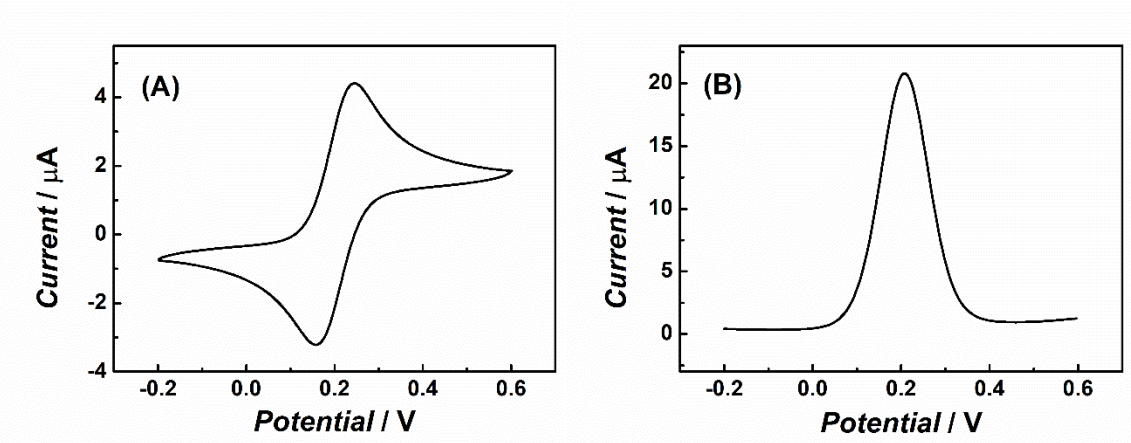

Figure 4.4.2 The Comparison between the results obtained with cyclic voltammetry (A) and square wave voltammetry (B) for oxidation of the 1 mM $K_4Fe(CN)_6$ in 0.1 M KNO_3.

SWV allows for more precise determination of the redox potential of the redox sample. For this reason the method was used for the simultaneous neurotransmitters detection experiments.

4.5 Scanning electron microscopy

Scanning electron microscopy (SEM) is a powerful imaging tool for visualizing objects in the micro- and nanoscale. The image is generated by scanning the sample with an electron beam while recording the number of electrons emitted from the sample. The electrons are accelerated by an electric field to an energy usually from 0.2 to 40 keV through a series of electron optics. The electron beam is focused by lenses on its way to the sample. The electrons, while interacting with the sample surface, lose some of their energy. As a result they can emit backscattered electrons, secondary electrons, cathodoluminescence, characteristic X-ray radiation or visible light.

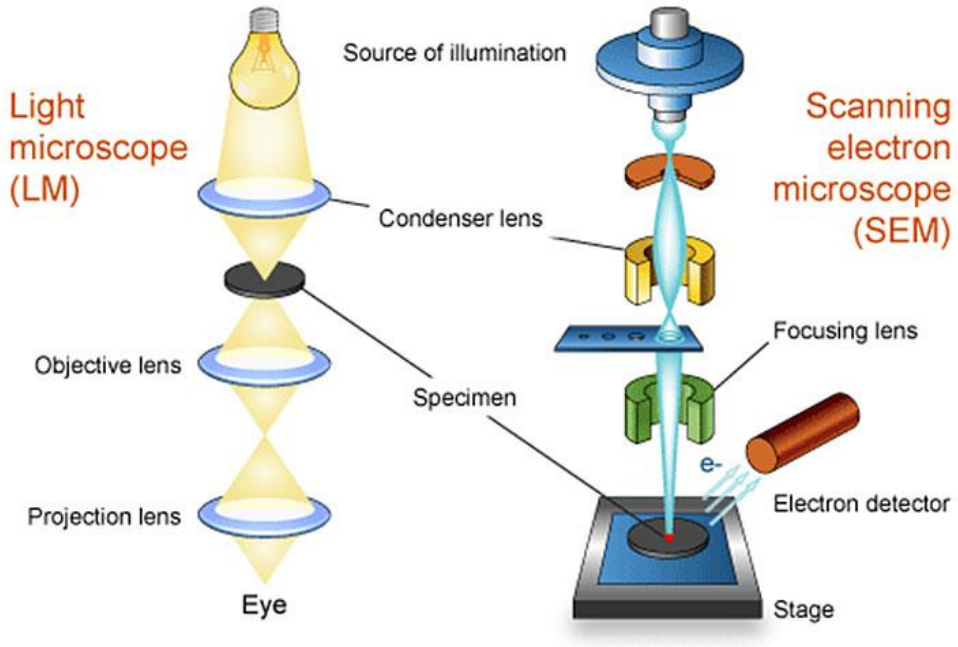

Figure 4.5.1 Comparison between an optical microscopy and Scanning Electron Microscopy. Adapted from [3]

With an application of a proper detector different signals can be obtained. Most SEM tools are equipped with low energy secondary electron detectors which allow for observation of the topography of the sample with high resolution and precision. However, application of a detector for backscattered electrons leads to images with higher composition contrast.

In this work SEM have been used for imaging the coverage of the ITO surface with different carbon materials, later used as working electrodes.

4.6 Particle Image Velocimetry

Particle Image Velocimetry (PIV) is a method which allows for determination of the flow velocity of fluids. It can be applied to testing both gases and liquids. The method is based on dispersing particles in the tested fluid and observing their movement under certain illumination of the sample. The particles should possess a unique set of properties such as a density similar to the density of the measured sample, proper size, matched viscosity.

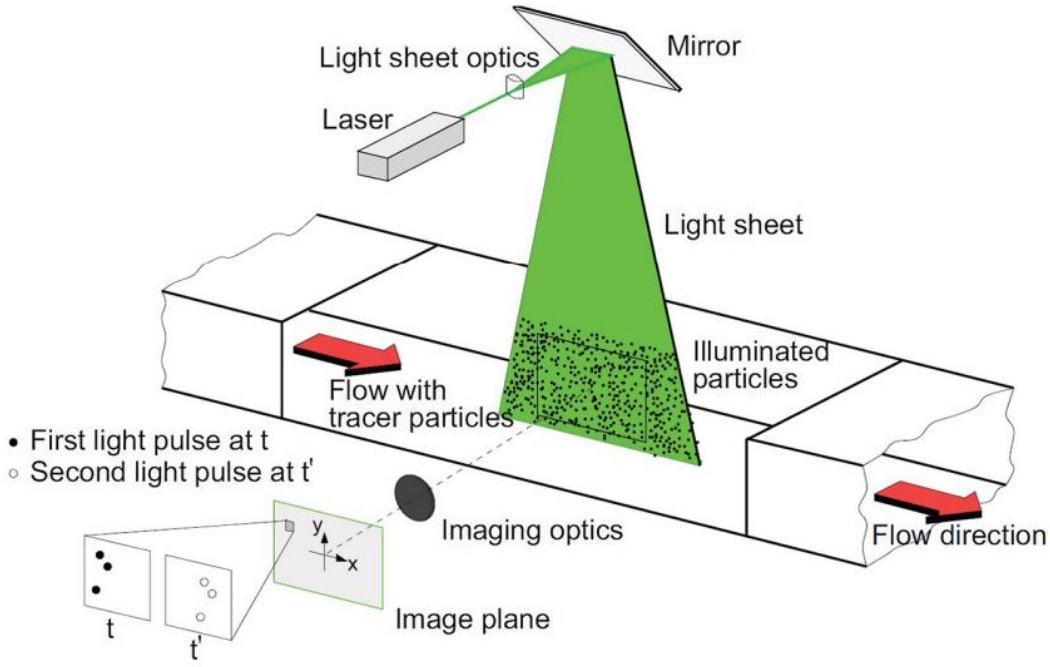

Figure 4.6.1 Basic 2-D-PIV setup in a channel. Adapted from [5].

Usually in PIV either fluorescent particles are used or particles with colour different from the observed fluid. In case of fluorescent particles the absorption wavelength differ from the emission wavelength. This phenomenon is used for the majority of cases, where lasers are used as the illumination source. The bigger the energy of the illumination source, the bigger the illumination effect on the seeding particles. However, there are some techniques which use the LED illumination. The recording methods are varied. The simplest method shows the 2 dimensional view of the observed fluid flow. However, superposition of many images from different angles with earlier calibration allows for creation of stereo PIV, which is a sort of 3D view of the fluid flow.

In principle correlation between the position of the illuminated particles in frames taken at known time intervals allows the velocity of the fluid to be determined (shown in Figure 4.6.1). Assembling of the average vectors over the whole sample shows the velocity profile in the sample.

In this work the PIV was used for experimental determination of the velocity profile in the rotating droplet system.

Bibliography

[1.] Bard, A. J.; Faulkner, L. R. *ELECTROCHEMICAL METHODS Fundamentals and Applications Allen*; 1985; ISBN 9780123813749.

[2.] Chen, A.; Shah, B. Electrochemical sensing and biosensing based on square wave voltammetry. *Anal. Methods* **2013**, *5*, 2158, doi:10.1039/c3ay40155c.

[3.] SEM image Available online: https://embryology.med.unsw.edu.au/embryology/index.php/File:Microscopy_LM_and_SEM_cartoon.jpg .

[4.] Mazue, G.; Viennet, R.; Hihn, J.-Y.; Bonnet, D.; Barthes, M.; Bailly, Y.; Albaïna, I. Influence of a perpendicular liquid flow on a cleaning process using 20 kHz ultrasound: Characterization of the agitation at vicinity of the surface opposite to the transducer. *Can. J. Chem. Eng.* **2015**, *93*, 201–205, doi:10.1002/cjce.22079.

[5.] Raffel, M.; Bauknecht, A.; Ramasamy, M.; Yamauchi, G. K.; Heineck, J. T.; Jenkins, L. N. Contributions of Particle Image Velocimetry to Helicopter Aerodynamics. *AIAA J.* **2017**, *55*, 2859–2874, doi:10.2514/1.j055571.

Chapter 5.
Optimization and testing of the Rotating Droplet setup

5.1 Introduction

The research on Rotating Droplet setup, presented in this thesis fits to the everlasting trend for faster and more efficient electrochemical systems. In terms of electroanalytical measurements, they can be performed faster, with smaller usage of reagents and with lower detection limits. The Rotating Droplet (RD) system is a modification of the well-known Rotating Disc Electrode (RDE) system, but it uses much smaller volume of reagents. Contrary to the RDE, where only commercial tips serve as a working electrodes, any flat electrode material can be used as a working electrode in the RD. In this and following chapters I will present the results obtained during my research on the RD system. Here I present the optimization of the RD system and its first application in enzymatic oxygen reduction.

The need for implementation of hydrodynamic methods in electrochemical investigations was already mentioned in Chapter 1 of this thesis. In this chapter I want to show in more detail the basis of the Rotating Droplet technique, its applications and its advantages over standard hydrodynamic methods especially the Rotating Disc Electrode. Commonly used microfluidic and nanofluidic systems are believed to use small volume samples, however the filling of the syringes and tubing are sometimes very sample consuming. Standard experiments with RDE uses at least 100 ml of sample. For experimenters who have only small (few tens of microliter volume) samples, usage of standard hydrodynamic methods is impossible. The RD system needs only 70 μL of the sample. The promising results of the optimization of the system and characteristic open walls the RD system encouraged us to check the possibilities of usage of the RD system in the oxygen reduction reaction (ORR). In order to investigate the enzymatic ORR a certain electrode

surface modification was needed. I used a number of different modifications with application of carbon nanomaterials and enzyme immobilization with the use of sol-gel encapsulation. The electrode preparation is shown in details way in section 5.3.

5.2 Setup configurations

The objective of this part of the project was to create a system based on the rotating disc electrode principles, but using smaller sample volume and enable the use of electrode materials that are not available as RDEs. The system consisted of a working electrode surface, in this case ITO-coated glass, masked with Teflon tape glued with one side to double sided scotch tape, whereas the second side of the scotch tape was glued to the ITO electrode. The mask from the Teflon tape, due to its hydrophobic properties, confined the solution to a small area and let it create a drop-like shape on the electrode surface. From the top a rotating ring-disc electrode (RRDE) tip was placed at an optimized height which was kept constant for further experiments. The 70 µL sample volume, inserted gently between the surfaces of the RRDE tip and the working electrode surface, took a cylindrical shape as it was held in place by surface tension. Such a trapped droplet was forced to rotate due to the rotation of the RRDE tip.

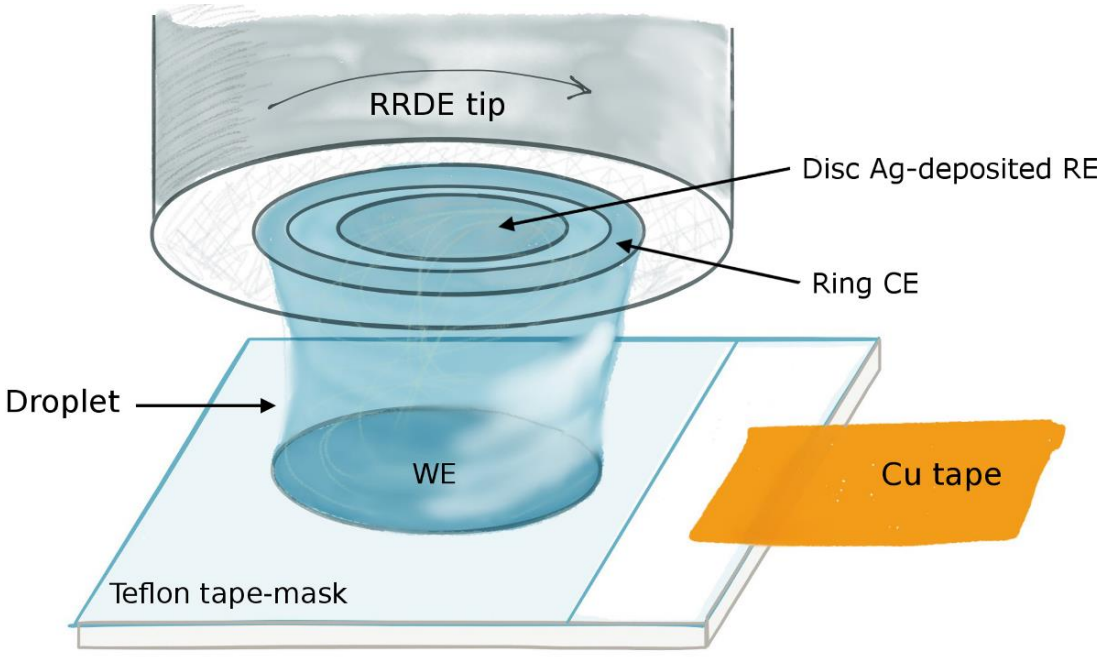

Figure 5.2.1 Schematic view of the system. Adapted from II.

Rotating ring-disc electrode tip in the presented system was adapted to work as reference and counter electrodes and is described below.

5.3 Electrode modification

The electrochemical measurements can be performed on various electrode materials. The working electrodes are often made from metals such as platinum, gold or mercury. Some experiments are performed on carbon based electrodes, where the Glassy Carbon electrode (GCE) is the most popular type. However, for some purposes a semiconductor electrode such as tin-doped indium oxide (ITO) works better. In the case of ITO electrode, its great advantage is transparency for visible light, which is why ITO electrodes are often used in spectroelectrochemistry. A great number of electrochemical experiments require a modification of the electrode surface either for bigger active electrode surface or for catalytic properties, for faster electrode reactions. The influence of electrode surface modifications on electrochemical measurements was already described in subchapters 2.2 and 2.3 of this thesis. Contrary to the standard (Gold or GC) electrodes, ITO electrode surface can be efficiently modified with the use of sol-gel matrices. The ITO outer layer consists of hydroxylic groups which allows for easy connection between the ITO surface and the modification layers. Utilization of the sol-gel matrices is especially important for creation of electrode surface material stable in hydrodynamic systems. In the studies presented in this thesis a majority of the electrochemical experiments were performed on ITO electrodes. In my research ITO electrodes were chosen because of their low price in comparison to the standard macro-electrodes, and ease of modification of their surface with sol-gel matrices stable under hydrodynamic conditions, which are crucial for the investigated RD system.

5.3.1 Carbon-based nanomaterials

Owing to their remarkable electrochemical properties, such as excellent electrical conductivity and high surface area, carbon-based nanomaterials are often used as an element for modification of electrodes. We can distinguish a number of possible modification materials such as single wall carbon nanotubes, multi wall carbon nanotubes, graphene or carbon nanoparticles. Carbon-based nanomaterials are used for a number of electrode applications in sensor and biosensors[1], various energy storage devices[2], photovoltaic devices and as catalysts for electrochemical reactions[3].

In this chapter I present data obtained with usage of electrodes modified with single wall carbon nanotubes (SWCNTs), reduced graphene oxide (rGO) and carbon nanoparticles (CNPs). SWCNTs were purchased from Shenzhen Nano-tech Port Co. Ltd, rGO was prepared by Hummer's method. CNPs were a gift from Cabot Corporation. The CNPs, sold under the name

Emperor 2000, have phenylsulfonate functionalities (negatively charged) and are used as a filler or a pigment. The negative charge of the CNPs has a great impact on their hydrophilicity. Positively charged carbon CNPs were obtained by functionalisation of the negatively charged nanoparticles with the etylendiamine [4] They were obtained as a gift from prof. Frank Marken's group. We used positively and negatively charged CNPs for modification of electrodes with layer by layer method. All used carbon nanomaterials SWCNT, rGO and CNPs were used to increase the electrode active surface area. Moreover, the unique property of the CNPs to influence the potential of certain electrode processes was noticed and used for further investigation presented in the next chapters.

5.3.2 Electrode preparation

In this chapter all experiments were performed with a traditional three electrode setup: a working electrode, a reference electrode and a counter electrode.

5.3.3 Preparation of working electrodes

- Bare ITO

The base material for the working electrode was glass support coated with indium-tin oxide, later called ITO slide/electrode. The ITO slides were cleaned with acetone, isopropanol, ethanol and distilled water and heated in a tube furnace to a temperature of 500˚C for 10 minutes in order to remove all organic residues. Such prepared electrode surfaces were used for the optimization of experiments, as shown in figures 5.4.1.1, 5.4.1.2 and 5.4.2.1.

In order to choose the best modification material for oxygen reduction studies (chapter 5.4.2) and further studies on neurotransmitters detection (shown in chapters 6 and 7), different nanomaterials were tested. Below, I describe the electrode modification with application of layer-by-layer modification with carbon nanoparticles (CNPs), drop-coating with carbon nanomaterials immobilization in the silica sol-gel matrices (described in Table 5.3.1),

- ITO CNP 3 (+/-)

The layer by layer method is based on alternate immersion of the electrode support (ITO slide) in suspensions of positively or negatively charged nanoparticles, as described in [5]. Here we used 3 layers of positively and 3 layers of negatively charged CNPs. Similarly as it was observed by Szot et. al [6], the increased number of layers caused loss of the mechanical stability of the electrode modification.

- ITO CNP TMA/ TMOS

For the application of the system for the enzymatic oxygen reduction reaction, the procedure of cleaning electrode was followed with modification of the surface with CNPs encapsulated in a *TMA/TMOS* silica matrix together with enzyme dissolved in the buffer solution, following the procedure in Table 5.3.1. CNPs provide the connection with the enzyme T1 center, facilitating the oxygen reduction by enabling direct electron transfer between the enzyme and the electrode.

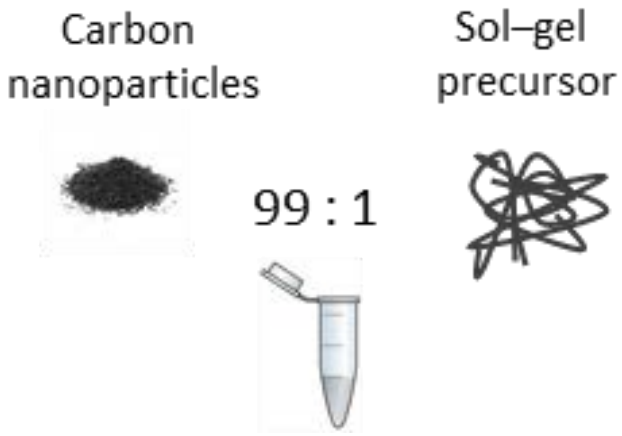

Figure 5.3.3.1 Schematic preparation of modification mixture with carbon material and silica sol-gel matrix (ITO CNP TMA/TMOS).

Carbon nanotubes or nanoparticles were dispersed in a water or buffer solution to obtain a dispersion of 3 mg of carbon material per 1 mL of solution, whereas the enzyme was dispersed in the buffer solution, to get 2 mg enzyme/ 1.

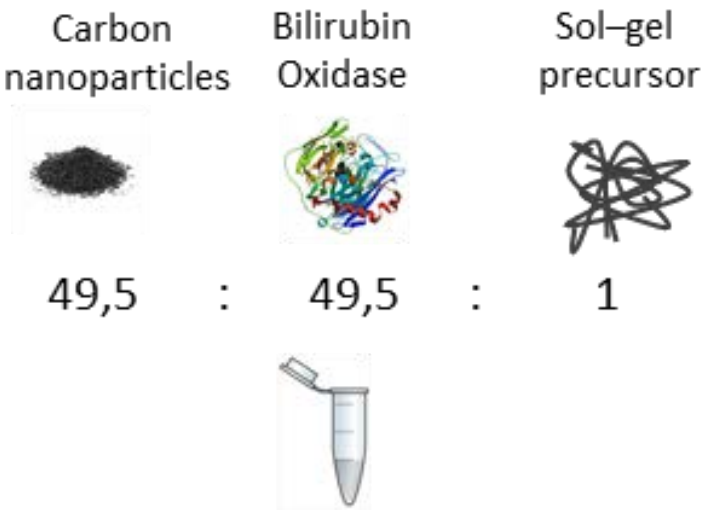

Figure 5.3.3.2 Schematic preparation of modification mixture with carbon nanoparticles and enzyme for encapsulation in silica sol-gel matrix (ITO CNP BOx TMA/TMOS).

Precursor	Composition	Procedure of preparation
MTMOS	375 µl of methanol, 250 µl of MTMOS and 14 µl of 11M HCl	Mixing with CNTs dispersion in volume ratio 1 : 99, drop coating on the tape limited electrode area.
TMA/ TMOS	270 µl TMOS, 54 µl of methanol, 35 µl of water, 6 µl of TMA µl and 1 µl of 11 M HCl	Mixing with CNPs dispersion or mixture of CNPs and enzyme solution in volume ratio 1 : 99, drop coating on the tape limited electrode area.

Table 5.3.3.1 Procedure of the electrode surface modification with sol-gel matrices based on MTMOS and TMA/TMOS precursors.

Such prepared solution of mixtures containing either carbon material or carbon material with enzyme were drop-coated on the masked surface of ITO electrode and dried in room temperature.

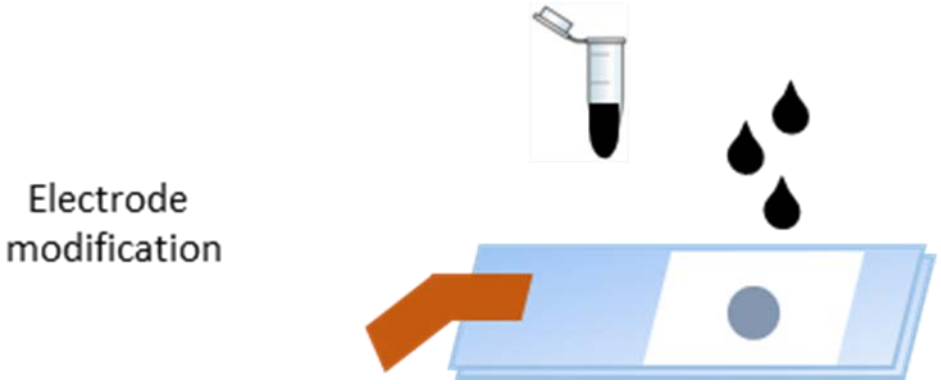

Figure 5.3.3.3 Schematic electrode surface modification.

For standard RDE measurements the Glassy Carbon Rotating Disc Electrode (GC RDE) tip was used and modified identically as the ITO electrode. The ITO surface was masked with tape to unify the surface to be a circle with diameter of 0.2 cm.

5.3.4 Reference electrode

The disc of a rotating ring-disc tip (both disc and ring are platinum) was treated as follows to work as a (pseudo)reference electrode: the disc was modified electrochemically by cyclic voltammetry, where 30 scans in the potential window of -0.1 to 0.1 V was applied in 20 mM solution of $AgNO_3$. As a result a silver layer was obtained on the disc. For the RDE measurements a standard Ag|AgCl reference electrode was used.

5.3.5 Counter electrode

The platinum ring from the Pt/Pt ring-disc tip electrode was used as a counter electrode. For a standard GC RDE experiment the platinum wire was used as a counter electrode.

5.4 Results

5.4.1 Rotating Droplet system optimization

The rotating droplet method turned out to be very sensitive to the height of the droplet system. Because of that a set of experiments was performed in order to define the optimal height of the droplet.

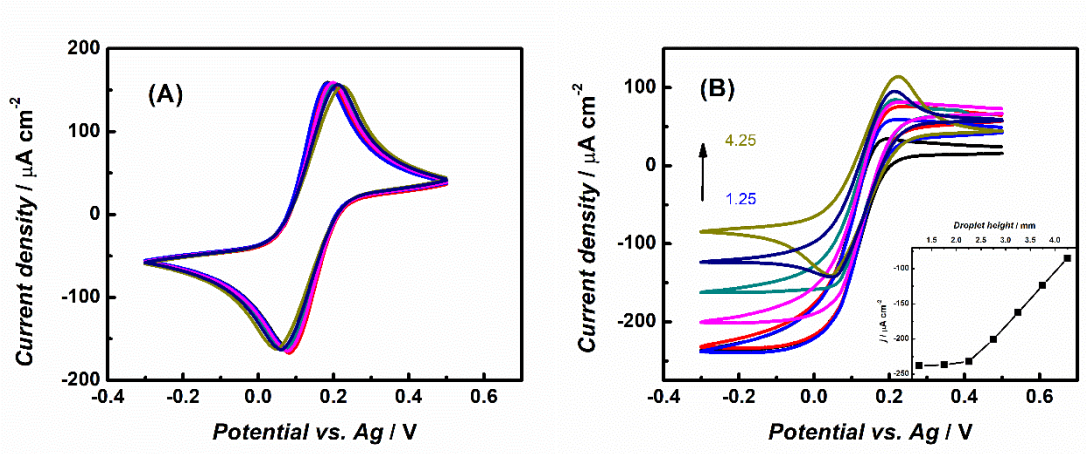

Figure 5.4.1.1 Cyclic voltammograms of 0.1 mM $K_3Fe(CN)_6$ in 0.5 M KNO_3 at (A) 0 rpm and (B) 500 rpm in RD system at different droplet heights (in millimeters), registered with bare ITO. Adapted from II.

Figure 5.4.1.1 shows the results for (A) stationary system, were no movement of the droplet was implemented and the part (B) where the droplet is rotated with 500 rpm, in both cases the height of the droplet was investigated in range from 1.25 to 4.25 mm. For the stationary droplet the peak shape is conserved and in the investigated range of the droplet height, no differences were observed in current registered on the working electrode. When the rotation is turned on it is clearly visible that the height of the droplet influences the measured currents. For the height lower than 3 mm, the results obtained in the rotating droplet system show a sigmoidal curve. As a result I decided to keep a constant height of the droplet at 2.75 mm (pink curve in the figure 5.4.1.1 (B)). It was a compromise between hydrodynamically controlled mass transport and not making it too hard to add the fluid between the working electrode and the RRDE tip. Keeping the droplet

height constant made sure that the hydrodynamic properties of the rotating droplet system were consistent in each experiment.

The new technique, based on the rotating disc electrode principle, had to be compared with the results obtained with usage of the mother method. For this reason the same redox probe was examined with using both standard RDE (Fig. 5.4.1.2 (A)) and the RD (Fig. 5.4.1.2 (B)) techniques. $K_4Fe(CN)_6$ in 0.5 M KNO_3 was tested with using the Glassy Carbon Rotating Disc Electrode (GC RDE), with Ag/AgCl as a reference and Pt wire as a counter electrodes in the range of 0, 50, 100, 200, 400, 700 and 1100 rpm. The inset in Fig. 5.4.1.2 (A) shows the Levich-plot for this experiment. Fig. 5.4.1.2 (B) shows the oxidation of the same $K_4Fe(CN)_6$ in 0.5 M KNO_3, but with set of electrodes appropriate for already mentioned RD setup. Inset in plot 5.4.1.2 (B) is a representation of the Levich-plot for the experiment shown in 5.4.1.2. Both systems, RDE and RD, show the similar dependency of the current on the rotation rate. However, we also see a difference in the slope of the line connecting the current and the square root of the rotation rate.

$$I_l = 0.620\, nFAD^{2/3}\nu^{-1/6}\omega^{1/2}C_0 \qquad \text{Levich equation for RDE system}$$

If we assume that the behavior of the other parameters in Levich equation are the same, we arrive at a different value of the constant in the beginning of the equation. For the RDE this was calculated by Levich to be 0.620, whereas in our system we can fit the value of 0.325. However, we have not tested the influence of the change of the other parameters. Viscosity and diffusion coefficient in the RD system can possibly affect the mass transport and ultimately influence the Levich equation.

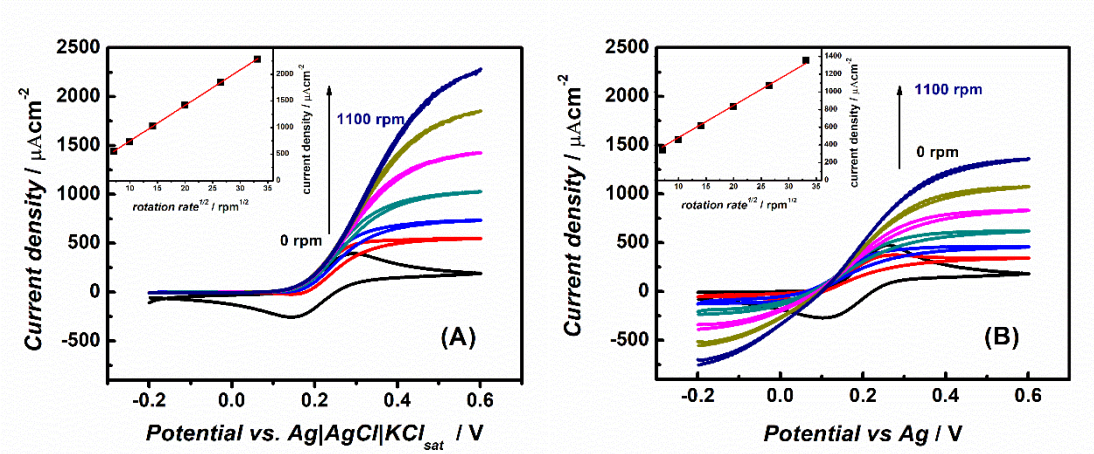

Figure 5.4.1.2 Cyclic voltammograms 0.1mM $K_4Fe(CN)_6$ in 0.5 M KNO_3 in (A) GC RDE system, (B) Bare ITO RD system under different rotation rates, scan rate 20 mV s^{-1}. Adapted from II.

The same shape of curves showing an increase of the total current value with increasing rotation rate for a fast reaction such as in the case of $K_3Fe(CN)_6$ in 0.5 M KNO_3 solution presented in Fig. 5.4.1.2. In the case of the RDE system no cathodic current was registered, whereas for the RD system cathodic current was significant. The difference between the system's responses can be explained by the use of the small volume sample and close proximity between the WE and CE in the RD system. Small volume and close distance between working and counter electrodes favor the fast transport of the products from WE to the CE. This phenomenon is explained in more detail in Chapter 6.

5.4.2 Carbon modified electrodes in RD system

Application of bare ITO electrode have been shown and proven to be useful for certain purposes, however as I already mentioned in Chapter 2, for many reasons modification of the electrode surface is needed. We wanted to use carbon modified electrodes for studying the oxygen reduction reaction - data presented in the next subchapter. Carbon modified electrodes were used for construction of a RD sensor for neurotransmitters detection, presented in the chapters 6 and 7 of this thesis. Before the application of the specific material we wanted to check the stability of the modification material, matrices which were used for modification, but also check if the porosity of the carbon material affect the RD system responses. In this subchapter I tested bare ITO electrodes, ITO electrodes modified with porous carbon nanoparticles with the layer by layer method (ITO CNP(+/-)) and ITO with carbon nanotubes encapsulated in a MTMOS sol-gel silica matrix. The electrode preparation is described in Chapter 5.3. For the simplification of the study, the various carbon materials and method of surface modification was tested with usage of an oxidized form of redox probe with known electrochemical behavior. For all experiments in this subchapter the solution of 0.1 mM K_3FeCN_6 in 0.5 M KNO_3 was investigated with cyclic voltammetry, 20 mV/s, in potential window from 0.25 V to -0.35 V and backwards. On the presented plots always the second scan is shown. Results obtained on the bare ITO electrode are presented in Fig. 5.4.2.1, cyclic voltammograms show an increase of the cathodic current with increasing rotation rate in the system, which stays in similar to the data presented above for oxidation of K_4FeCN_6.

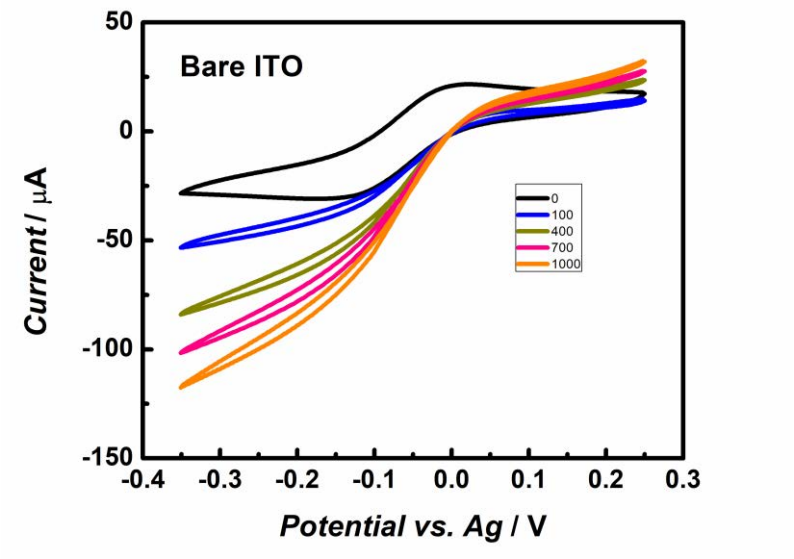

Figure 5.4.2.1 Cyclic voltammograms 0.1mM $K_3Fe(CN)_6$ in 0.5 M KNO_3 in RD system, registered with bare ITO electrode under different rotation rates, scan rate 20 mV s^{-1}.

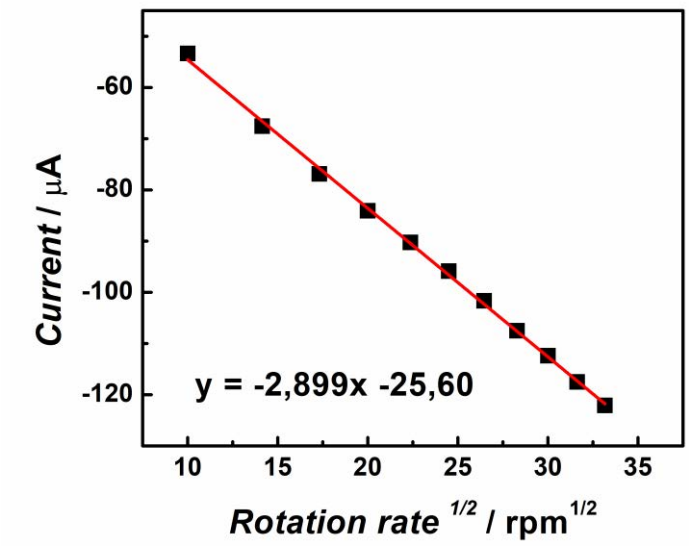

Figure 5.4.2.2 Levich plot for 0.1mM $K_3Fe(CN)_6$ in 0.5 M KNO_3 in the RD system, registered with bare ITO electrode. Current registered at -0.35V.

The increase of the limiting current indicates that the observed reaction is no longer limited by diffusion but the convection governs mass transfer limitations. However, the shape of curves visible in Fig. 5.4.2.1 indicate that the kinetic limitations still exist. On this type of electrode more negative potential has to be applied to reach the mass transfer limitations, and this could result in side reactions. The linear response for Levich plot shows that, in the measured rotation range, the electrode reaction is characterized with fast kinetics.

The next step in the performed comparison was to measure the response of the system with usage of the CNP layer by layer modified electrode, Fig. 5.4.2.3. Observed cyclic voltammograms show the increase of cathodic current as a function of rotation rate, but also simultaneously quite significant increase of the anodic current. This phenomenon comes from the fact that the layer-by-layer method lead to a highly porous material, which tends to keep the chemical probes in close proximity to the working electrode surface, staying in electric contact with it. As a result, products can be consumed while the electrode is polarized with positive potential and can be oxidized. Observed behavior of the redox probe can be used for some investigations, however one has to be very careful with interpretation of the current responses obtained on such porous electrode materials.

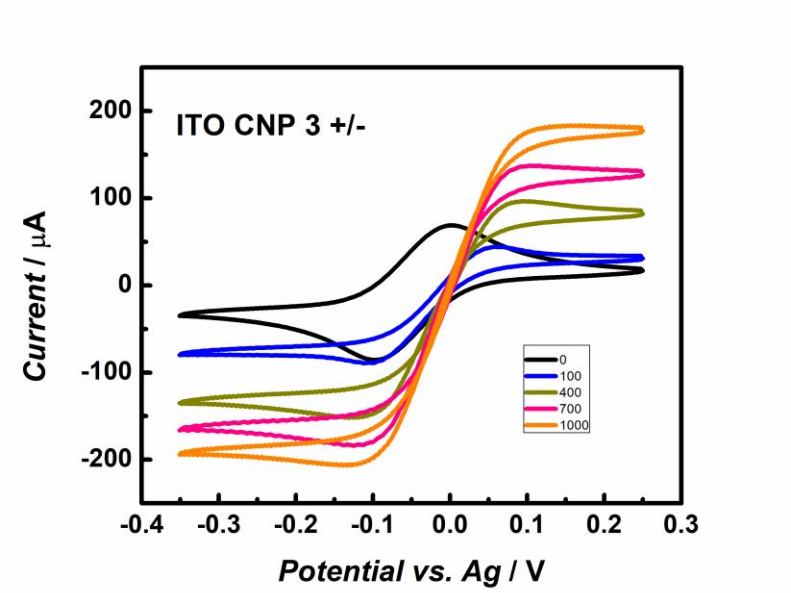

Figure 5.4.2.3 Cyclic voltammograms 0.1mM $K_3Fe(CN)_6$ in 0.5 M KNO_3 in RD system, registered with ITO electrode modified with layer-by-layer method with carbon nanoparticles under different rotation rates, scan rate 20 mV s^{-1}.

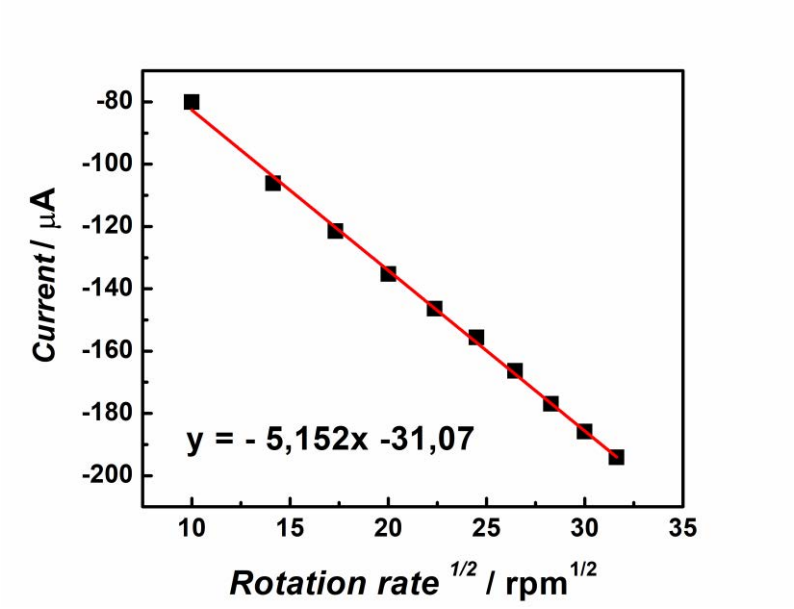

Figure 5.4.2.4 Levich plot (A) for 0.1mM $K_3Fe(CN)_6$ in 0.5 M KNO_3 in RD system, registered with ITO electrode modified with layer-by-layer method with carbon nanoparticles.

Despite the fact that the porous material present on the electrode surface was blocking the electroactive species trapped inside it, the linear Levich plot was registered. The Levich response shows that the carbon nanoparticle film electrode is not changing the rate of the electrochemical reaction, and definitely the reaction rate is not slowed down with application of this modification, and only mass transport of the reactant to the electrode surface is a limiting factor.

Highly desired electrode surface development with carbon material is often biased with the surface blocking or slow diffusion of the reaction product from the porous material. However, it is possible to immobilize the carbon material with sol-gel matrices. Such modification enables maintenance of the carbon on the electrode surface, but also coating of the carbon material to be less adsorptive for chemical reactants. Application of the silica matrices in the following subchapters will show to be a successful choice for immobilization of both enzymes and carbon nanoparticles for some detection purposes described in next chapters of the thesis. Taking advantage of well-known and used before silica matrix based on MTMOS precursor I have constructed an electrode modified with carbon single walled nanotubes encapsulated in a matrix. The created electrode enabled us to measure almost as high current as for the highly porous layer-by-layer modified carbon nanoparticles electrode, see Fig. 5.4.2.5. Application of the silica matrix have limited the possibility of adsorption of the reaction product close to the electrode surface and as a result we observed a high increase of the reductive current, while increasing the rotation rate with tiny increase of anodic current, when polarizing electrode in high positive potentials.

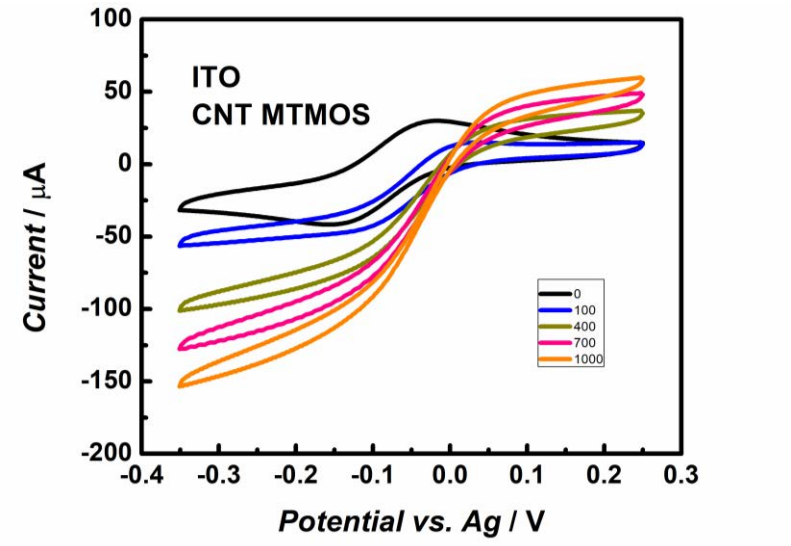

Figure 5.4.2.5 Cyclic voltammograms 0.1mM $K_3Fe(CN)_6$ in 0.5 M KNO_3 in the RD system, registered with ITO electrode modified with matrix encapsulated carbon nanotubes under different rotation rates, scan rate 20 mV s^{-1}.

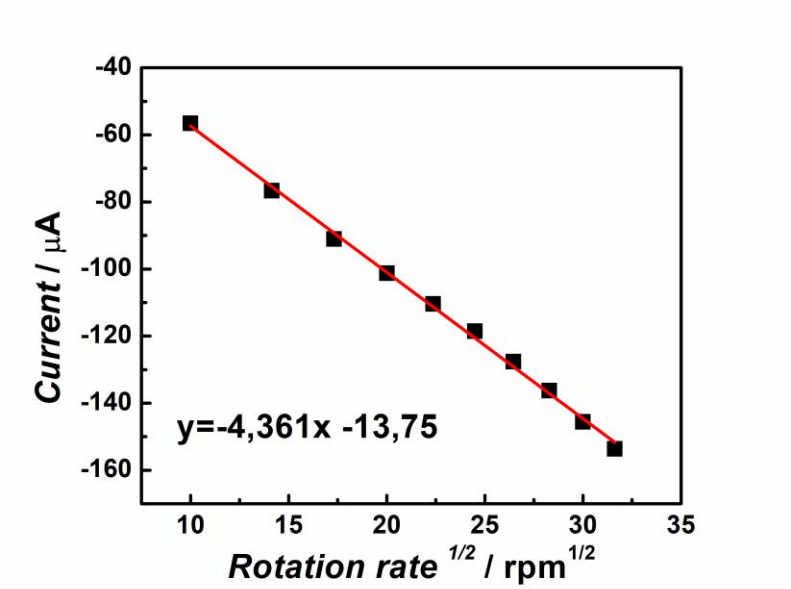

Figure 5.4.2.6 Levich plot (A) for 0.1mM $K_3Fe(CN)_6$ in 0.5 M KNO_3 in RD system, registered with ITO electrode modified with matrix encapsulated carbon nanotubes.

Linear response in the examined rotation rate shows that the oxidation of $K_3Fe(CN)_6$ on the carbon nanotubes film is also characterized with fast kinetics, and the mass transfer of the products to the electrode surface is the only limitation.

Performed experiments have led us to a conclusion that the rotating droplet system act as a new economic alternative for the already known hydrodynamic method and can be used for further

investigation and applications. Moreover, application of a proper, hydrodynamic resistant matrix allows for the efficient modification of the electrode surface, which can act as an integrated part of the Rotating Droplet system.

5.4.3 Oxygen reduction in a Rotating Droplet system

The importance of the investigation of the oxygen reduction reaction was already mentioned in the Chapter 1. The Department of Electrode Processes of the IPC PAS, which our group is part of, gave a substantial contribution into the study of enzymatic oxygen reduction [7]–[9]. The direct electron transfer enabled by various electrode modifications inspired me toward studies on enzymatic oxygen reduction under hydrodynamic conditions. During my master thesis I was working on enzymatic oxygen reduction, catalyzed by the enzyme Bilirubin Oxidase (BOx). We have observed that direct electron transfer between the enzyme and electrode surface is possible provided that the electrode surface is covered with nano carbon materials. I took advantage of the new RD system, where the easily modified ITO electrode can act as a working electrode, and decided to check, whether the RD system can be useful and efficient tool for enzymatic oxygen reduction reaction. For studies with enzyme immobilized on the electrode surface I have applied the sol-gel matrices. Sol-gel matrices encapsulate the enzyme molecules on the electrode surface which assure hydrodynamic durability but does not impair enzyme's function.

The first set of experiments was performed for solution with dissolved enzyme, which is the unusual way of performing such experiments. We used the solution of 0.5 M Na_2SO_3 and electrode modified with carbon nanotubes MTMOS matrix. The enzyme Bilirubin Oxidase catalyzes oxygen reduction in a 4-electron reaction. For the purpose of this experiment the first trial was performed in air saturated solution. As a result the oxygen reduction reaction was observed. From the data shown in figure 5.4.3.1 one can see that the increase of the rotation rate influences the registered current. For 50 rpm and 100 rpm we can see the increase of the cathodic current, but with time and with application of higher rotation rate we can see that the cathodic current decreases.

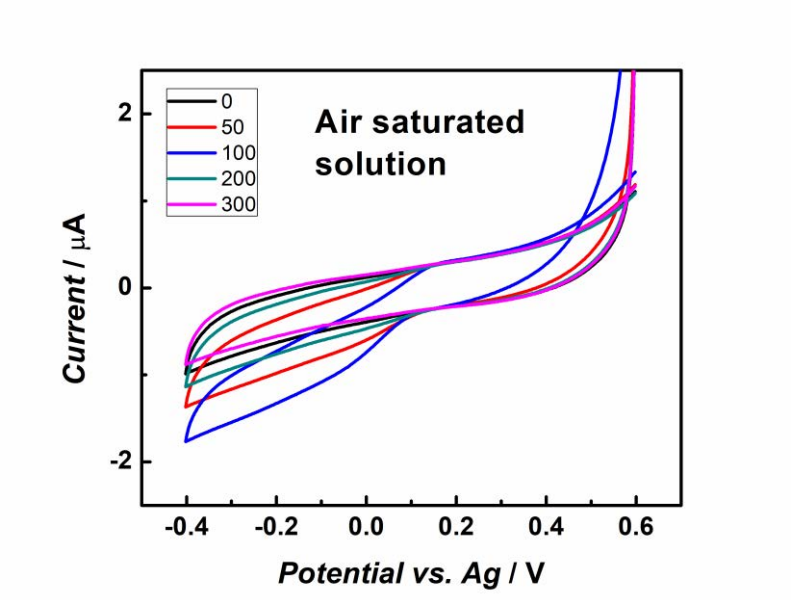

Figure 5.4.3.1 Cyclic voltammograms registered in Air saturated solution of 1 mM BOx in 0.5 M Na_2SO_3 on ITO electrode modified with carbon nanotubes encapsulated in MTMOS matrix, scan rate 20 mV s^{-1}.

Moreover, experiments performed in the oxygen saturated solution Fig. 5.4.3.2 show that the oxygen reduction reaction starts at higher potential and also that the increase of rotation rate of the RD system causes the increase of the cathodic current. The current observed in the experiment with oxygen saturated solution is almost one order of magnitude higher than in the case of the air saturated solution. This proves that the observed results show the oxygen reduction reaction.

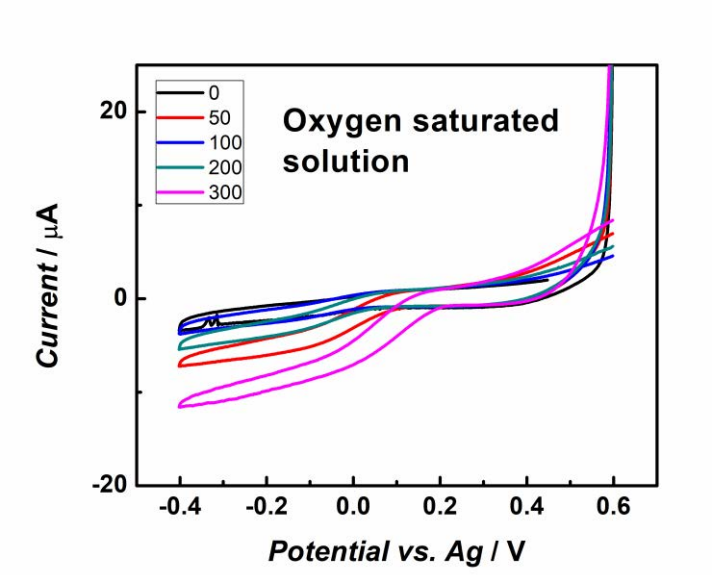

Figure 5.4.3.2 Cyclic voltammograms registered in Oxygen saturated solution of 1 mM BOx in 0.5 M Na_2SO_3 on ITO electrode modified with carbon nanotubes encapsulated in MTMOS matrix, scan rate 20 mV s^{-1}.

As a control experiment the set of measurements with argon saturated solution was performed. From results shown in Figure 5.4.3.3 we can draw the conclusion that there is no oxygen reduction in the same potential range that for the above-mentioned examples which proves the results for air and oxygen saturated solutions.

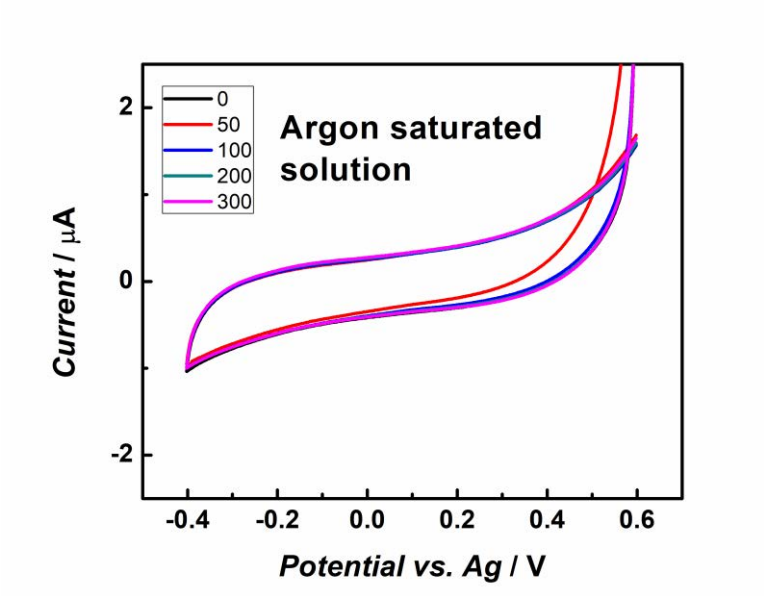

Figure 5.4.3.3 Cyclic voltammograms registered in Argon saturated solution of 1 mM BOx in 0.5 M Na_2SO_3 on ITO electrode modified with carbon nanotubes encapsulated in MTMOS matrix

In further sections I will show the study done in order to find a more efficient electrode material and method for encapsulation both the electrode (carbon material and enzyme). We developed the method for efficient encapsulation of the electrode carbon material and enzymes with silica matrix based on the TMA precursor, which occurred to be more stable under hydrodynamic conditions. In the next series of experiments, I performed a set of measurements for both cases with the enzyme dispersed in the electrolyte solution of and with the enzyme encapsulated on the electrode surface.

At first we used the electrode modification with carbon nanotubes. As we can see in Fig. 5.4.3.4 the oxygen reduction for Bilirubin Oxidase dissolved in the electrolyte solution case (A). The cathodic current is small and it is hardly dependent on the rotation rate, which can indicate that the collisions of the Bilirubin Oxidase capable of catalyzing the oxygen reduction is not efficient, contrary to the experiment performed with enzyme encapsulated with silica matrix on the electrode surface (B). Plots C. and D. show respectively the Levich and Koutecký-Levich plots for the experiment C (with enzyme on the surface). From the Koutecký-Levich plot we can calculate the maximum current value for this electrode reaction which is -363µA/cm^2. This is

done by extrapolating the current values in the Koutecký-Levich plot to infinite rotation, in effect ensuring an infinite supply of analyte.

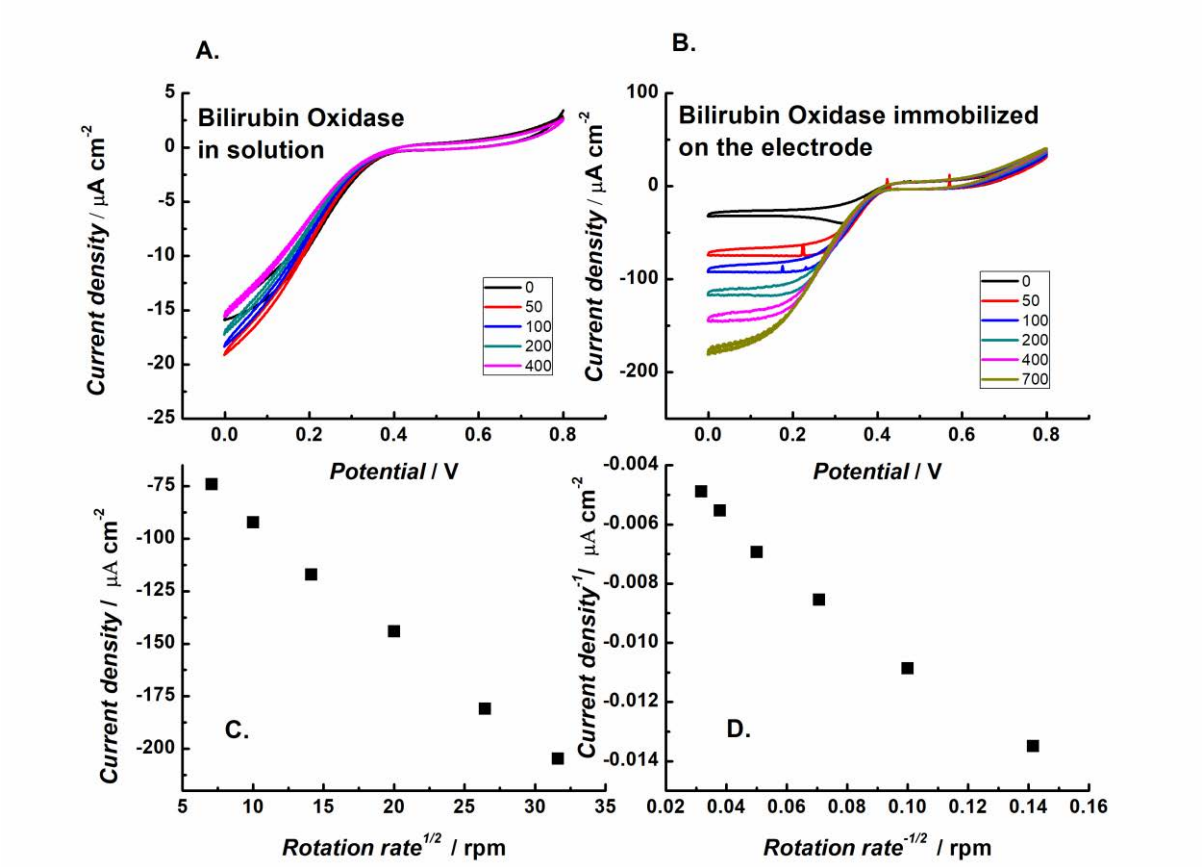

Figure 5.4.3.4 Cyclic voltammograms of oxygen reduction with Bilirubin Oxidase dispersed in the solution (A), Bilirubin Oxidase immobilized on the electrode surface (B), Levich dependency for the oxygen reduction on the electrode modified with carbon nanotubes in MTMOS matrix (C) and Koutecký-Levich dependency for the oxygen reduction on the electrode modified with carbon nanotubes in MTMOS matrix (D). Scan rate 2 mV s^{-1}.

The further investigation lead us to the application of other carbon material which was carbon nanoparticles. Similarly to the experiments presented in Figure 5.4.3.4 we performed the experiment with the enzyme dispersed in the solution of the electrolyte and with the enzyme encapsulated on the electrode surface with help of the silica matrix based on TMA precursor. As a result in plot (A) we can see that the oxygen reduction when enzyme is dispersed in the solution is completely insufficient, whereas the oxygen reduction catalyzed with enzyme encapsulated with TMA matrix on the electrode surface gives bigger cathodic current than the carbon nanotubes shown previously. Moreover, in plots (C) and (D) one can find the Levich and Koutecký-Levich plots. Maximal current value for this reaction with using modification with carbon nanoparticles equals -943 μA/cm^2. However, the shift of the reference electrode may influence this result.

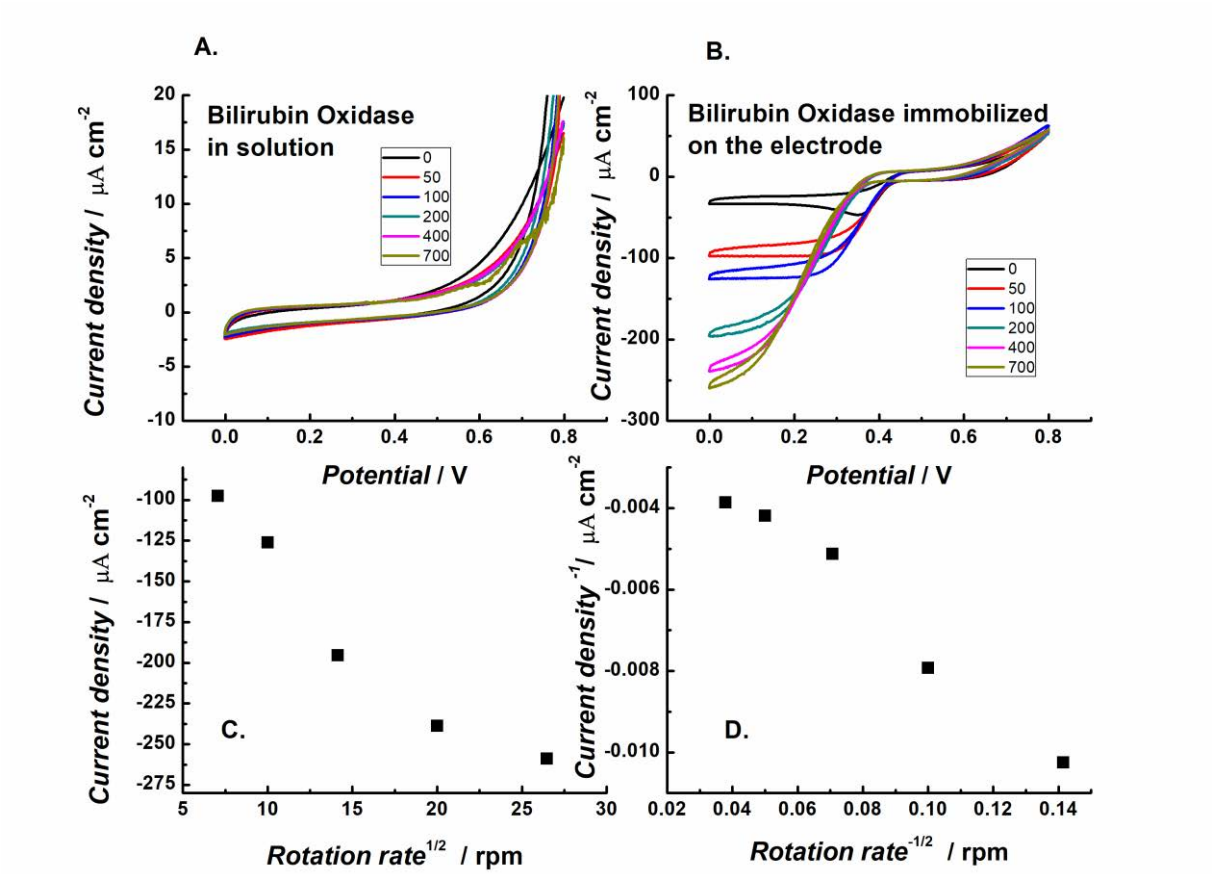

Figure 5.4.3.5 Cyclic voltammograms of oxygen reduction with Bilirubin Oxidase dispersed in the solution (A), Bilirubin Oxidase immobilized on the electrode surface (B), Levich dependency for the oxygen reduction on the electrode modified with carbon nanoparticles in TMA matrix (C) and Koutecký-Levich dependency for the oxygen reduction on the electrode modified with carbon nanoparticles in TMA matrix(D), limiting current taken at 0.0 V. Scan rate 2 mV s^{-1}.

We have also tried to investigate reduced graphene oxide as a supporting carbon like material for electrode surface modification. I performed the same type of modification and as in case of CNP modification checked the electrode efficiency for the enzyme catalyzed oxygen reduction. The plot 5.4.3.6 shows the electrode responses together with Levich and Koutecký-Levich plots. The maximal current calculated from Koutecký-Levich plot equals to -546 µA/cm^2. The variation between the maximum current densities for the different electrodes comes from the material used for the electrode surface modification, the amount of enzyme that adsorbs on the surface with proper orientation and the specific interaction between the electrode surface and the enzyme.

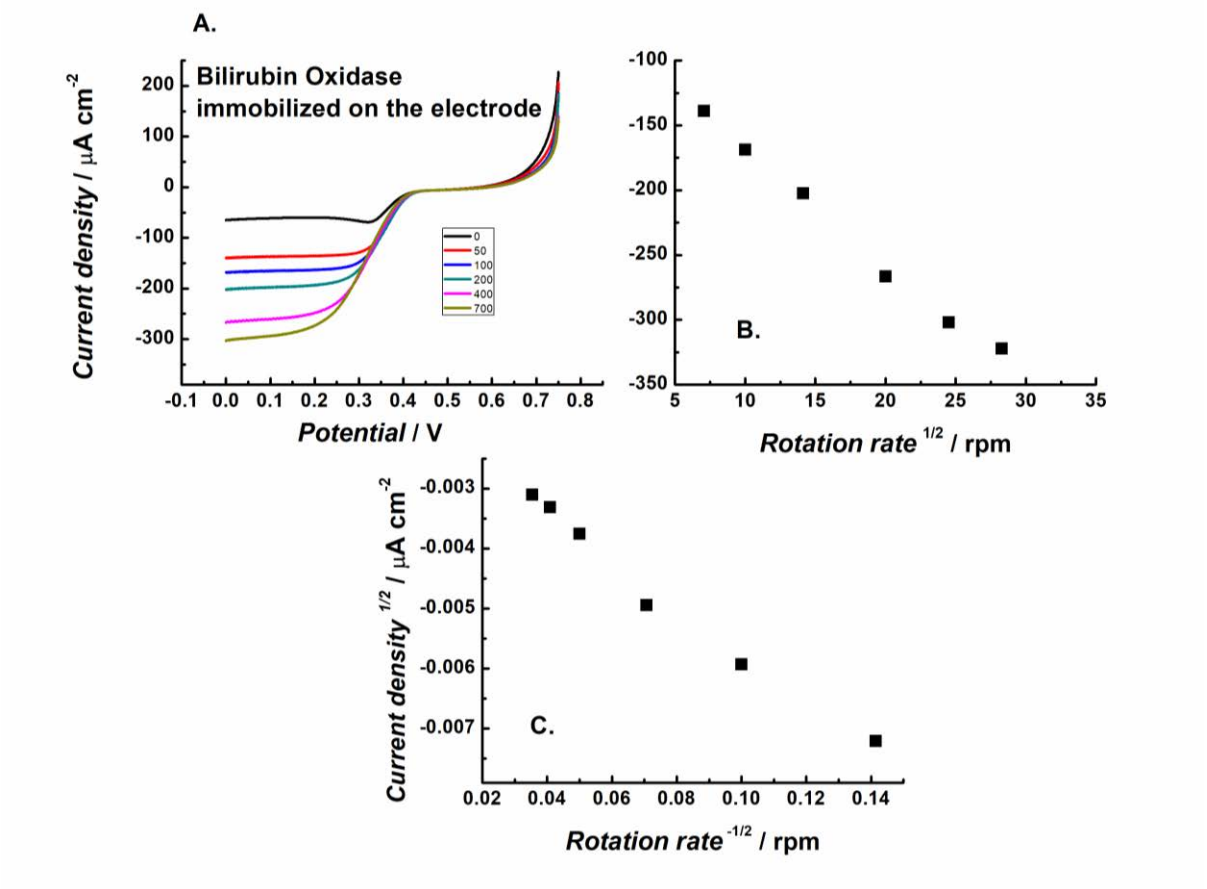

Figure 5.4.3.6 Cyclic voltammograms of oxygen reduction registered on ITO electrodes modified with reduced graphene oxide and Bilirubin Oxidase immobilized with TMA matrix with different rotation rates (A.), Levich (B.) and Koutecký-Levich dependency (C.) for the oxygen reduction on the electrode modified with reduced graphene oxide immobilized in TMA matrix, limiting current taken at 0.0 V. Scan rate 2 mV s^{-1}.

Rotating droplet system has been characterized as an instrument for enzymatic oxygen reduction. Fig. 5.4.3.7 shows comparison between the RD system utilizing ITO electrode and results obtained with (GC RDE). In both cases Bilirubin Oxidase was encapsulated on the working electrode surfaces with TMA sol-gel matrix. As a result, the signals registered with standard GC RDE (black curve on plots) in oxygen saturated electrolyte solution showed the oxygen reduction signals, where the cathodic current increase with rotation rate. For comparison, the same reaction but for air saturated solution was registered using the Rotating Droplet system (blue curve) and here also the cathodic current increase with increased rotation rate. Moreover, despite the more pore in oxygen electrolyte solution gave the higher cathodic current than in the standard beaker RDE case. Comparison with the oxygen saturated solution is shown as a red curve on the plot, where the significant increase of cathodic current can be observed. The inset presented on the plot 5.4.3.7 (D) shows Koutecký-Levich plot for oxygenated and aerated solution in RD system and oxygenated solution in the RDE system.

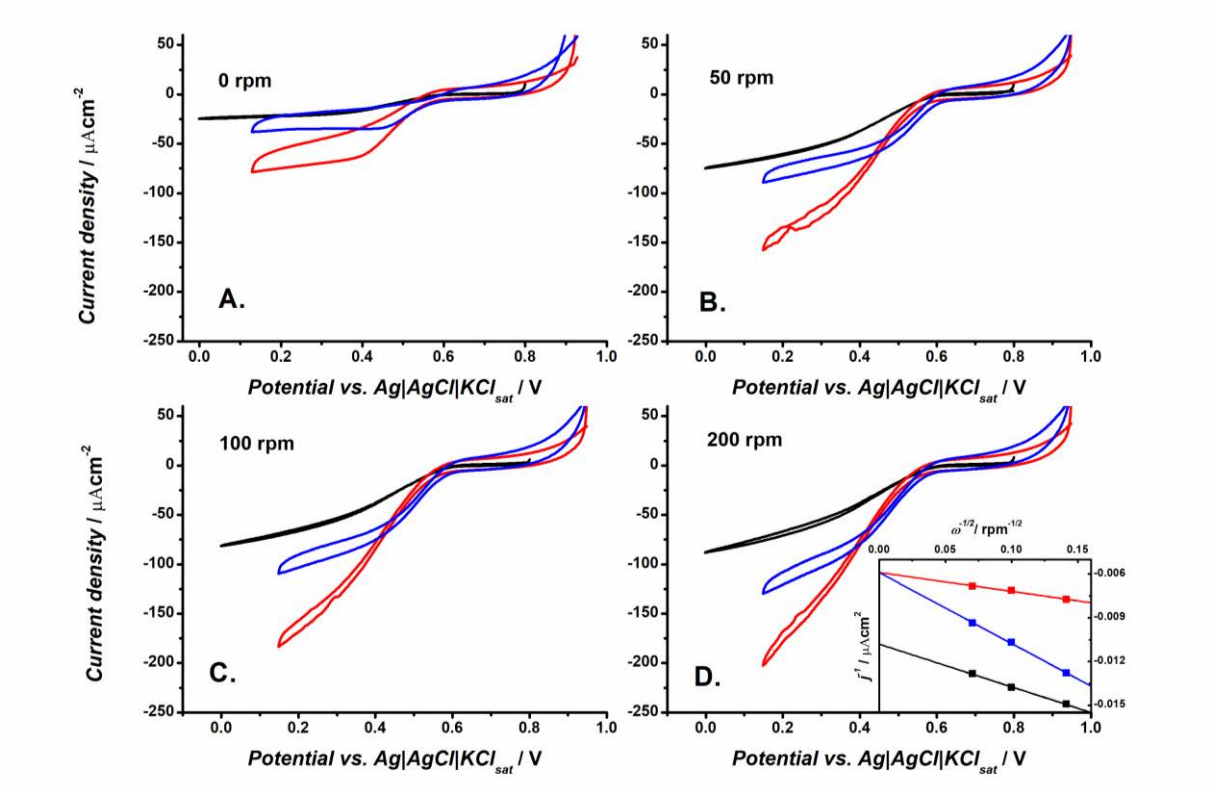

Figure 5.4.3.7 Cyclic voltammograms in 0.1mMPBS buffer pH 4.8 in air saturated solution on ITO electrode (blue curve), air saturated solution on glassy carbon RDE (black curve) and oxygenated solution on ITO electrode (red) with different rotation rates. BOx was immobilized on the electrodes. Koutecký-Levich plot for air and oxygenated solutions on RD and oxygenated solution on RDE. Scan rate 2 mV s-1, j taken at 0.2 V.

Data presented in the Fig. 5.4.3.7 show significant increase of the oxygen reduction reaction efficiency for the rotating droplet system in comparison with the standard RDE with the same electrode material modification applied in both cases. The behavior registered with RD system can indicate that the specificity of Rotating Droplet system geometry allow for better diffusion of gases through the droplet wall and bigger amount of the oxygen can reach the working electrode surface, where it consumed in reduction process.

Figure 5.4.3.8 presents the chronoamperommetric response of the Rotating Droplet system with ITO electrode modified with Bilirubin Oxidase and carbon nanoparticles, where the changing atmosphere around the droplet was measured. For the sake of this experiment only one rotation rate 50 rpm was checked. The Rotating Droplet system was enclosed in an external cylinder for a better control over the atmosphere around the droplet. The cylinder was filled with oxygen or argon. As presented in Fig. 5.4.3.8 (A) the change in atmosphere around the droplet resulted in immediate change of the current (the time for reversing the current was ca. 2 s). Fig. 5.3.4.8 (B) shows the difference in reaction time in systems with and without rotation with conserved manner

of changing the atmosphere around the droplet. As a result we can observe that the shape of chronoamperommetric curves is much sharper for the case with rotation applied, which indicated faster reaction for forced convective conditions.

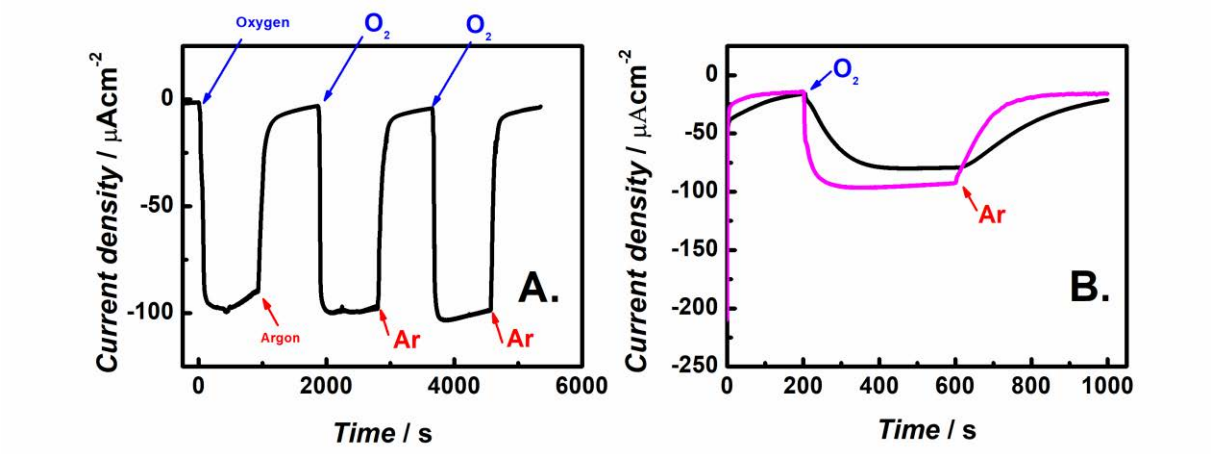

Figure 5.4.3.8 *Chronoamperommetric responses of ITO CNP BOX electrodes to changing atmosphere. In A with 50 rpm rotation, in B comparison between with (magenta) and without rotation (black). Adapted from II*

Both the open walls of the rotating droplet system and the forced convection inside are favorable for the oxygen reduction reaction inside the RD system, which exceeds the standard methods.

Conclusions

In this chapter I have presented the first part of the research devoted to optimization of the rotating droplet system and its utilization for oxygen reduction studies. The RD system utilize smaller sample volume than most electrochemical systems , and any flat electrode material can be used as a working electrode support. The open walls of the system and hydrodynamic condition inside the system favor the enzymatic oxygen reduction, while the enzyme is immobilized on the working electrode surface. The specific geometry of the droplet system helps with observation of fast atmosphere changing around the system and can be used as an oxygen sensor in the atmosphere. In combination with of other electrode modifications, the RD system could be used for detection of other compounds in the air.

Bibliography

II M. Kundys, W. Adamiak, and M. Jönsson-Niedziółka, “Rotating droplet as a new alternative for small volume electrochemical measurements,” *Electrochem. commun.*, vol. 72, pp. 46–49, 2016.

[1] L. Rassaei, M. J. Bonné, M. Sillanpää, and F. Marken, “Binding site control in a layer-by-layer deposited chitosan-carbon nanoparticle film electrode,” *New J. Chem.*, vol. 32, no. 7, pp. 1253–1258, 2008.

[2] G. Lota, K. Fic, and E. Frackowiak, “Carbon nanotubes and their composites in electrochemical applications,” *Energy Environ. Sci.*, vol. 4, no. 5, pp. 1592–1605, 2011.

[3] N. Cheng *et al.*, “One-step growth of 3-5 nm diameter palladium electrocatalyst in a carbon nanoparticle-chitosan host and characterization for formic acid oxidation,” *Electrochim. Acta*, vol. 55, no. 22, pp. 6601–6610, 2010.

[4] J. D. Watkins *et al.*, “Carbon nanoparticle surface functionalisation: Converting negatively charged sulfonate to positively charged sulfonamide,” *Phys. Chem. Chem. Phys.*, vol. 12, no. 18, pp. 4872–4878, 2010.

[5] M. Kundys *et al.*, “Electrochemical determination of selected neurotransmitters at electrodes modified with oppositely charged carbon nanoparticles,” *Anal. Methods*, vol. 6, no. 18, p. 7532, 2014.

[6] K. Szot, M. Jönsson-Niedziolka, E. Rozniecka, F. Marken, and M. Opallo, “Direct electrochemistry of adsorbed proteins and bioelectrocatalysis at film electrode prepared from oppositely charged carbon nanoparticles,” *Electrochim. Acta*, vol. 89, pp. 132–138, Feb. 2013.

[7] A. Zloczewska and M. Jönsson-Niedziolka, “Efficient air-breathing biocathodes for zinc/oxygen batteries,” *J. Power Sources*, vol. 228, pp. 104–111, 2013.

[8] E. Rozniecka, M. Jonsson-Niedziolka, J. W. Sobczak, and M. Opallo, “Mediatorless bioelectrocatalysis of dioxygen reduction at indium-doped tin oxide (ITO) and ITO nanoparticulate film electrodes,” *Electrochim. Acta*, vol. 56, no. 24, pp. 8739–8745, Oct. 2011.

[9] M. Jönsson-Niedziolka, A. Kaminska, and M. Opallo, “Pyrene-functionalised single-walled carbon nanotubes for mediatorless dioxygen bioelectrocatalysis,” *Electrochim. Acta*, vol. 55, no. 28, pp. 8744–8750, Dec. 2010.

[10] M. Kundys, W. Adamiak, and M. Jönsson-Niedziółka, “Rotating droplet as a new alternative for small volume electrochemical measurements,” *Electrochem. commun.*, vol. 72, pp. 46–49, 2016.

Chapter 6.
Generation-collection experiments in a Rotating Droplet system

6.1 Introduction

Utilization of a Rotating Droplet system to enzymatic oxygen reduction reaction was presented in the previous chapter. Here I would like to present a nonconventional way of application of the RD electrochemical setup. Generation-collection is a known field of research in electrochemistry. The principles of a generation-collection experiment are that in the same setup two working electrodes are used, one as a generator and second as a collector. When a potential is applied to the generator electrode, a certain reaction occurs. Simultaneously on the collector electrode a different potential is applied, which drives different electrochemical reaction. Properly chosen potential programs and parameters on both generator and collector allow to perform the following steps of the electrochemical reactions. Generation-collection experiments are used also to filter out other signals or to increase signal from a reversible reaction. There are known various systems which utilize this phenomenon. First approach to the generation-collection experiments was made in stationary conditions. Sanderson *et al.* performed the generation-collection experiments on double band electrodes separated from each other with a distance of 100 μm [1]. Further investigation of the generation-collection experiments was done by Amatore and coworkers who defined limiting current in such system as a function of the electrode width-to-gap ratio [2]. Later the system with alternately arranged numerous electrodes acting as generator and collector, called interdigitated electrodes was proposed [3], authors found that the efficiency of the system is mainly affected by the interelectrode gap width, the smaller the gap the higher the efficiency, caused by more efficient redox cycling. The interdigitated electrodes were shown to be useful for

filtering out the signal from weaker reductor in presence of the stronger due to the redox cycling Dam et. al [4]. Another known type of generation-collection systems are so called trench electrodes proposed by Dale et. al [5], for measurements of a local pH solution changing. The closely spaced electrodes were used in micro-fabricated nanochannels for detection of a single redox active molecules [6]. This detection of individual molecules was supported with numerical simulations and confirmed that the system can find a wide range of applications.

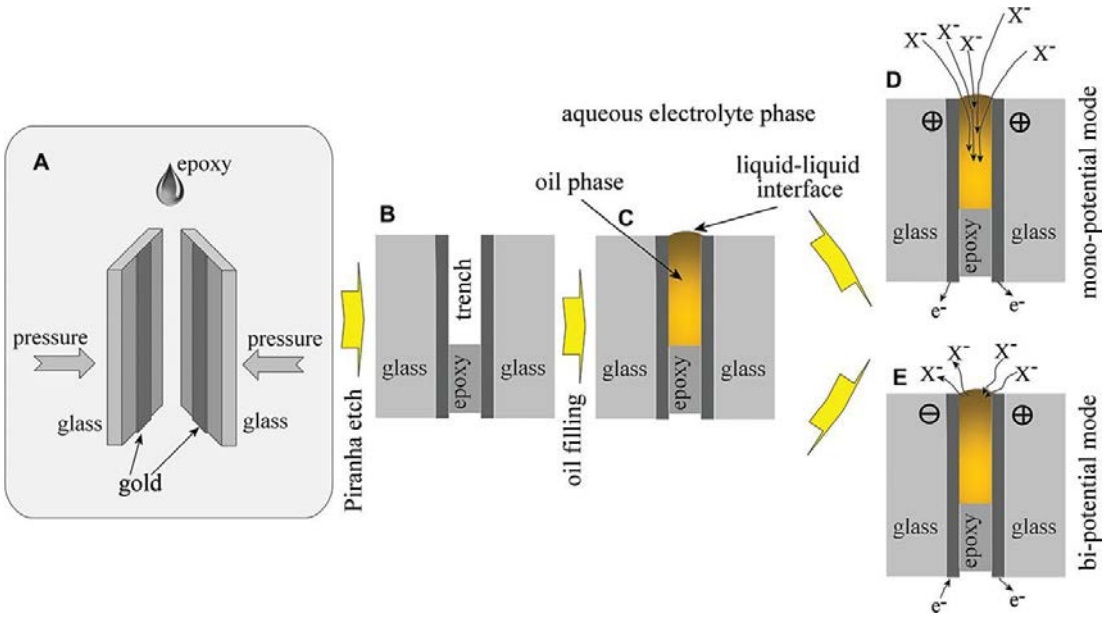

Figure 6.1.1 Schematic drawing of (A) the assembly of two gold electrodes, (B) trench formation with etching, (C) filling with redox active oil, (D) mono-potentiostatic anion transfer, and (E) bi-potentiostatic anion transfer. Adapted from [5].

There are also reports where the generation-collection systems are used in hydrodynamic conditions, such as microfluidic interdigitated electrode nanochannels proposed by Goluch et. al [7].

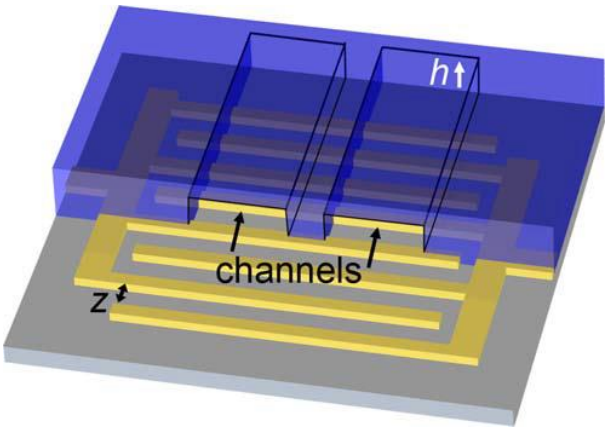

Figure 6.1.2 Schematic representation of a nanofluidic interdigitated electrodes system. Adapted from [7].

The most known example of generation-collection system is the Rotating Ring Disc Electrode (RRDE) described in Chapter 1 of this thesis. The RRDE system is used e.g. in the ORR to distinguish between 2- and 4- electron processes. A recent modification of this was presented by Ahn *et al.* [8], where they showed the rocking disc electrode.

The generation-collection systems based on the principle of the RDE system such as RRDE, Rocking Disc Electrode, and most of the presented examples are cases when bulk solutions of redox active species have been uses. This means that most of reagent after generator reaction diffuses to the bulk and never reaches the collector surface. In the following chapter of the dissertation I want to present a Rotating Droplet system used for generation-collection purpose, where the small droplet volume improves the performance of the system. The small sample volume prevents diffusion of products from the generator reaction to the bulk of solution.

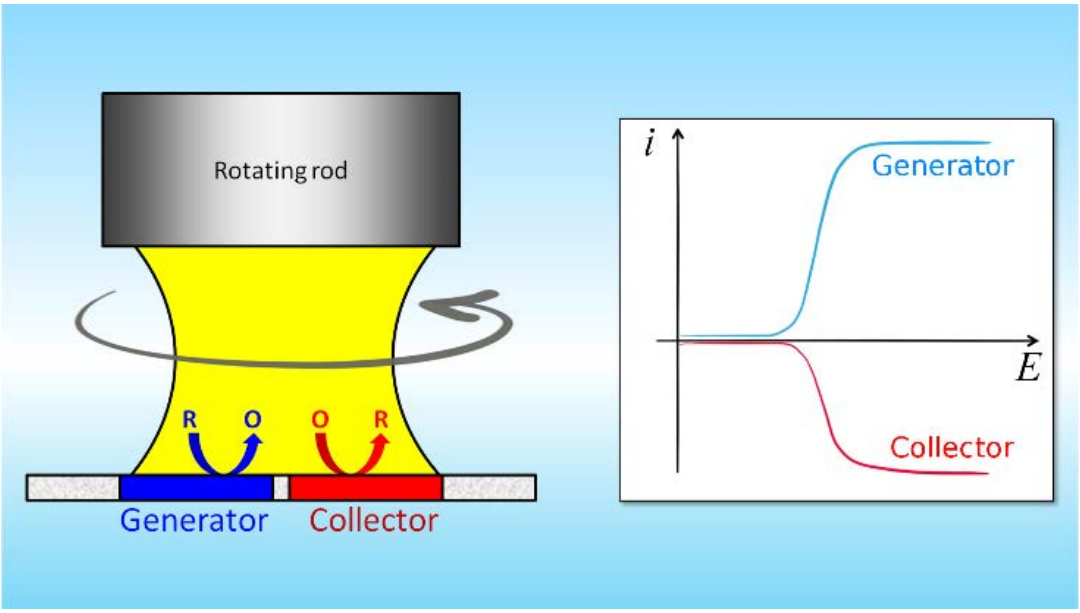

Figure 6.1.3 Schematic representation of the Rotating Droplet system in generation-collection experiment and the schematic results of generation-collection voltammetry

In order to obtain the two working electrodes in such small system, we took advantage of the flat surface and constructed working electrode setup on the bottom of the system. As it was mentioned in the previous chapter ITO electrode is a glass material covered with a thin layer of tin-doped indium oxide. The layer of ITO is 120 – 160 nm thick, because of that we tried to remove a narrow slit in the ITO cover to obtain two ITO electrodes separated by a small gap. Other properties of the system were preserved: the top electrode was a rotating ring-disc electrode with the disc covered with silver acting as reference electrode and the platinum ring acting as counter

electrode. Generation-collection experiments can be performed in different modes. The most commonly used is the CV-CA mode, where cyclic voltammetry is performed on the generator and chronoamperometry on the collector. The second mode often used is CA-CA, where both generator and collector are performing chronoamperommetric measurements. In this chapter, applications of both CV-CA and CA-CA modes are shown.

For a fair comparison of a certain generation-collection systems a parameter called collection efficiency was defined (mentioned already in Chapter 1) as the ratio between the total value of the collector current to the total value of the current on generator. Collection efficiency is often given as a % value.

6.2 Electrode surface modification

The working electrode surfaces described in this chapter were prepared by making a slit between the ITO electrodes on clean ITO surfaces. The first gaps I prepared by simply scratching of the ITO layer from the glass slide with a diamond knife. As a result I removed the 150 nm thick layer of ITO and created two separated ITO surfaces. The scratching method was fast, simple, but resulted in uncontrollable gap widths, in the majority of cases greater than 150 μm. Moreover, the curvature of the scratch was irregular which could result in wider and narrower gaps in different parts of the scratch, see Figure 6.2.1 (A). Because of those disadvantages I created ITO gaps with more accurate widths using photolithography. In this case the ITO / glass slide was covered with positive photoresist, later exposed to UV light, with application of an appropriate mask with an accurate gap width. In this procedure, the unprotected part of the ITO surface (the gap) was etched with the photoresist developer and as a result the gap between ITO surfaces was created. With application of photolithography, designed and more precise gap widths were obtained. However, the resolution of our masks was insufficient to create gaps smaller than 20 μm. Not -sharp edges are characteristic for the gaps prepared with photolithography, which makes it difficult to precisely measure the gap width under the optical microscope. Edges are visible as a yellow-orange lines in Figure 6.2.1 (B).

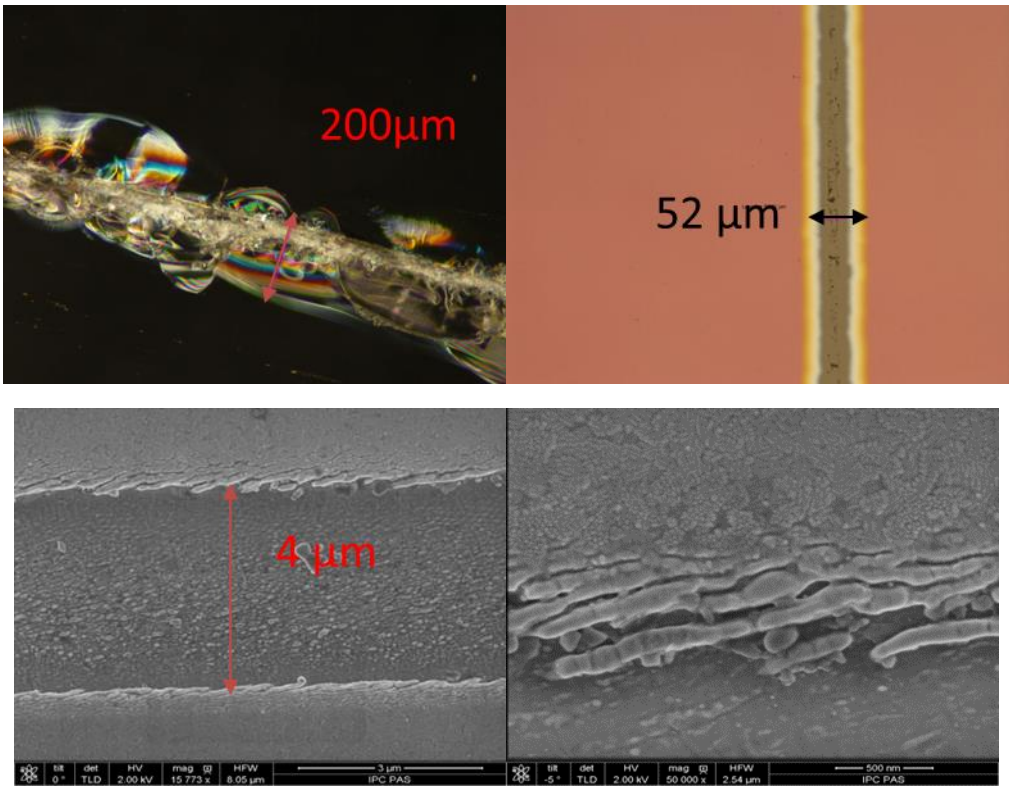

Figure 6.2.1 A. An optical microscope image of interelectrode gap between ITO electrodes fabricated by mechanical scratch on ITO, B. Optical microscope image of interelectrode gap between ITO electrodes fabricated by photolithography process, C. and D. SEM images of the interelectrode gap between ITO electrodes fabricated by the laser ablation technique and close-up of the edge of the gap.

In order to create precise and narrow gaps between the ITO electrodes we cooperated with the Laser Center at IPC PAS, where a technique for such cutting based on femtosecond laser ablation was already available. By using proper settings on the laser cutter, the ITO layer was evaporated from the glass support, which resulted in creating a gap between two ITO surfaces. With the application of the laser cutter, as narrow, as few µm interelectrode distance could be obtained with relatively sharp edges. Moreover, the whole range of the gap widths could be created. Figure 6.2.1 (C) shows the SEM image of the 4 µm wide interelectrode gap and (D) the edge of the melted ITO surface. The electrodes prepared in this way are used for majority of experiments presented in this chapter. Additionally, for detection of dopamine and epinephrine (shown in section 6.3.4) the ITO electrodes were covered with carbon nanoparticles in a sol-gel matrix based on TMA/TMOS precursor, described in electrode preparation in Chapter 5. With help of scanning electron microscopy, we performed a thorough analysis of the ITO modification with carbon nanoparticles (CNPs) immobilized with TMA/TMOS sol-gel matrix. The obtained coating

creates a quite homogenous and porous surface on the whole modification area. Some of the nanoparticles create aggregates visible as hills.

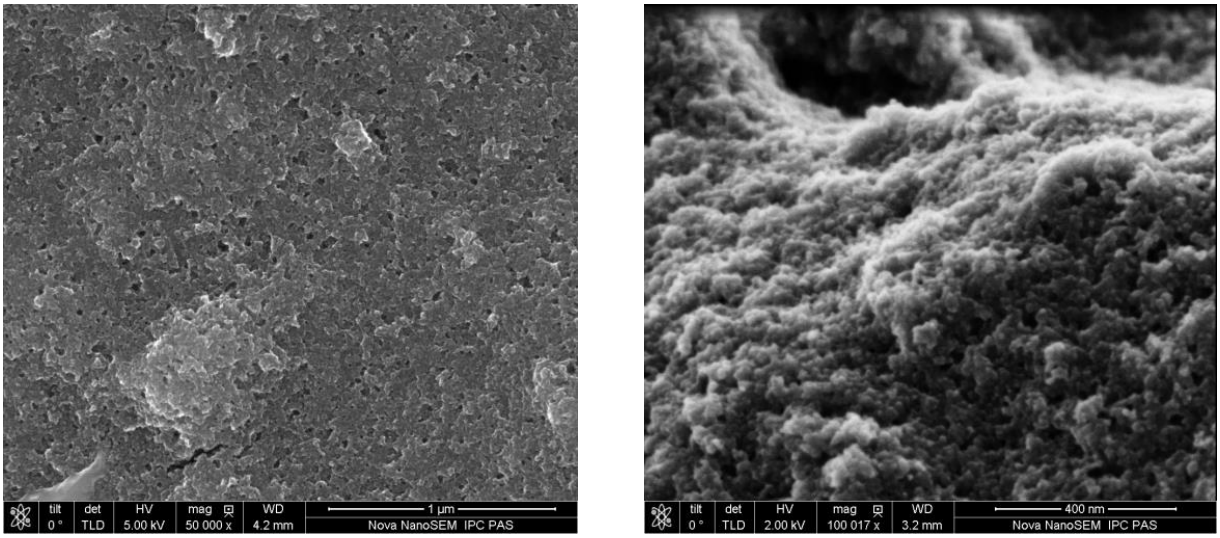

Figure 6.2.2 images of CNP-TMA modified ITO electrode surface.

The electrodes prepared in this way, due to the electrocatalytic properties of the CNPs enabled the neurotransmitters analysis.

6.3 Results

6.3.1 Generation-collection in RD and RRDE systems

The most often used system for investigation of generation-collection phenomena is Rotating Ring Disc Electrode (RRDE). Its principle was already shown in Chapter 1.2.2. In this section I would like to compare the results obtained with the Rotating Droplet system with the results from RRDE. $K_4[Fe(CN)_6]$ *in 0.1 M* KNO_3 was used in both sets of experiments, where CVs in a 0.6 V range were registered with changing rotation speed. Simultaneously on collector the CA was measured at a potential -0.1 V in the RDE system and -0.15 V in RD. The difference between potential applied comes from the utilization of the Ag|AgCl electrode for standard RRDE electrode and Ag pseudoreference electrode for RD system.

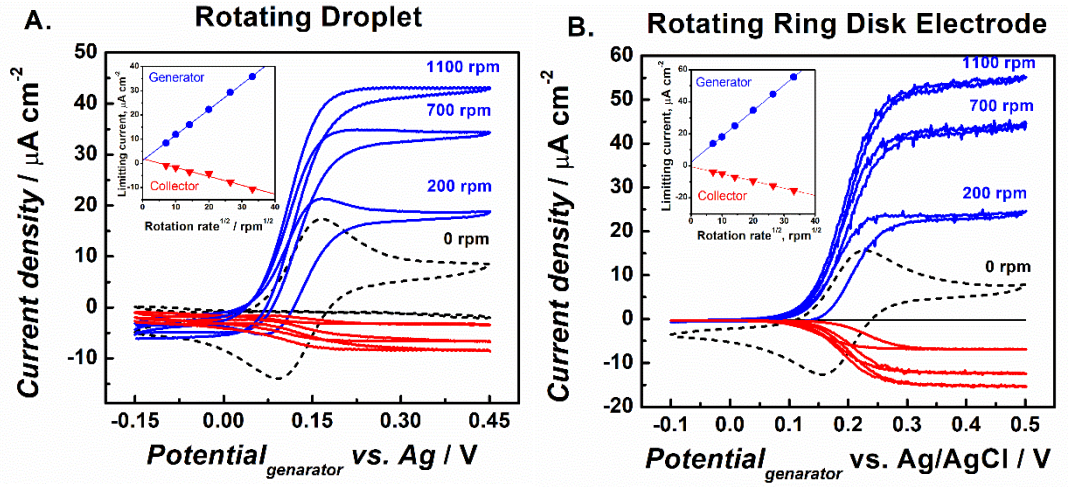

Figure 6.3.1.1 CV−CA signals for rotating droplet (RD; A) and rotating ring disk electrode (RRDE; B) at different rotation rates. The insets show Levich plots for the generator and collector limiting currents as a function of the square root of the rotation rate. The scan rate of the CV was 25 mV/s. The solution was 1 mM $K_4[Fe(CN)_6]$ in 0.1 M KNO_3. The generator−collector distance was 18 μm in RD and 1 mm in the commercial RRDE tip. The collector CA potentials were −0.15 and −0.1 V for RD and RRDE methods, respectively. Adapted from III. (C.)

As it is shown in Figure 6.3.1.1, the current on the generator electrode increases as expected with the increase of the rotation rate. The increase of the generator current is followed by an increase of collector current. The observed behavior of generator-collector setup is identical for both RD and RRDE systems. Insets included in Figure 6.3.1.1 (A) and (B) show the linear Levich dependency of both generator and collector.

6.3.2 Generation–collection experiment in RD system: visualization with electrochromic measurements

One of the simplest generation collection experiments is performed in CV-CA mode, where cyclic voltammetry is applied to generator and the reaction product reacts on collector electrode at certain applied potential. Results obtained using CV-CA mode were shown already for comparison between the RD generation-collection system and standard RRDE in Figure 6.3.1.1.

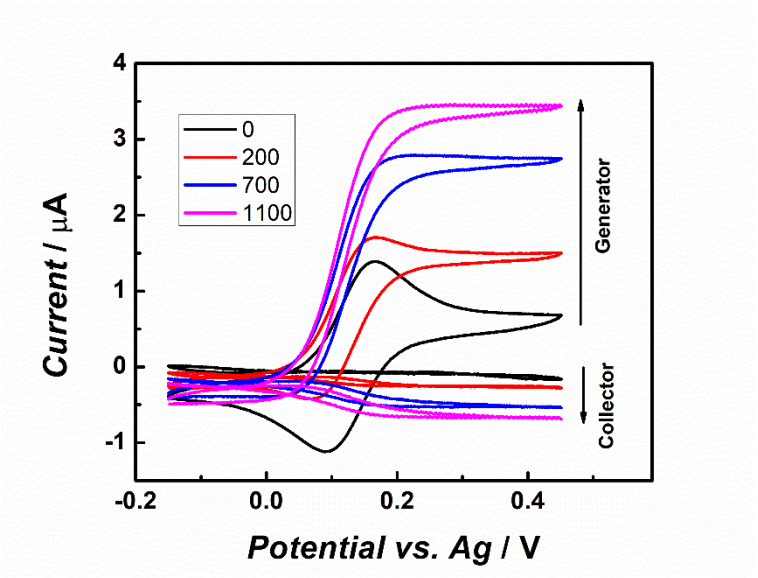

Figure 6.3.2.1 CV−CA signals for rotating droplet at different rotation rates. The scan rate of the CV was 25 mV/s. The solution was 1 mM $K_4[Fe(CN)_6]$ in 0.1 M KNO_3. The generator−collector distance was 18 μm. The collector CA potentials was −0.15 V.

Figure 6.3.2.1 shows a typical program of cyclic voltammetry registered on generator and chronoamperometry registered on collector program for $K_4[Fe(CN)_6]$ in 0.1 M KNO_3, on unmodified ITO-ITO generator-collector electrodes, where the interelectrode distance was 18 μm. The increasing current on generator creates more product, which due to the applied potential can be consumed on the collector. CV-CA mode was also used for visualization of RD generation-collection system shown below (figure 6.3.3.1).

In order to show the mass transport of the product from the generator to the collector I performed a set of experiments with oxidation of an electrochromic redox probe 1 mM ABTS in 0.1 M KCl solution. In the experiment shown in Fig. 6.3.2.2 (A) only the generator was turned on. As a result, the transparent $ABTS^{2-}$ was oxidized and the greenish ABTS was created. Because of the rotation, the generator product is transported to the whole volume of the droplet. Fig. 6.3.2.2 (B) presents the situation when the generator product (ABTS) is transported to the droplet volume, but the collector is ON. As a result, the product of generator reaction can be regenerated on the collector, visible as a light shadow after depletion of the green ABTS.

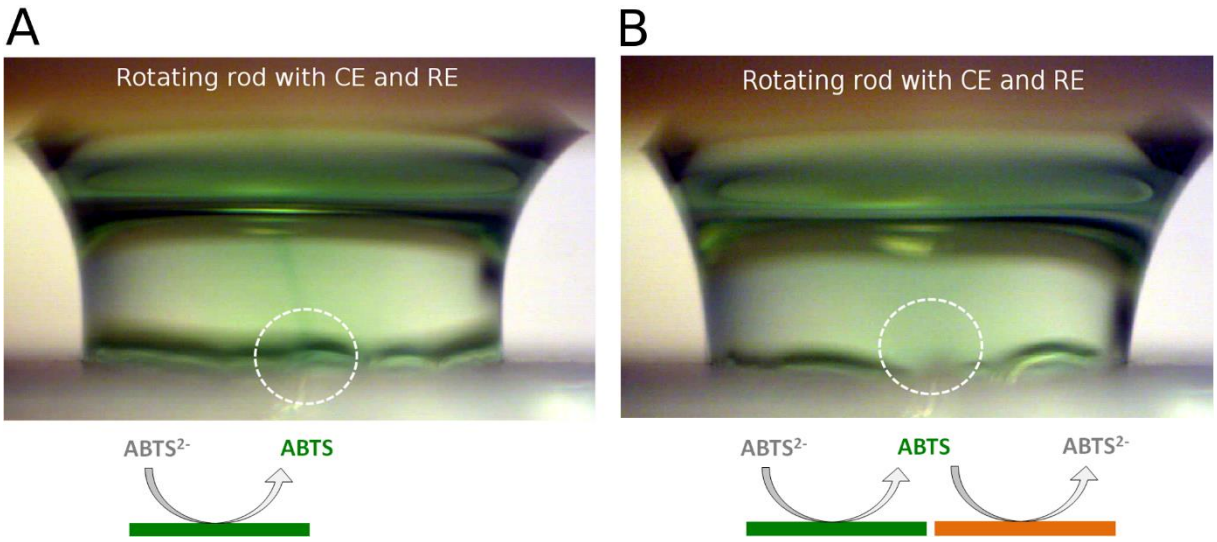

Figure 6.3.2.2 Photographs of ABTS2− oxidation to ABTS inside the rotating droplet when the collector is OFF (A) and when the collector is ON (B). The rotation rate was 200 rpm. The circles indicate the interelectrode gap between the generator and the collector.

Application of the generation-collection system is shown also in terms of collector enhancement of ABTS reactions. The electrochemical data shown in Fig. 6.3.2.3 is registered in CV-CA mode. A plot shown in Fig. 6.3.2.3 as red curves represents signals in the system where only generator works, and black curves correspond to the system, where both generator and collector are ON.

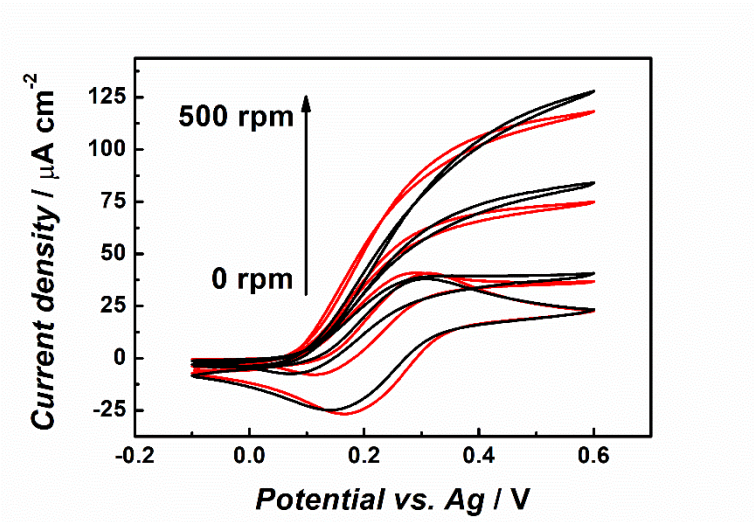

Figure 6.3.2.3 Cyclic voltammetry of 1 mM ABTS in 0.1 M KCl solution oxidation. Red curves are for generator only, black are for the collector regeneration at - 0.1 V. For various rotation rate of: 0, 50, 200, 500 rpm. Scan rate 25 mV/s.

It is visible that application of a collector electrode enhances the generator current signal a little. In the next sections I will describe a systematic investigation on the influence of the gap width

and rotation rate on the efficiency of the generation-collection experiments, and application of the system to neurotransmitter detection.

6.3.3 Investigation of the collection efficiency in RD system

Application of the CV-CA mode shown for redox probe and ABTS oxidation (Fig. 6.3.2.1 and 6.3.2.3) results in poor collection efficiency of ca. 19%. Much higher collection efficiency can be obtained with application of a CA-CA mode, in the same system with application CA-CA mode collection efficiency ca. 40 % can be reached. For these systematic studies I used an RD system where on both generator and collector chronoamperometry with constant potential was measured. As above, the redox probe 1 mM $K_4[Fe(CN)_6]$ in 0.1 M KNO_3 was oxidized on the generator (0.6 V applied), whereas on collector (-0.15 V) the reversible reaction occurred.

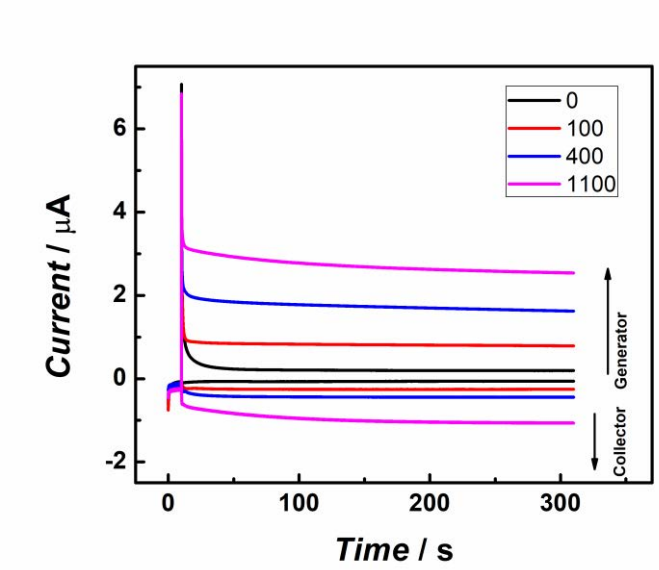

Figure 6.3.3.1 CA−CA signals for rotating droplet at different rotation rates. The solution was 1 mM $K_4[Fe(CN)_6]$ in 0.1 M KNO_3. The generator−collector distance was 18 μm. The generator CA potentials were 0.6 V vs Ag. The collector CA potentials were −0.15 V vs. Ag .

In Fig. 6.3.3.1 we can observe the increasing generator current as a function of the increasing rotation rate in combination with an increasing collector current. The collector signal is related to the amount of products created on the generator that can be consumed on the collector electrode. The ratio between the total collector current and generator current was taken at 200 s, giving the current enough time to stabilize. The dependency of the gap width and rotation range on the collection efficiency is shown in Fig. 6.3.3.2. . One can clearly see that the collection efficiency is a function of both the gap width and the rotation rate.

The systematic study on the Rotating Droplet generation-collection experiments with a various interelectrode gap and various rotation rate gave an overview on the usage of the RD system. Fig.

6.3.3.2 shows the collection efficiency of the generation –collection experiments performed by registering the chronoamperometric signals on both the generator and the collector. As mentioned before, the electrode reaction was the oxidation of 1 mM $K_4[Fe(CN)_6]$ in 0.1 M KNO_3 on the generator at 0.6 V and the reduction of the oxidized products on the collector at -0.15 V. The data shown below is a result of the series of experiments performed for generation-collection Rotating Droplet system with different gap widths of 3, 18, 33, 150, 325, 415, 487 µm prepared with laser ablation and one gap prepared with simple scratching of the ITO surface with the diamond knife.

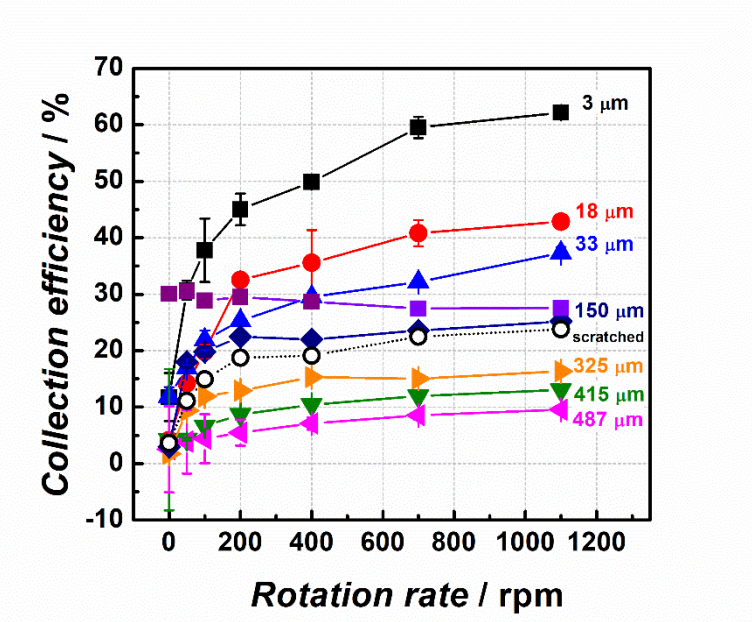

Figure 6.3.3.2 Collection efficiencies obtained for different generator − collector distances, plotted as a function of the rotation rate. Adapted from III.

Each of investigated gap widths was tested with the same range of the rotation rates applied to the RD system. As a result, we can see the collection efficiency dependency as a function of rotation rates and interelectrode gap widths. The faster the rotation and the smaller the interelectrode gap width the higher the collection efficiency. For the most optimal (1100 rpm and 3 µm of gap width) conditions collection efficiency reaches over 63 %, which is more than double as much as in the case of the standard RDE. The obtained high collection efficiency parameter is the result of the small droplet (reactor) volume and the very close proximity between the generator and the collector. Within a 70 µl volume the products from generator reaction can be transported quickly to the collector, where they can be further consumed. Presented data prove the uniqueness of the RD system as a new generation-collection system.

6.3.4 Generation-collection enhancement of neurotransmitters detection

In the following subchapter I would like to present the data concerning the application of the RD generation-collection system for the analysis of neurotransmitters. I investigated presence of

dopamine (DA) and epinephrine (EP) in presence of common interferents such as ascorbic (AA) and uric (UA) acids. The electroactive neurotransmitters such as DA and EP are known to have an oxidation potential similar to each other and their concomitant interferents. Typically, signals detected with unmodified electrodes, from a solution containing DA or EP and UA and AA mixture, are undistinguishable, as visible in the inset plot in Fig. 6.3.4.2.

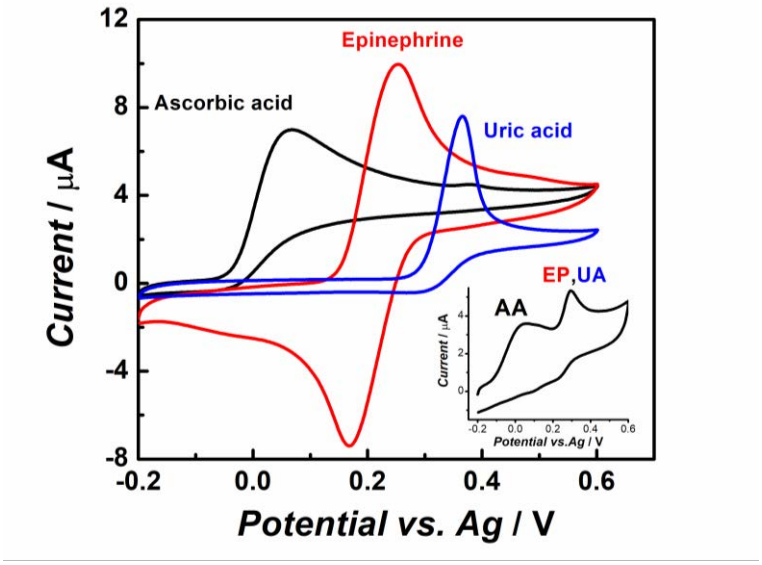

Figure 6.3.4.2 Cyclic voltammograms of 1 mM ascorbic acid, 2 mM epinephrine and 1 mM uric acid recorded in RD at 0 rpm on CNP-TMA-modified generator electrode. Inset: Cyclic voltammogram recorded in the mixture of 1 mM AA, 2 mM EP, and 1 mM UA at 0 rpm at non-modified electrode. Adapted from III.

Modification of the ITO surface with CNPs allows for distinguishing the signals from different components of the mixture. The biggest advantage visible on the main part of Figure 6.3.4.2 is that signal from epinephrine is shifted ca. 100 mV towards more negative potentials, which enables to separate signals form EP and UA. Data presented above shows significant feature - reversibility of the EP signal and irreversible oxidation on the AA and UA. I decided to perform the set of experiments in order to filter out signals from interferents while the EP signal would be regenerated on the second working electrode. The oxidation potential (0.6 V) applied to the generator electrode caused the irreversible oxidation of both AA and UA, and oxidation of EP, while reductive potential (-0.2 V) applied to the collector enabled regeneration of EP, which could be consumed on the generator again, data presented on plot 6.3.4.3 (A) for 1100 rpm rotation rate and 18 μm gap width.

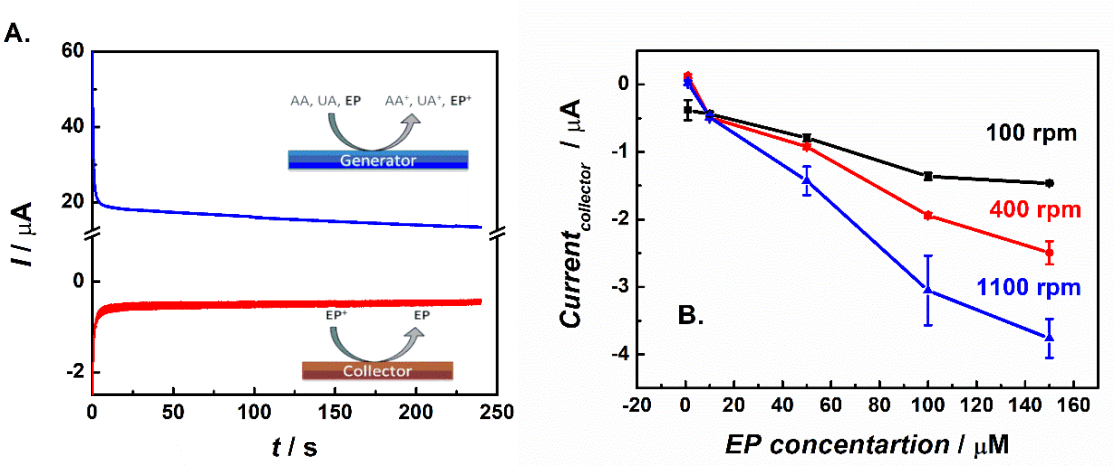

6.3.4.3 (A) Typical chronoamperograms (CA−CA signals) recorded on the generator and collector at 1100 rpm for 10 μM EP, 0.5 mM AA, and 0.5 mM UA. The generator and collector potentials were 0.6 and −0.2 V, respectively. The inset shows the mechanism of filtering out the interferents. The generator−collector distance was 6 μm. (B) Dependence of the collector limiting current on the EP concentration for different rotation rates. Adapted from III.

The same set of generator and collector electrodes was used for investigation of the concentration of EP which can be collected and regenerated on the collector. As a result, shown in plot 6.3.4.3 (B), the increase of the collector current as a function of increasing EP concentration and increasing rotation rate is visible.

Both electroactive neurotransmitters dopamine and epinephrine are characterized by reversible redox reactions.. In order to compare the systems with generator electrode and with generator and collector, a set of chronoamperommetric experiments was performed. Data presented in Fig. 6.3.4.4 (A) and (B) shows CA signals registered at 200s. The black plots show the signal for generator only, while the red plots show signals for the generator and collector experiments. Both for EP and DA, the signals registered on the generator were higher when the collector was ON. This indicates that the neurotransmitters are indeed regenerated on the collector. Moreover, for EP the enhancement of the generator signal increases with the increasing rotation rate.

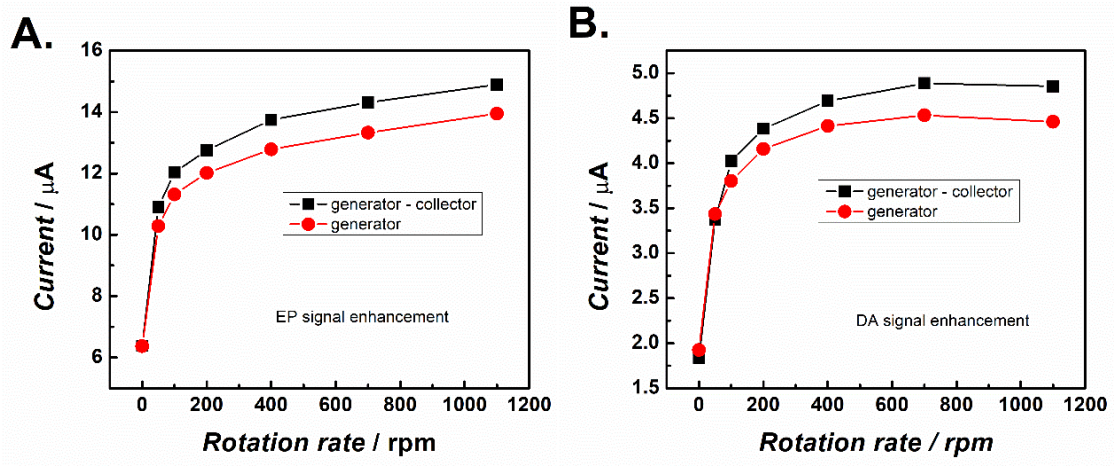

Figure 6.3.4.4 Generator and generator-collector signals for neurotransmitters signals enhancement epinephrine (A) and dopamine (B). Generator potential signal taken at 200 s.

Dopamine is a neurotransmitter known for its complicated electrochemistry with a tendency to polymerization at neutral pH. Fig. 6.3.4.4 (B) shows that the enhancement curvature is reaching a maximum, and starting to decrease after 700 rpm, which can indicate blocking of the working electrode surface by polymerized dopamine. In contrast, the signal from epinephrine keeps increasing with increasing rotation rate.

I performed a similar set of experiments using serotonin and the common interferents uric and ascorbic acids, expecting enhancement of the serotonin signal among the interferents, similarly to the case with EP and DA. Unfortunately, no enhancement of the serotonin oxidation signal in this type generation-collection system was seen. The complex, multistage electrochemistry of serotonin, as will be explained in chapter 7, was probably the reason for this.

Conclusions

In this chapter I presented a small volume Rotating Droplet generation-collection system. The RD generation-collection system was tested in a wide range of rotation rates and the gap widths. In the smaller the gap width and the faster the rotation rate is applied, the bigger collection efficiency in the system. I successfully used the RD generation-collection system for filtering out the interferents signal and enhancement of the oxidation signal for dopamine and epinephrine.

Bibliography

III M. Kundys, M. Nejbauer, M. Jönsson-Niedziolka, and W. Adamiak, “Generation–Collection Electrochemistry Inside a Rotating Droplet,” Anal. Chem., vol. 89, no. 15, pp. 8057–8063, Aug. 2017.

[1] D. G. Sanderson and L. B. Anderson, “Filar Electrodes: Steady-State Currents and Spectroelectrochemistry at Twin Interdigitated Electrodes,” *Anal. Chem.*, vol. 57, no. 12, pp. 2388–2393, 1985.

[2] B. Fosset, C. A. Amatore, J. E. Bartelt, A. C. Michael, and R. Mark Wightman, “Use of Conformal Maps To Model the Voltammetric Response of Collector-Generator Double-Band Electrodes,” *Anal. Chem.*, vol. 63, no. 4, pp. 306–314, 1991.

[3] O. Niwa, M. Morita, and H. Tabei, “Electrochemical Behavior of Reversible Redox Species at Interdigitated Array Electrodes with Different Geometries: Consideration of Redox Cycling and Collection Efficiency,” *Anal. Chem.*, vol. 175, pp. 447–452, 1990.

[4] V. A. T. Dam, W. Olthuis, and A. Van Den Berg, “Redox cycling with facing interdigitated array electrodes as a method for selective detection of redox species,” *Analyst*, vol. 132, no. 4, pp. 365–370, 2007.

[5] S. E. C. Dale, Y. Chan, P. C. Bulman Page, E. O. Barnes, R. G. Compton, and F. Marken, “A gold-gold oil microtrench electrode for liquid-liquid anion transfer voltammetry,” *Electrophoresis*, vol. 34, no. 14, pp. 1979–1984, 2013.

[6] M. A. G. Zevenbergen, P. S. Singh, E. D. Goluch, B. L. Wolfrum, and S. G. Lemay, “Stochastic sensing of single molecules in a nanofluidic electrochemical device,” *Nano Lett.*, vol. 11, no. 7, pp. 2881–2886, 2011.

[7] E. D. Goluch, B. Wolfrum, P. S. Singh, M. A. G. Zevenbergen, and S. G. Lemay, “Redox cycling in nanofluidic channels using interdigitated electrodes,” *Anal. Bioanal. Chem.*, vol. 394, no. 2, pp. 447–456, 2009.

[8] S. D. Ahn, P. E. Frith, A. C. Fisher, A. M. Bond, and F. Marken, “Mass transport and modulation effects in rocking dual-semi-disc electrode voltammetry,” *J. Electroanal. Chem.*, vol. 722–723, pp. 78–82, 2014.

Chapter 7.
Simultaneous neurotransmitters detection in the Rotating Droplet system

7.1 Introduction

It has been already shown that the Rotating Droplet (RD) system can be utilized for various purposes, such as the detection of gaseous components (Chapter 5), signal multiplication in generation-collection experiments (Chapter 6) or for filtering out the interferents signal while detecting neurotransmitters (Chapter 6). In the following chapter I would like to present the use of the RD system to simultaneous detection of many neurotransmitters in a small volume sample and in the presence of interferences. Data presented in this chapter is especially precious for me not only because the experiments shown here were performed within my own grant, but also due to its proximity to the field of human healing, which has always been my dream mission. Conventional neurotransmitter detection has been thoroughly described in Chapter 2 of this thesis. A number of different methods for analysis of the concentration of neurotransmitters already exists. However, the problem of large sample volume or the problem of low resolution in order to discriminate between many neurotransmitters still needs a solution.

7.2 Rotating Droplet setup configuration

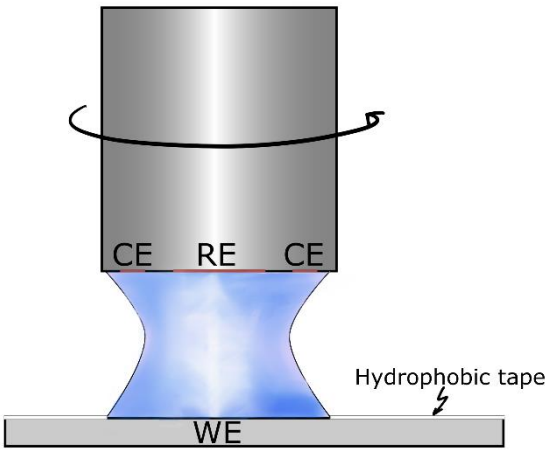

Figure 7.2.1 Schematic representation of the Rotating Droplet system. Adapted from V.

The Rotating Droplet system has been used as previously, where the bottom electrode acts as a working electrode surface and the upper RRDE tip disc as a reference electrode and the ring as a counter electrode. Between the bottom and the upper surfaces the 70 µL sample is gently placed. As a result, the hyperbolical shape of the droplet is created, the rotation of the disc-ring tip enforces rotation of the droplet.

Electrode preparations

The ITO electrode was used as an electrode support. It was first cleansed with a sonic bath in acetone, isopropanol, ethanol and distilled water, 15 min in each solution. Later it was dried with compressed air, in order to remove the water residues. Then the electrode substrate was masked with hydrophobic tape to get a few electrodes of the same area on the same ITO slide. Each electrode spot (black areas in Fig. 7.2.2.) was used only once, and for that reason they were prepared differently than shown previously in Chapters 5 and 6. Later ITO supports were covered with carbon nanoparticles (CNPs) in TMA/TMOS sol-gel matrix, as described already in Chapter 5 of this thesis. However, here we used various methods for modification such as: dip coating, drop coating, and spin coating. The obtained surfaces were characterized by different coverages. We were able to overcome the differences in the coverage by application of ozone treatment. This technique is known to make surfaces more hydrophilic. Additionally, activation of the ITO external hydroxylic groups facilitates binding of the silica matrix used for encapsulation of the carbon material. ITO clean slides were exposed to the ozone lamp for 15 minutes, and later masked with the Teflon tape and covered with the CNPs in the sol-gel matrix.

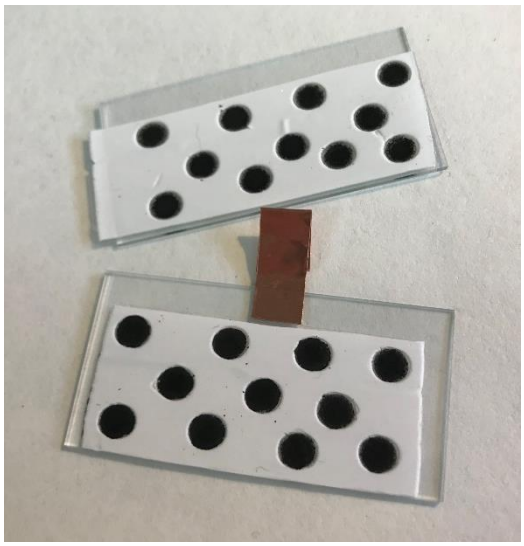

Figure 7.2.2 Photograph of the electrode used for experiments in neurotransmitters detection - electrode support masked with Teflon tape and modified electrode spots. Adapted from V.

7.3 System characterization

The electrode surfaces modified with different techniques were investigated with scanning electron microscopy to determine the homogeneity of the surface coverage with carbon nanoparticles. In Figure 7.3.1 electrodes prepared by dip coating, spin coating, or drop coating are presented. The SEM photograph shown in Figure 7.3.1 is characterized by similar coverage to the one where the electrode material was situated with additional treatment with organic solvents (Fig. 6.2.2). This observation may prove that there is no need for long electrode preparation procedure, as it was done for previous chapter's experiments.

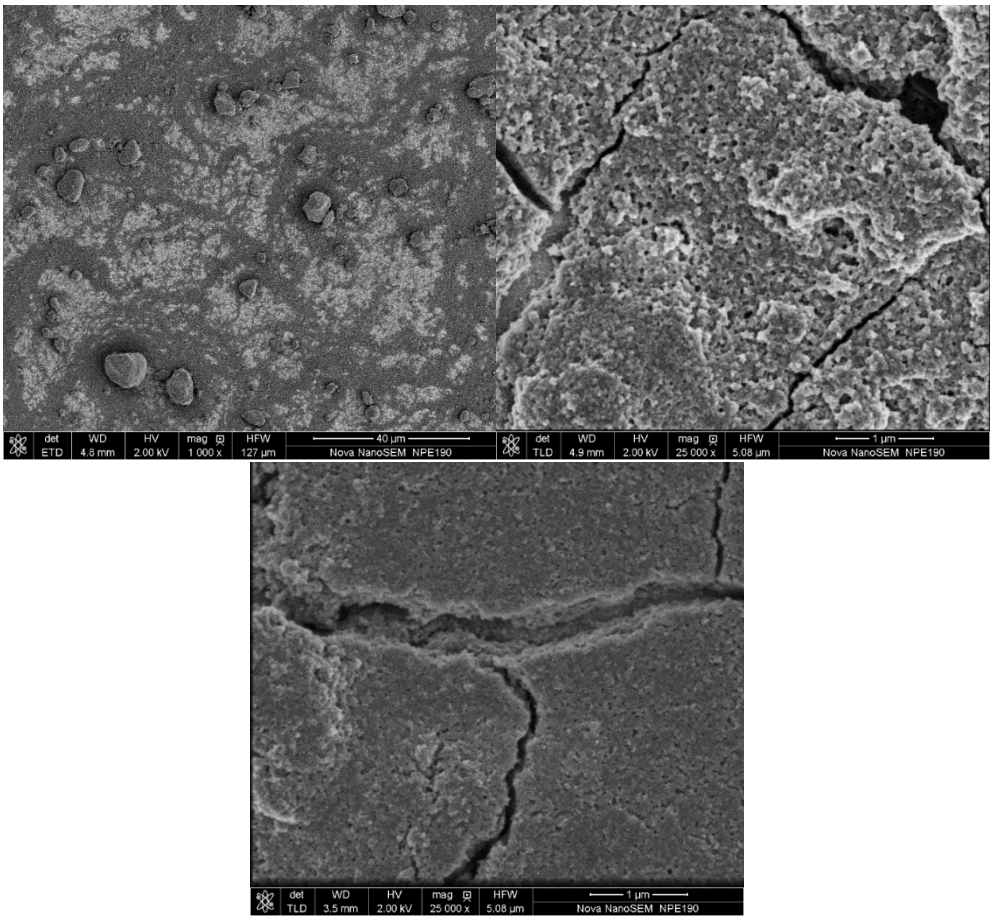

Figure 7.3.1 The SEM images of the ITO CNPs in TMA sol-gel matrix modified with (A) dip coating without ozone pretreatment, (B) using drop coating method on an ozone treated ITO support material (C) spin coating, without ozone pretreatment. Adapted from Supplementary Information in publication V.

Figure 7.3.1 (A) shows the ITO support modified with dip coating without the ozone pretreatment. The coverage of the surface with CNPs is not total and some light gray areas indicate the uncovered ITO surface. The best coverage was performed with application of drop coating or spin coating on the surface treated with ozone. Porous surface fully covers the ITO support. For the next experiments I used electrodes prepared by drop-coating of the CNPs encapsulated in sol-gel matrix on ozone pretreated surfaces of ITO supports. These electrodes assure mechanical stability of carbon material under hydrodynamic conditions.

I investigated the coverage of the electrode surface with the carbon nanoparticles in the TMA/TMOS sol-gel silica matrix electrochemically.

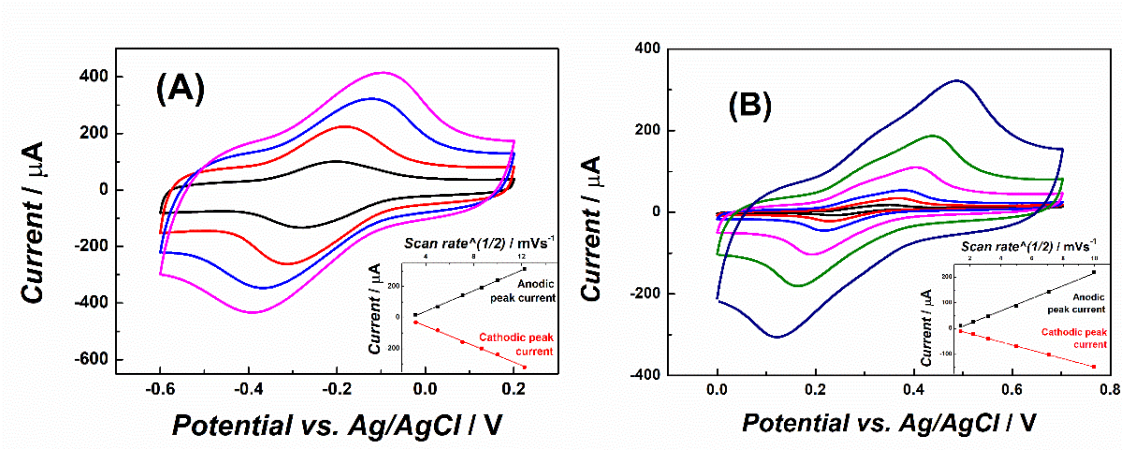

Figure 7.3.2 Cyclic voltammograms of (A) 1 mM $Ru(NH_3)_6Cl_6$ in 0.1 M KCl, (B) 1 mM Dopamine in 0.1 M PBS registered with variable scan rate. The insets show current as a function of the square root of the rotation rate. Adapted from Supplementary Information in publication V.

Data shown in Figure 7.3.2 presents the ITO CNPs TMA/TMOS electrodes responses in (A) 1 mM $Ru(NH_3)_6Cl_6$ in 0.1 M KCl, (B) 1 mM Dopamine in 0.1 M PBS for wide range of scan rates. Insets show the current as a function of a square root of the scan rate. The linear dependency between the peak current and the square root of scan rate indicate that the reaction performed on this electrode is controlled by diffusion only. Diffusion limitations can easily be overcome by application of forced convection systems such as the RD system.

7.4 Results

First tests were performed to check whether it was possible to simultaneously detect multiple neurotransmitters and interferents. Components of the sample were tested with square wave voltammetry as shown in Figure 7.4.1. Samples containing dopamine (A), serotonin (B) or both dopamine and serotonin (C) together with common interferents such as uric and ascorbic acids, in phosphate buffer saline pH 7.4 were tested in various range of neurotransmitters concentrations. Utilization of the electrodes modified with carbon nanoparticles enabled distinguishing between components of mixtures, which was shown already for detection of epinephrine (Fig. 6.3.2.1). The good separation between peaks allowed for simultaneous detection of the two neurotransmitters and two commonly occurring interferents.

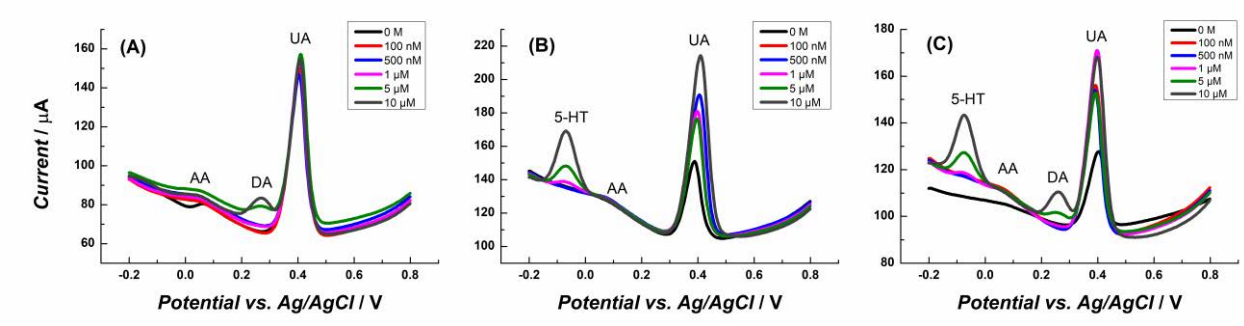

Figure 7.4.1 Square wave voltammograms registered on ITO modified with CNP(-) TMA/TMOS in solution of 0.5 mM UA and AA in 0.1 M phosphate buffer pH 7.4 in stationary system containing various concentration of (A) DA, (B) 5-HT and (C) both DA and 5-HT. Adapted from V.

Simultaneous detection of DA, 5-HT and UA, AA was tested in stationary conditions, where no convection was applied. The results obtained during the measurements showed that in stationary conditions the limit of detection for dopamine is 5 µM and for serotonin is 1 µM. The obtained limits of detections are high and not sufficient for objective analysis. Therefore, I performed further analysis with application of hydrodynamic conditions with using of the Rotating Droplet system, data shown in Figure 7.4.4.

Data presented in Figure 7.4.1 (B) and (C) is biased with the change of the peak height described as a UA oxidation. We found out that the peak from the uric acid oxidation registered in the presence of the serotonin must have been affected by the 5-HT itself. In order to investigate the influence of 5-HT on the UA signal I performed a set of experiments where the 5-HT solution was scanned. Figure 7.4.2 (A) shows the cyclic voltammograms (1st, 5th, 10th, 15th, and 20th scans) and (B) square wave voltammograms (1st, 5th, 10th, 15th, and 20th scans) of 10 µM serotonin dissolved in 0.1 M phosphate buffer saline pH 7.4. Both cyclic voltammograms and square wave voltammograms show the double peak which comes from the serotonin oxidation. The 5-HT oxidation peak observed at ca. +0.38 V (Figure 7.4.2) is exactly at the position of the UA oxidation peak in Figure 7.4.1. This observation explains the shift of the peak height in case of UA.

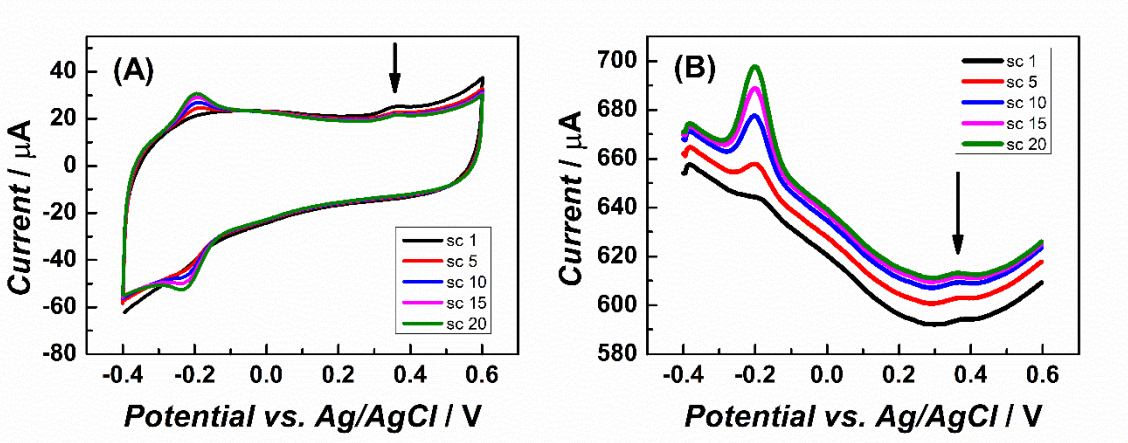

Figure 7.4.2 Solution of 10 µM 5-HT in PBS saline pH 7.4 (A) cyclic voltammograms 1st, 5th, 10h, 15th and 20th scans, Scan rate 20 mVs-1 (B) square wave voltammograms 1st, 5th, 10h, 15th and 20th scans, 0 rotation rate.

Data presented in Figure 7.4.2 clearly shows that the peak visible at negative potential (ca. -0.2 V) is growing with the scanning which is opposite to the peak registered at positive potential (ca. + 0.38 V). Moreover, the background of the square wave increases significantly. Both of those observations were taken into account for further analysis and are described in the text of this chapter.

At this stage of the research, we were sure that we were able to distinguish between two neurotransmitters and two interferents in the same sample. Electrochemically active neurotransmitters such as dopamine, epinephrine and norepinephrine are very similar in the chemical structure which was already described in Chapter 2 of this thesis. I performed a series of experiments to verify the possibility of detection of more neurotransmitters in one sample. I prepared several electrodes modified with isonicotynic acid, taurine and arginine and CNPs to distinguish between components of the mixture solution of dopamine, epinephrine and norepinephrine According to the literature, all of those modifications should allow for electrochemically based distinction between epinephrine and dopamine. However, none of the performed experiments made it possible to conclude how to improve electrodes' stability, sensitivity and limit of detection. Below I present the best results of oxidation of the dopamine, epinephrine and norepinephrine.

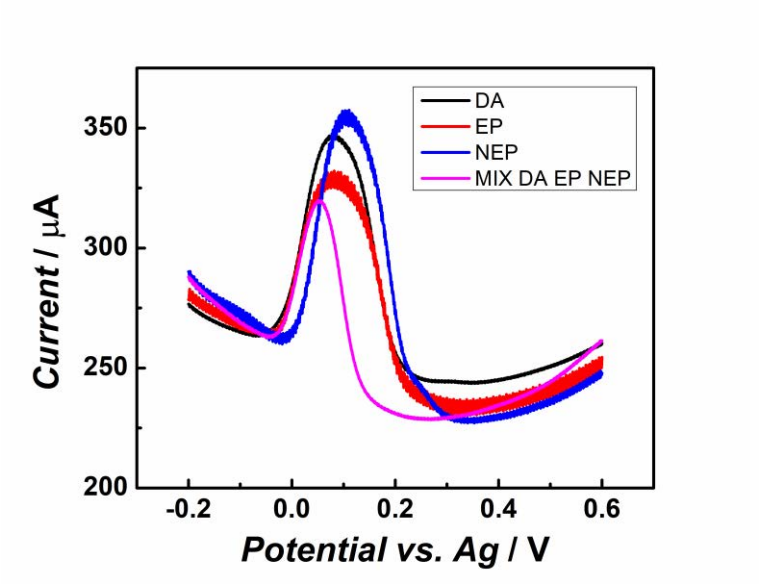

Figure 7.4.3 Square wave voltammograms registered in 2 μM solution of DA (black curve), EP (red curve), NEP (blue curve), and mixture of DA, EP, NEP (purple curve) in phosphate buffer solution pH 5, registered on ITO electrode modified with CNPs TMA/TMOS matrix.

Unfortunately, this result could not be used as a new direction in my research. Instead I focused my research on improving the limit of detection for dopamine and serotonin, together with uric and ascorbic acids.

Further analysis was performed with hydrodynamic conditions of the RD system for mixtures of DA, 5-HT, AA and UA in phosphate buffer saline pH 7.4. We studied lower range of neurotransmitters concentrations, with constant 0.5 mM concentration of acids. This concentration of interferences was fixed at the approximate values of concentration of UA and AA in human body. As a result, a set of increasing peak currents as a function of increasing rotation rate and increasing neurotransmitter concentration was obtained.

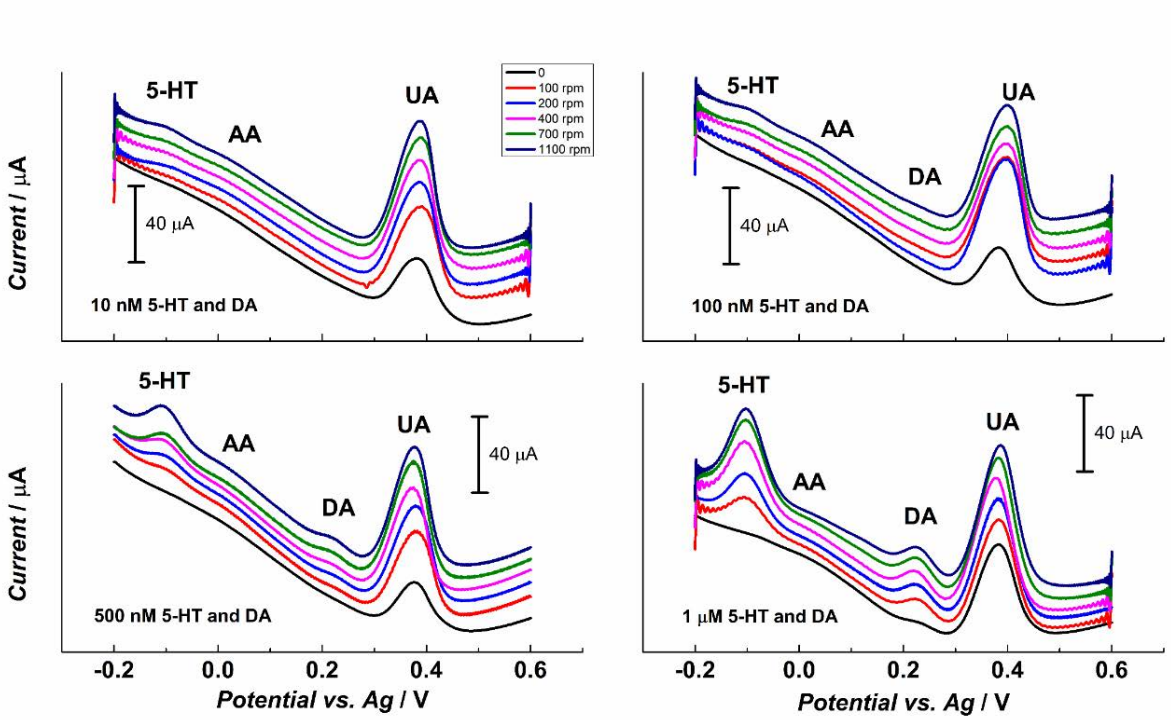

Figure 7.4.4 SW voltammograms, 3rd scans registered on ITO modified with CNP/TMA in solutions of 0.5 mM UA and AA and (A) 10 nM DA and 5-HT, (B) 100 nM DA and 5-HT, (C) 500 nM DA and 5-HT and (D) 1 uM DA and 5-HT in 0.1 M phosphate buffer saline pH 7.4 in a rotating droplet system for various rotation rates. Curves are offset for clarity. Adapted from V.

Square wave voltammograms in Figure 7.4.4 (A) show a well-established peak shape for 10 nM serotonin, with presence of 10 nM dopamine and 0.5 mM uric and ascorbic acids, the peak height was increasing with increasing rotation rate. Plot (B) presents the 100 nM limit of detection for dopamine with presence of 100 nM 5-HT, and 0.5 mM AA and UA in the solution. Even though the peak shape is not clearly visible the base line of the signal for DA oxidation differs between 0 rpm and 100 rpm rotation rate. Plots (C) and (D) present well visible signals for 500 nM and 1 µM concentration respectively of both DA and 5-HT, in the presence of 0.5 mM of AA and UA. In figure 7.4.5 I show the data for 1100 rpm with a subtracted baseline, to better show the change in the dopamine peak.

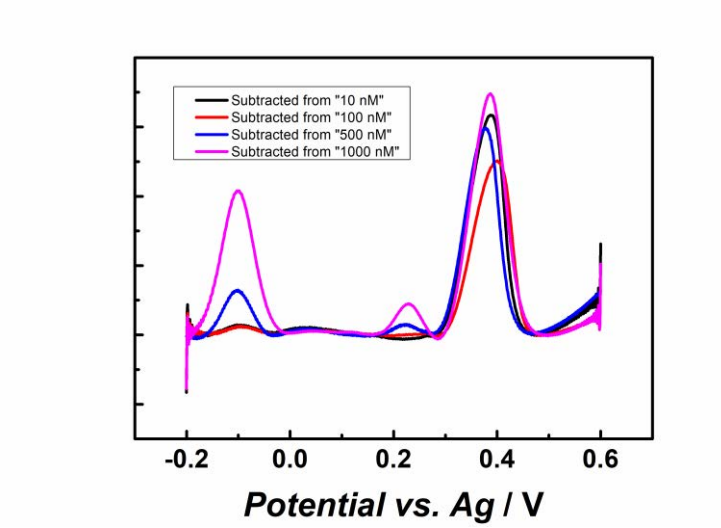

Figure 7.4.5 SW voltammograms with baseline subtraction, registered in 10, 100, 500 nM and 1 µM solution of 5-HT in PBS saline, pH 7.4 The rotation rate 1100 rpm for Adapted from supplementary information V.

During the measurements I observed that the background current was shifting from scan to scan. A thorough investigation led us to the conclusion that the porous material immobilized on the electrode surface is wetted in different time scales. Therefore to maintain the same background level we applied a so-called wetting procedure. For the experiments with analytes dissolved in the phosphate buffer solution we registered 5 scans in the pure buffer to assure that the whole electrode surface is used for the measurement. The wetting procedure was applied for each new spot at the electrode, before each measurement set.

The LOD as low as 10 nM for 5-HT, in presence of other substances, dominated the direction of further research. We decided to verify the shift of the background with bigger number of scans. In Figure 7.4.5 I present the square wave voltammograms measured on ITO CNPs TMA/TMOS electrodes in (A) 100 nM and (B) 500 nM 5-HT solutions in PBS saline solution pH 7.4 with application of a rotation of 400 rpm.

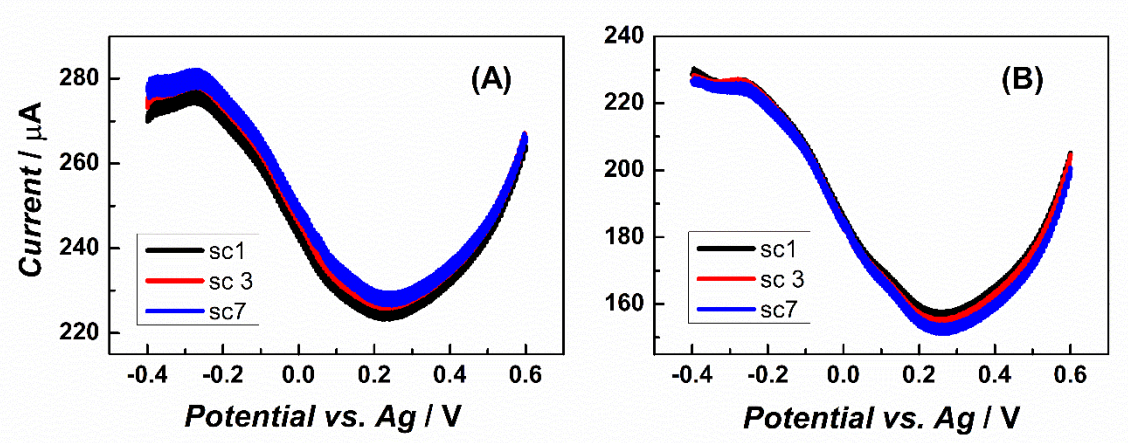

Figure 7.4.5 Square wave voltammograms of (A) 100 nM and (B) 500 nM of 5-HT in PBS saline solution pH 7.4, shown 1st, 3rd and 7th scans, 400 rpm. Adapted from Supporting Information V.

The presented data shows the change of the peak height current between the scans. For smaller concentration (100 nM) the subsequent scan results in a slight background shift, whereas the bigger concentration (500 nM of 5-HT) gives the response where no background shift is visible. However, our aim was to create the sensor suitable for low concentration of neurotransmitters measurements. We decided to use the peak height value instead of a total current value. By using the peak height value we could avoid the low concentration deviation. The increasing trend of peak height corresponding to the oxidation of 5-HT with increase of concentration and rotation rate led to determination of a calibration curve in phosphate buffer saline pH 7.4 for stationary conditions (0 rpm), 400 rpm and 1100 rpm. The unstable peak height for stationary conditions and increasing concentration of serotonin eliminated possible determination of 5-HT concentration under these conditions, and no calibration curve for 0 rpm was obtained. This was probably caused by contamination of porous material and inconstant flux of serotonin from the bulk solution, and diffusion of serotonin oxidation products from the electrode surface. Contrary to the stationary conditions, both 400 and 1100 rpm rotation rate resulted in a stable increase of the peak current with increasing concentration of serotonin. Results presented in Figure 7.4.6 show calibration curves for both 400 and 1100 rpm rotation rate. Both rotation rate measurements were repeated 3 times.

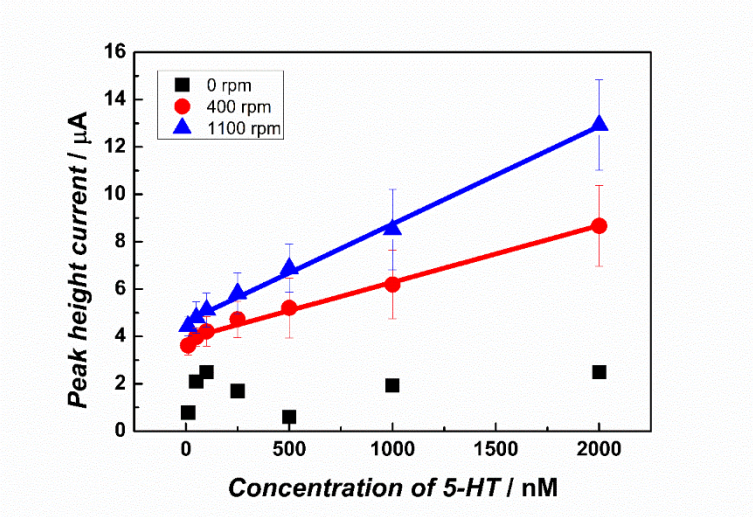

Figure 7.4.6 Calibration curve, obtained for 5-HT oxidation in PBS solution, scattered lines show the data for 10, 50, 100, 250, 500 nM and 1 and 2 µM for 0, 400 and 1100 rpm, lines show linear fits to the data. Adapted from V.

The responses for two rotation velocities resulted in different slopes of the calibration curve, which indicates the increase of sensitivity of the applied method with increase of the rotation rate.

The promising results for limit of detection of serotonin with concomitant substances and creation of the calibration curve performed in the phosphate buffer saline pH 7.4 led to the experiments in biological environment. For that purpose we used mice blood serum, received from Nencki Institute of Experimental Biology[5]. The mice blood was collected from 3 months old C57BL6J male mice from Jackson Laboratory (Białystok, Poland), centrifuged at 2500 g and later stored at -20˚C. Samples prepared in such way are called mice blood serum. Mice blood serum was stored frozen and thawed in small portions suitable for measurements' needs. Figure 7.4.7 (A) shows square wave voltammograms registered after scan in mice blood serum. The signal obtained during oxidation of the sample gives peak signals at -0.16 V and +0.37 V. However, during progressive scanning the peak at more positive potentials decreases while the peak at more negative potentials increases. This phenomenon, which is due to the mechanism described above, was used as a main feature for determination of serotonin concentration in the sample. We are aware that the signal at -0.16 V can be considered as a product of the first oxidation of serotonin at higher potential. However, the peak height at -0.16 V corresponds to the concentration of the serotonin added to the solution. For that reason the peak at -0.16 V was used for further analysis. Fig. 7.4.7 (A) shows the stabilization of the peak height for 3rd and further scans, despite the movement of the background current. The addition of serotonin to the mice

[5] The mice blood serum was received during the sacrifice of mice used for other purposes. No mouse life was taken for the sake of this thesis.

blood serum sample is presented in Fig. 7.4.7 (B). The increasing concentration of serotonin in the sample results in the increasing peak height.

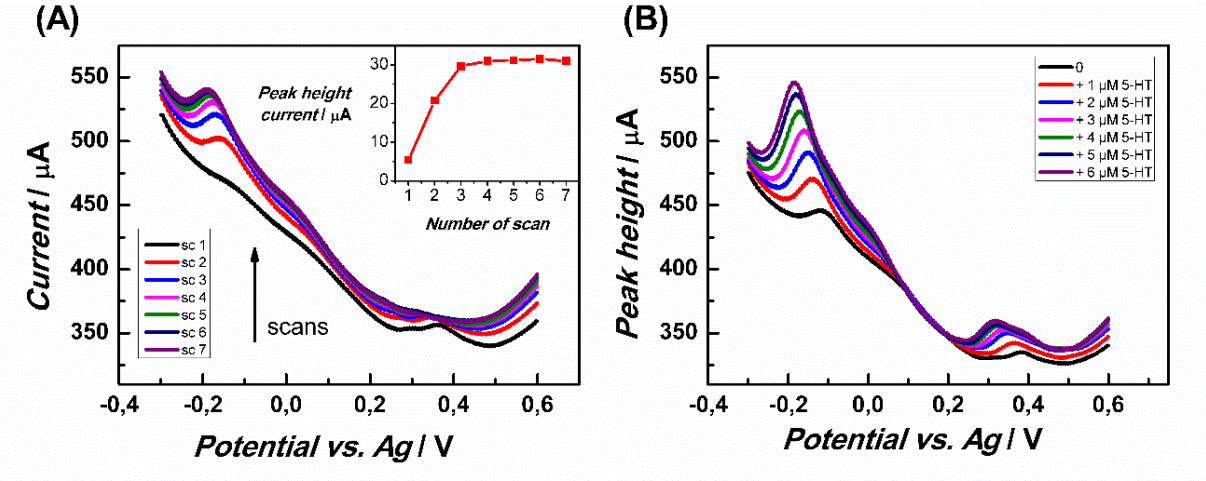

Figure 7.4.7 Square wave voltammograms obtained with ITO CNP/TMA electrode in the RD system at the 400 rpm for (A) mice blood serum 7 scans, (B) mice blood serum and 6 consecutive scans of addition of the 1 µM of the 5-HT each. Adapted from V.

Experiments performed with utilization of the mice blood serum were biased with even bigger background current shift than in case of the phosphate buffer solution. For this reason the pre-wetting procedure was altered with additional scanning of the pure mice blood serum for 7 scans. The pre-wetting procedure for experiments in serum consisted of 5 scans with pure phosphate buffer saline to wet porous carbon material on the electrode surface and 7 scans with pure mice blood serum to standardize the serum level, before internal probe addition. This observation was a base for obtaining a calibration curve for determination of the serotonin concentration in the unknown sample. A set of measurements with an internal addition of 5-HT for 400 rpm was registered. Rotation rates higher than 400 rpm caused wobbling of the droplet which was probably caused by higher viscosity of the serum in comparison to the water solution for which the Rotating Droplet system was optimized and used so far. For further experiments we kept the 400 rpm rotation speed of the RD system. Each of the experiments was performed for a number of scans and with three repetitions in order to determine the accuracy of the method. As it was shown in Fig. 7.4.7 (A), the first and second scan of the mice blood serum resulted in significant increase of the background current and the changes in the peak height registered at -0.16 V. For that reason each measurement consisted of 7 scans to assure the stable peak height for a given concentration of serotonin added to the mice blood serum solution.

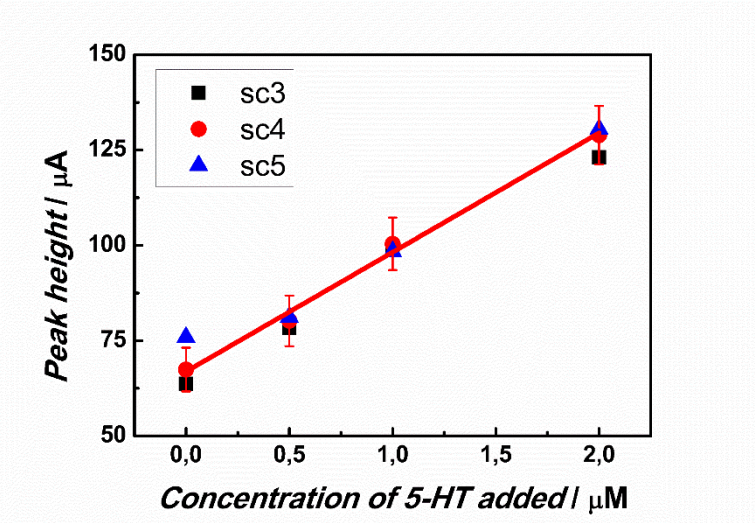

Figure 7.4.8 Calibration curve for 5-HT internal addition, constructed for 5-HT oxidation in mice blood serum solution, for 3rd, 4th and 5th scans, taken with 400 rpm, and the linear fit for the 4th scan, with R^2 value 0.9926. Adapted from V.

Figure 7.4.8 shows the results for the internal addition calibration curve. As a result we obtained a perfectly linear response (R^2 value 0.9926). As it is seen in this figure, the 4^{th} scan response is closest to the linear range of calibration. With usage of the internal probe addition we were able to determine the basal serotonin concentration in the pure mice blood serum which was: 2.14 μM. The calculated value of the serotonin is in good correlation in the mammalian human blood content of serotonin (0.5-2.0 μM)[1]. I was looking also for a medical laboratory, which would be able to perform a sample analysis, but the volume of the sample was too small for any commercial analysis.

Conclusions

Data presented in this chapter shows that the RD system can be used for simultaneous detection of multiple neurotransmitters in presence of interferences. Both dopamine and serotonin can be detected in very low concentration in presence of commonly occurring interferents such as uric and ascorbic acids. The registered voltammograms allowed us to obtain the calibration curve for 5-HT, for two rotation rates. The results for mice blood serum show that the method can be applied for detection of serotonin in a biological samples without preceding preparation of a sample, except centrifugation. Moreover, the reproducibility of the method was sufficient for creation of the calibration curve for the 5-HT. Internal addition to the mice blood serum sample allowed for determination of serotonin content in an unknown sample.

Bibliography

V M. Kundys-Siedlecka, E. Bączyńska, and M. Jönsson-Niedziółka, “Electrochemical Detection of Dopamine and Serotonin in the Presence of Interferences in a Rotating Droplet System,” Anal. Chem., p. 91, 10908-10913, 2019.

[1] G. S. Lee *et al.*, “Measurement of plasma, serum, and platelet serotonin in individuals with high bone mass and mutations in LRP5,” *J. Bone Miner. Res.*, vol. 29, no. 4, pp. 976–981, 2014.

Chapter 8.
COMSOL calculations for electrochemistry and description of the flow inside the RD system

8.1 Introduction

The importance of computational predictions of the mechanisms ruling the experimental setups was already mentioned in Chapter 3 of this thesis. Parallelization of calculations for various parameters can significantly support the measurements and reduce the experimental time. For some cases computations are crucial not only for choosing optimal factors but also for avoiding construction errors. In this chapter I would like to present computations which I performed using the COMSOL Multiphysics software for applications in electrochemical systems. The results obtained during those computations had a positive influence on the process of creating new configurations of electrochemical setups. I performed a number of COMSOL calculations to understand the movement inside the Rotating Droplet system, and to simulate the electrochemical properties of the system. I will also present results concerning the flow profile in the RD system obtained with using Particle Image Velocimetry.

8.2 COMSOL Multiphysics for electrochemistry

8.2.1 Application of COMSOL Multiphysics

The benefits and examples of successful application of COMSOL Multiphysics for solving the electrochemical problems were already mentioned (Chapter 3). The number of different issues which can be resolved with this software makes it a very popular tool to support experimental data.

Modules

Problems in COMSOL are implemented as 1D, 2D or 3D models, which are governed by a few physico-chemical laws. In the case of chemical engineering calculations COMSOL Multiphysics can support scientists with modules such as:

- Chemical Reaction Engineering
- Batteries & Fuel Cells
- Electrodeposition
- Corrosion
- Electrochemistry.

Application of the modules mentioned above are mainly used for solving chemical equations. For multiphysics problems modules from other disciplines can be combined within COMSOL Multiphysics calculations. Within each module there are several sets of pre-defined "Interfaces" that help the researcher solve the most common equations within several areas of physics, chemistry and engineering. All the data showed in this chapter is the result obtained with the module *Microfluidics* using the Interface *Fluid flow*, where the transport properties of the system (the Navier-Stokes equations) were solved and the *Chemical species transport*, was used for electrochemistry calculations (Nernst-Planck and Butler-Volmer equations). Even though COMSOL has an *Electrochemistry* module, it didn't work well for our model[6]. For that reason we decided to implement the Butler-Volmer equation as boundary conditions within the normal chemical transport interface. While solving the multiphysics problem in COMSOL, one can choose to solve several problems in parallel, e.g. the flow profile and the diffusion equations.

Geometry

The possibility to carry out simulations in complicated geometries is one of the key advantages of COMSOL and similar software packages. Independently from the performed calculation type, the geometry of the problem can be either uploaded form an external source (e.g. AutoCAD) or defined within COMSOL Multiphysics. Computations presented in this chapter were based on geometries written within COMSOL Multiphysics (calculations concerning microfluidic channels, post electrodes and Rotating Droplet system).

[6] Calculations of cyclic voltammograms were very slow in previous versions of COMSOL. This seems to have improved with the latest updates.

8.3 Calculations of the concentration profile and efficiency of the electrochemical reaction in posts based microchannel device.

Microfluidic devices are very popular among research groups and many modifications are being made to improve their functioning. One of the ideas is to increase the efficiency of electrochemical microfluidic devices by insertion of more efficient electrodes into the system. The utilization of pencil pillars as electrode material into a microfluidic device gave the opportunity for creation of a competitive system for e.g. p-nitrophenol detection. The study performed in our research group needed some computational assistance. My task was to create a model within the COMSOL Multiphysics software which could compare the flow profiles in a standard band electrode system (as seen in Fig. 8.3.1 A) and in a pencil pillar system (Fig. 8.3.1 B). After determination of the flow in both systems, I implemented the electrochemical study to calculate the efficiency of the system, where various numbers of pillars were applied. Moreover, the computation with COMSOL allowed us to test several possible configurations to determine which could give better result.

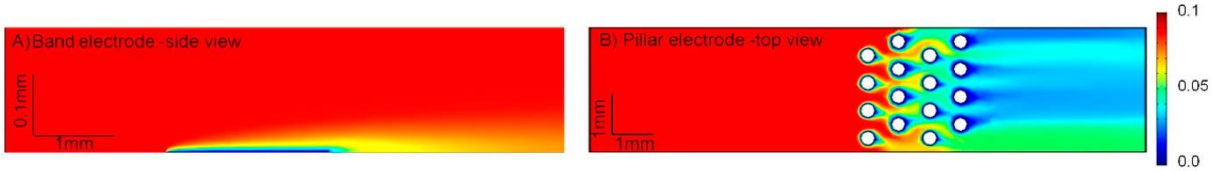

Figure 8.3.1 Concentration profiles of the analyte (mol L−1) in a simplified electrochemical reaction in a microfluidic channel calculated using COMSOL Multiphysics 5.3. (A) using a microband electrode (side view) and (B) using 16 vertical posts as electrodes (top view). The channel dimensions, flow rates (Vf) and over-potential are the same in both systems. Red color denotes high concentration and blue color low concentration. In (A) the collection efficiency is a mere 3% compared to 81.5% in (B). Adapted from IV.

Data presented in Fig. 8.3.1 shows the side view of the band electrode (A.) and the top view on the pillar electrode (B). For reason of fair comparison the applied volumetric flow rate and channel dimensions were the same in both cases (Fig. A and B). As is visible in Fig. (A) most of the substrate passes through the microchannel high above the band electrode and never interacts with the electrode surface. The pillar electrode shows much better efficiency (Fig. B) where after the region of electrodes most of the substrate is consumed, and only small portion is visible in the stream.

I performed a thorough analysis with application of various numbers of pillars as active electrodes. I calculated the flow for a geometry with 1, 2, 3 or 4 rows of pillars and simulated the

electrochemical reaction (chronoamperometry) on the results. The initial results showed straight lines, which suggested current values proportional to the flow rate. Those calculation results deviated from the experimental data. For that reason, I implemented an additional resistivity, characteristic for the pencil lead material, to the pencil electrodes.

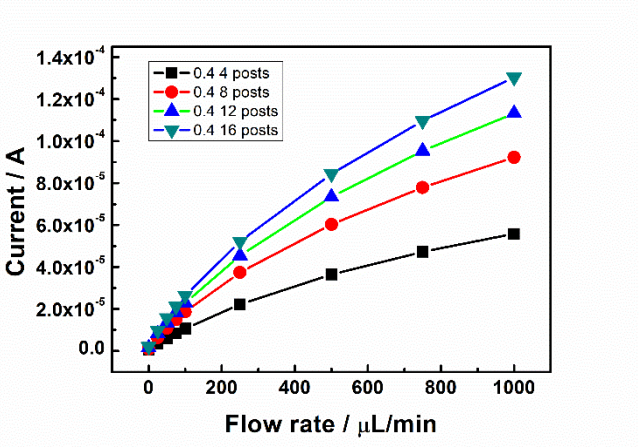

Figure 8.3.2 Current vs. flow rate for different number of posts and various flow rate (0, 25, 50, 75, 100, 250, 500, 750, 1000 μL/min). Adapted from supplementary material IV.

As a result, we can see an increasing current value calculated on a pillar electrode with increasing number of electrodes and increasing velocity of the stream. The computational results showed behavior identical to the experimental results. The increase of the current is slower than the increase of the flow rate. Moreover, the computation which I performed revealed that the resistivity of the electrode material in such sensitive devices plays a crucial role.

A second set of computations was performed in order to describe the efficiency of electrodes composed into a system of microfluidic channel for a detection of certain substances with utilization of cyclic voltammetry. In this case I simulated the flow in a wide range of velocities (0, 10, 25, 50, 75, 100, 250, 500, 750, 1000 μL/min). I set the calculated flow profile as a starting point for the electrochemical simulation of the cyclic voltammetry.

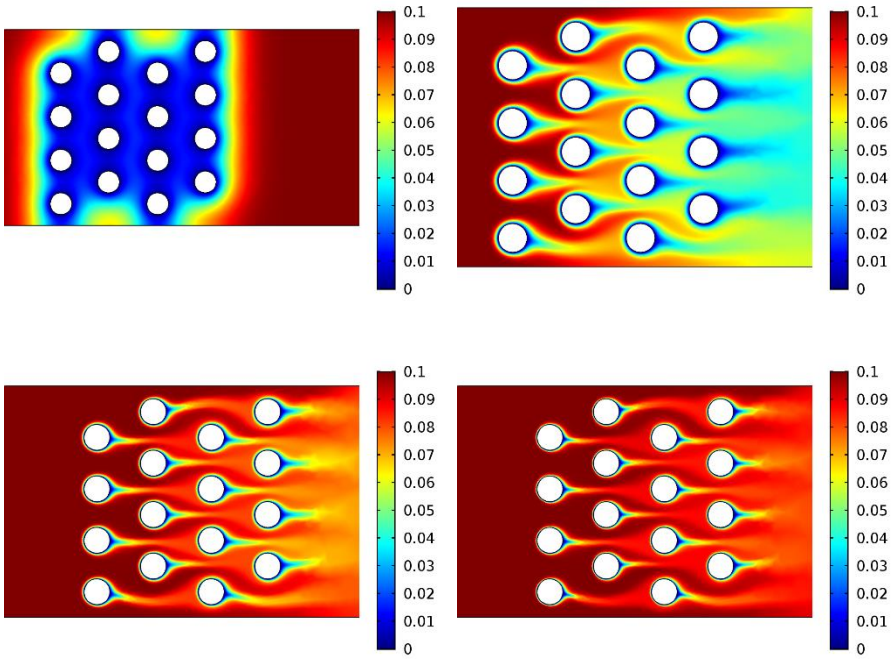

Fig 8.3.3 Concentration profile of the reduced form of the Redox probe around the electrodes for different flow rates: A) 0 µl/min, B) 10 µl/min, C) 25 µl/min, D) 100 µl/min. The image is saved at the turning point in the CV. The flow is from the left to the right side. Adapted from supplementary material IV.

As it is visible in Fig. 8.3.3 (A) the 0 flow rate results in a fast consumption of the substrate (red color), and in the closest proximity to the pillars the substrate concentration equals zero (blue color). With application of the flow rate shown in Fig. (B) 10 µL/min, (C) 25 µL/min and (D) 100 µL/min the substrate consumption is smaller and smaller with increase of the flow velocity.

The obtained results visible in Fig. 8.3.3 were key for determination of the efficiency of the system. For this system the efficiency can be understood as a ratio between the input of the concentration to the output of the substrate concentration. Not surprisingly the best efficiency of the system was obtained for the maximal 4 rows (16 pillars) of electrodes. Moreover, I have shown how important is the fluid flow rate for the analysis of the system.

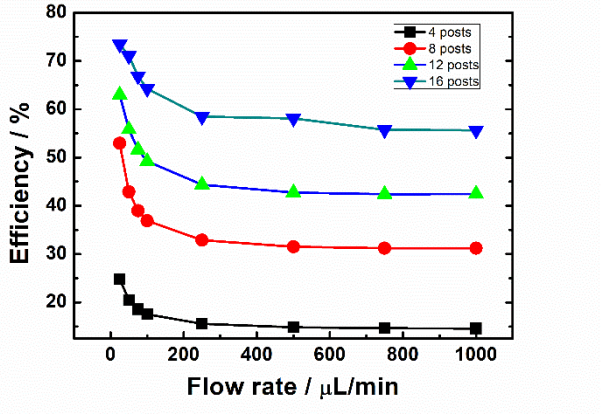

Figure 8.3.4 Efficiency as a function of a flow rate for 4, 8, 12 and 16 posts. Data collected from the cyclic voltammetry simulation.

As it is shown in Fig. 8.3.4 application of 25 μL/min instead of 250 μL/min can help with increasing the system efficiency by more than 10 percentage points, which indicates that to reach the maximal efficiency of the fluidic electrochemical system one has to use flow rate small enough to assure consumption of the substrate at the electrode surface.

Based on the successes with computation of the physico-chemical properties of this system, I would like to present a set of calculation results obtained for a gravitationally driven microfluidic biofuel cell.

8.4 Calculation of the electrochemical depletion zone in a microfluidic channel

One of the experiments performed in our research group concerned a gravitationally driven microfluidic biofuel cell. On the anode ascorbic acid was oxidized, whereas on the cathode enzymatic oxygen reduction, catalyzed by Bilirubin Oxidase, took place. In the experiment the anode was placed upstream in the channel and the cathode downstream. The ascorbic acid (used as fuel in this fuel-cell), caused fuel crossover, since the anode and cathode were made of the same material, and this was affecting the cathode performance. Ascorbic acid is also known as a potential inhibitor of Bilirubin Oxidase. To overcome the problem of cathode inhibition, proper construction of the system was needed. I performed computations of the electrochemical depletion zone, i.e. an area behind the anode where the concentration of ascorbic acid is lower, in the microfluidic channel using COMSOL. The goal of the simulation was to find an optimal configuration of a length of the electrodes and a distance between the cathode and anode in the microfluidic gravitational bio-fuel cell (manuscript under preparation). I was looking for the best

length of the anode, which could affect the depletion zone of the ascorbic acid, so that only a small portion of that compound was transported to the cathode surface. I tested several options of the distance between anode and cathode, and the volume flow rate.

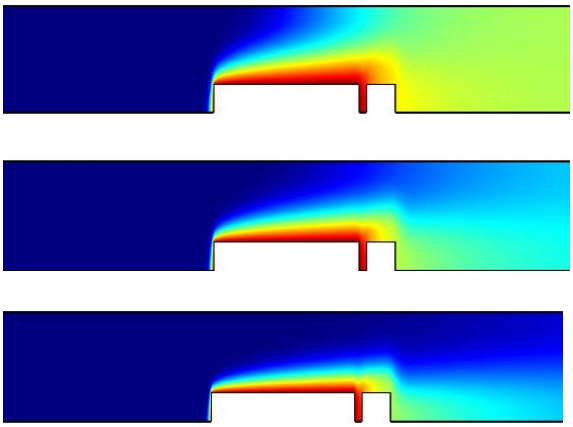

Fig 8.4.1 Scheme of the depletion zone effect in microfluidic biofuel cell. The flow is from the left to the right side. The results present the depletion of the concentration of fuel (ascorbic acid) after reaction on the anode, for 1, 2 and 5 µL/min, from top to the bottom respectively.

The intuitive solution with application of a very long anode and very closely spaced cathode had its limitation. The microfluidic channel has limited dimensions as well as the closest proximity of the one electrode to the other. Within the computation I simulated a number of different settings of flow velocities and how extending the anode would affect the performance of the cathode. I also calculated how much the cathode is protected with different configurations of certain parameters of the system. On the basis of this simulation I was able to find the most promising solution and construct the most efficient system for microfluidic bio-fuel cell, where the flow rate was 1ul/min and the anode length was five times longer than the length of the cathode. We thought that more complicated calculations should be taken into consideration, such as possible reaction of the ascorbic acid oxidation on the cathode. But this reaction was much more complex and difficult to represent in a computer simulation. During further experiments the oxygen reduction reaction appeared to be the rate limiting factor, so that the ascorbic acid oxidation at the cathode was not limiting the efficiency of the bio-fuel cell.

The experience gained during calculations concerning the microfluidic channels helped me with computations on Rotating Droplet system, which I present in the next section.

8.5 COMSOL calculations results for the RD system

Depending on the complexity of the results of the calculation, the data can be presented as a single number, as it was in case of the collection efficiency presented in section 8.3, or a larger set of data. More complex results can be expressed as a 2D graphs or 3D visualizations of the obtained result with the image changing over time.

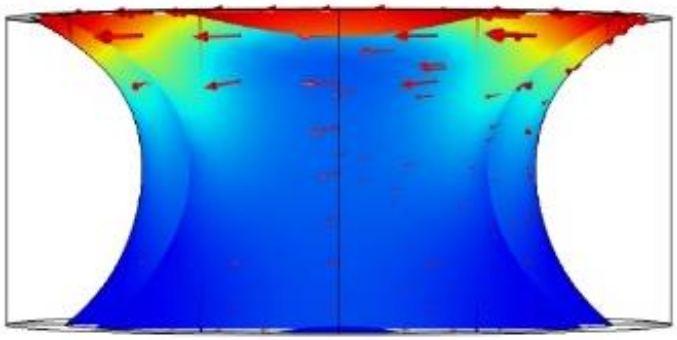

Figure 8.5.1 Graph visualization of the movement inside a Rotating Droplet system, color indicate the velocity of the movement. The graph shows several cut planes taken vertically through the droplet. The arrows show the direction of the flow.

The graph presented in Figure 8.5.1 shows an example of the velocity inside a Rotating Droplet system. The closer to the top wall (which is set as a rotating wall) the faster the movement of the fluid, arrows shows the direction of the flow. This result will be presented in more detail in this section of the thesis.

Velocity inside a Rotating Droplet system

The Rotating Droplet system works on the basis of the well-known Rotating Disc Electrode principles. However, the movement profile for the RD and RDE systems are different. In the standard RDE the reactants are disappearing from the surface of the electrode, pushed radially and are diluted into a large volume, whereas in the RD system reactants are being moved around in a much smaller volume, from where they can easily reach the counter electrode or move back to the working electrode surface. For this reason, the description of the flow profile inside a Rotating Droplet system was very important to understand the results of electrochemical measurements made using the system.

I performed a number of different simulations in order to describe a flow profile inside a Rotating Droplet. The main difficulty was based on proper description of properties of the different droplet walls. The droplet boundary comprises three types of walls, where the bottom – working electrode

wall – was described as a non-slip wall[7], the side walls of the droplet were implemented as slip walls[8], and the top wall (the one which was created from the rotating ring-disc tip) was set as a moving wall. The velocity of the top wall around its axis was applied as:

$$V = -r * \omega * \cos(\phi) + r * \omega * \sin(\phi) \qquad \textit{Eq. 8.5.1,}$$

where r is radius of the Rotation Droplet system, ω is the rotation rate and ϕ the angle in the cylindrical coordinate system.

As a result, I obtained the profile of the movement of the fluid inside the Rotating Droplet visible in Figure 8.5.2 (A) and (B).

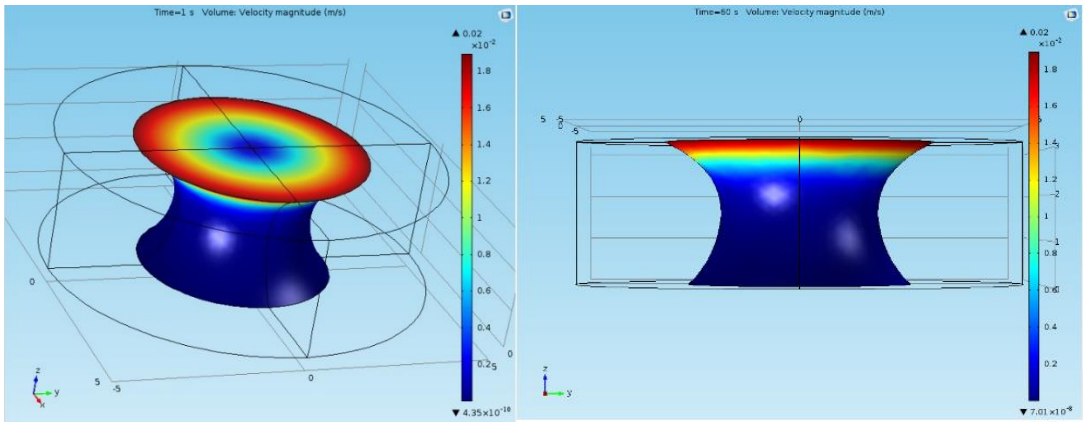

Figure 8.5.2 The graphical representation of the velocity magnitude inside a Rotating Droplet, simulation for 50 rpm.

The flow profile inside a rotating droplet can help with explanation of the trajectory of the transported species in the body of the Rotating Droplet. Unfortunately, as it is presented in the graphical representation in Fig. 8.5.2 (A) and (B), close to the simulated electrode surface (bottom wall of the droplet) the velocity is practically zero. I repeated simulation with many different rotation rates. However, even for high rotation rates no movement close to the bottom droplet wall was observed. The experiments performed during the research on the RD system optimization, its utilization to generation-collection experiments and neurotransmitters detection (shown in Chapters 5, 6 and 7 of this thesis) have shown that the movement close to the electrode surface exists even for rotation rates as small as 50 rpm. To be able to better define the motion inside the system we decided to make experimental measurements of the liquid motion in the RD system using particle Image Velocimetry (PIV). These measurements are described in the next section.

[7] A wall where the velocity of the liquid at the wall is zero.
[8] A wall where the velocity of the liquid normal to the wall is zero, but the motion parallel to the wall is not hindered.

8.6 Particle Image Velocimetry

We made several attempts to define the movement of the droplet with home-made methods. We tried to see the motion path with an addition of a dye to the rotating drop. This method had some drawbacks, because the dye was changing the volume of the droplet and the injection procedure was affecting the shape of the system. We tried to observe the movement of the air surrounding the droplet, and on this basis infer the velocity inside the system[9]. With time we learned about the Particle Image Velocimetry (PIV) which is a technique used for description of the velocity and the motion path in a wide range of the systems. PIV was briefly described in the Chapter 4 (Methods) of this thesis. PIV system for observation of the setups such as the RD system demanded the special treatment because of its dimensions. Typical PIV setups are dedicated to a vast system such as wind tunnels or helicopter aerodynamics [1], which are several meters high and long. There are also micro-PIV setups, but those are dedicated to microfluidic chips on the microscale [2]. The volume of interest in the RD system is distributed in a geometry which is smaller than usual PIV system and bigger that the micro-PIV. Its biggest difficulty comes from the moving wall. The refracting walls of the RD system which are very advantageous for electrochemical purposes, turned to be very problematic for the PIV measurements. The RD system is not enclosed in any type of external walls. Despite a number of difficulties to be overcome, I performed a set of PIV measurement and analysis for Rotating Droplet measurements shown in section 8.6.1.

8.6.1 PIV results for Rotating Droplet

PIV measurement is based on registering a movie with visible movement of the fluid and processing of the data. The preparation of the movie requires specialized elements, such as:

- Light source (laser, in our case 532 nm)
- Optical path for expanding and collimating the illumination path (lenses)
- Mechanical slit (used to cut-of the rest of the unnecessary illumination)
- The seeding (fluorescent particles distributed in the volume of interest)
- Camera and computer for recording of measurement

[9] One of the applied methods was based on using smoke, which was blown in through a tube to the closest surrounding of the droplet. From this experiment we drew conclusions about movement of the air which surrounds the droplet. This observation let us better define further COMSOL models.

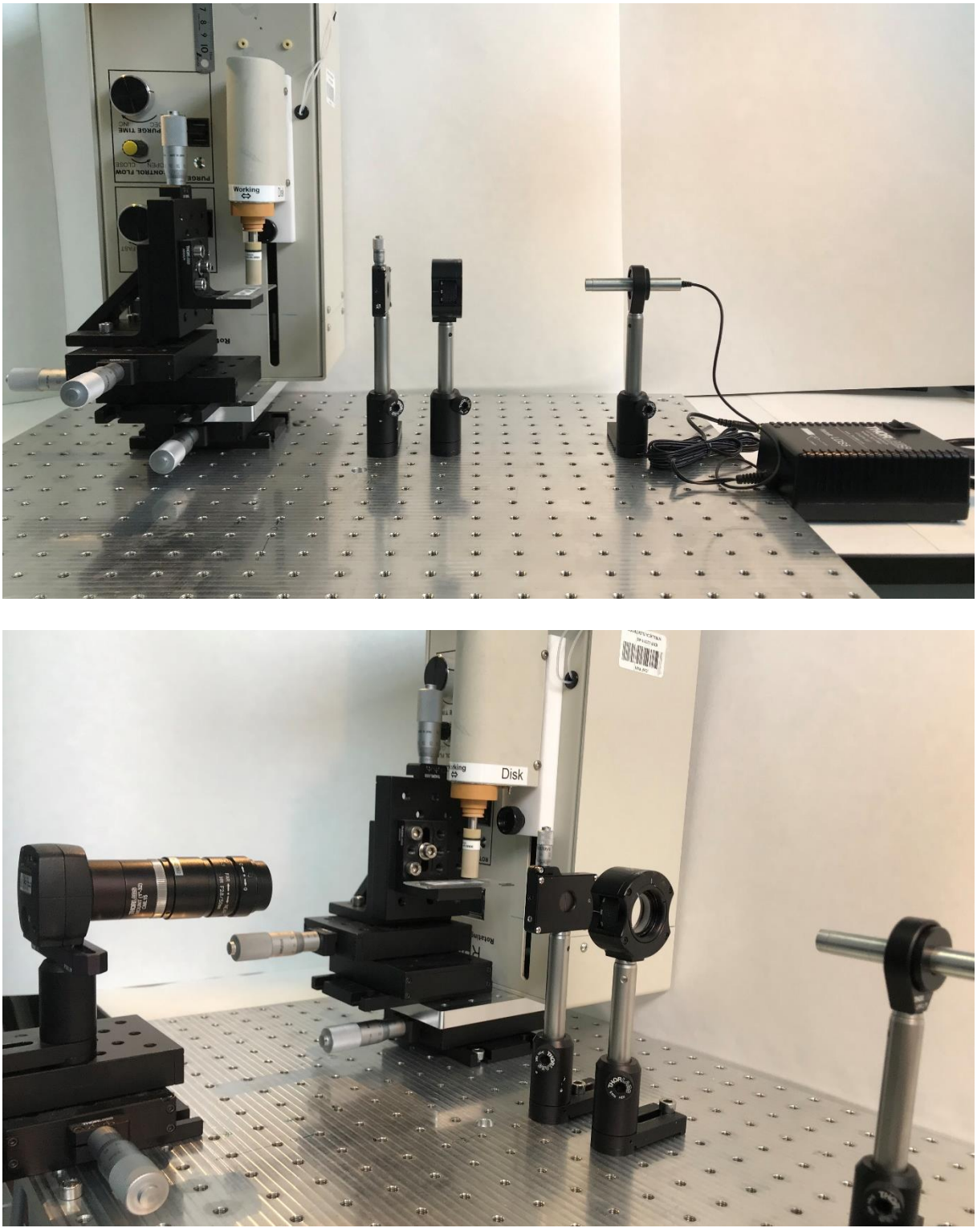

Figure 8.6.1.1 The photograph of the PIV setup for Rotating Droplet PIV measurement.

Collection of the data for Rotating Droplet velocity was demanding not only because of reflection from the open walls of the droplet, but also due to its complicated flow profile. The flow inside

a droplet is axial symmetric and to define the flow profile we decided to "cut" the droplet volume into illuminated slices of the droplet volume[10].

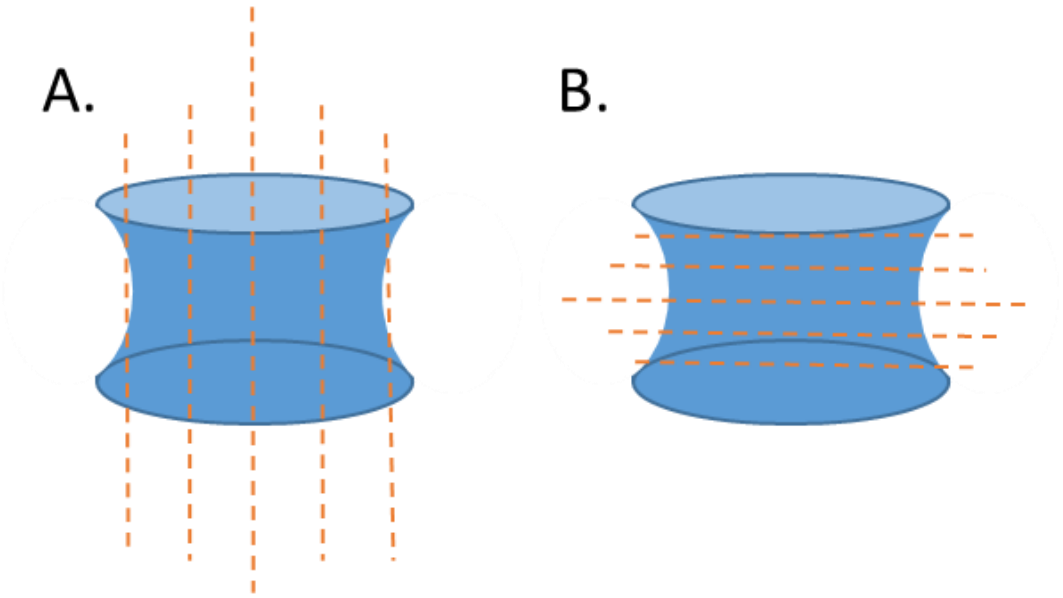

Figure 8.6.1.2 The schematic representation of the division of the droplet volume into illuminated droplet slices, A. side view, B. bottom view.

The PIV experiments were very difficult to perfom because of the interaction of the illumination source and the moving, reflection drop wall. I tried to register the PIV recording for a several types of the seeding particles and power of illumination. Below I present the ten consecutive frames out of tens of thousands regisered frames for this system.

[10] During my stay in DLR, Gottingen, Germany I learned how to build a setup, record and analyze the data from PIV measurements. The specificity of the RD system attracted attention of other employers, one of the comments was: "You want to do PIV on such small system? And you want to do PIV on a droplet of water which behave like a lens by itself? And you want to record PIV for this droplet while its moving? Hmmm Peculiar…". Even though it supposed to demotivate me, I decided to try anyway.

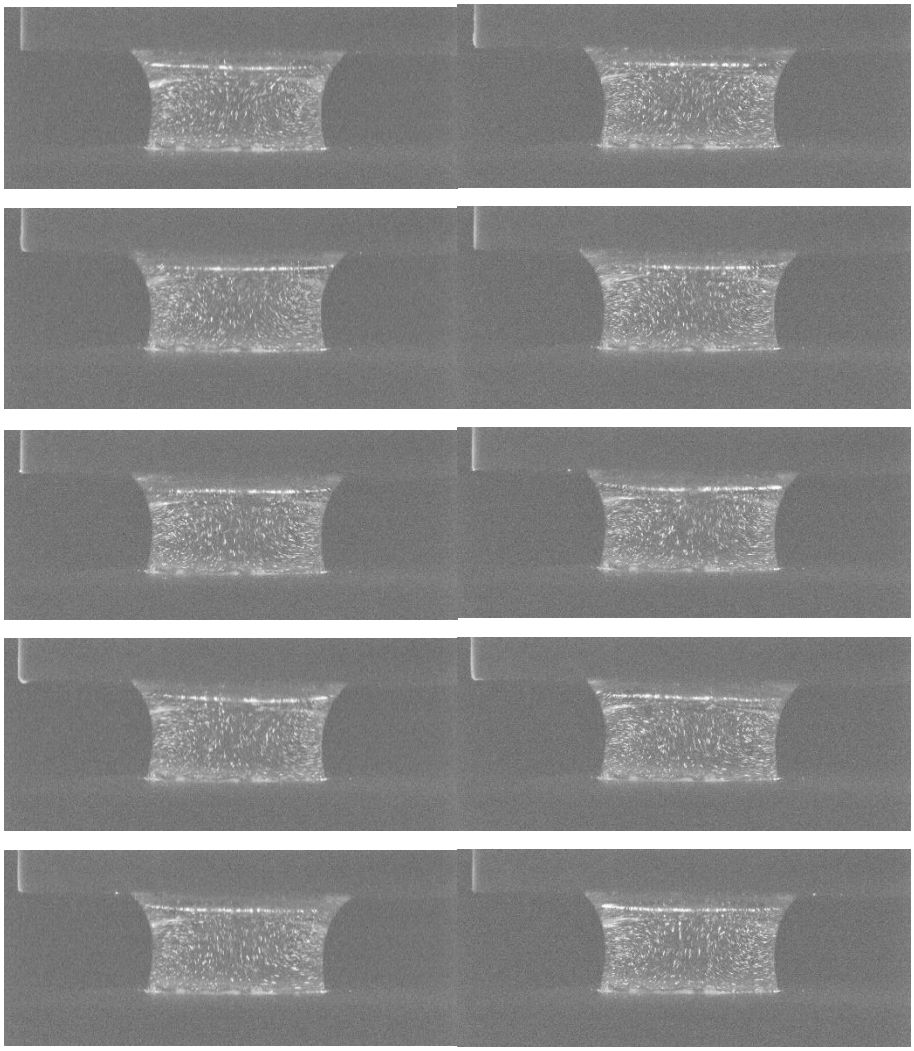

Figure 8.6.1.3 The representation of the PIV data, frame by frame for a Rotating Droplet system, 60 rpm velocity applied to the system.

Even though the frames presented as it is visible above were used for final computation of a velocity profile, it is much easier to observe the movement of the droplet on the videos, see links:

http://bit.ly/31vIRlp

http://bit.ly/2J7xABJ

http://bit.ly/2Pcl0oF,

where bigger number of rapidly changing frames allows to see a movement path.

The obtained data had to be analyzed with an external software, we used the student's version of the Matlab plugin called PIVlab capable of computing time-resolved digital particle image velocimetry. PIVlab allows for automatic, statistical analysis of the data. A complement to the PIVlab software is the free Open Source Physics software Tracker [3]. The advantage of free

access to the software is balanced with the time-consumption and labor-intensity of it. In Tracker the movie can be split into a single frames, but the position of a single particle has to be manually marked on each frame. As a result one can obtain a nice pattern of a movement inside an observed volume.

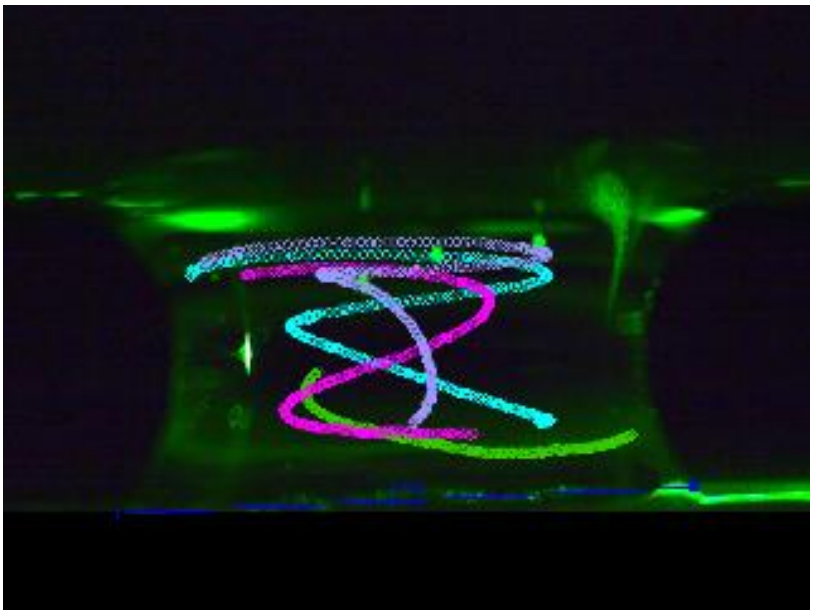

Figure 8.6.1.4 The representation of the PIV data analysis with Tracker TM. The single point corresponds to the position of the tracked particle visible in a single frame of the registered movie.

Within the computation the pixels from the seeding particles their position is tracked between frames. Having knowledge about time between frames and the dimensions of the observed objects enables calculation of the velocity of the particles, which is assumed to be the same as the velocity of the fluid. Data collected for the experiment was analyzed and as a result we obtained the velocity profile inside a droplet.

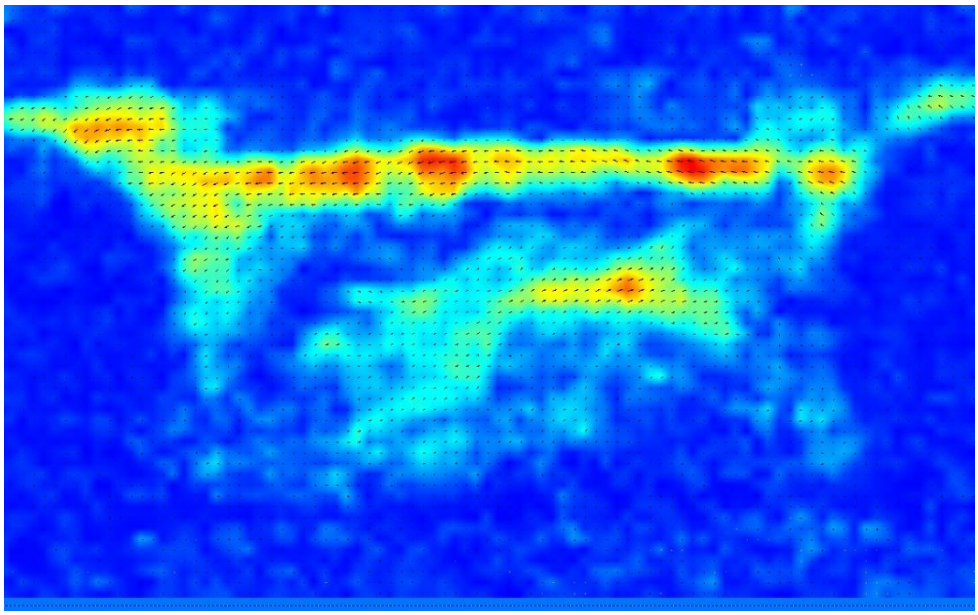

Figure 8.6.1.5 The velocity profile inside a Rotating Droplet system obtained with home-made PIV system, analyzed with PIVlab.

The results obtained with PIVlab allowed for a creation of a velocity map inside a Rotating Droplet system. The plot presented in the fig. 8.6.1.5 has some missing points which indicate lacking data, but this comes from the limitation of the home-built system. I calculated a set of experiments and performed many analyses to plot the average velocity in sections of the droplet. The data from PIVlab was correlated with Tracker data to make sure the calculated velocities are valid. To give a wide look on the droplet velocity I divided the droplet volume into five cutoffs in front view and five cutoffs in the look from bottom to the top, as it was presented in the figure 8.6.1.2.

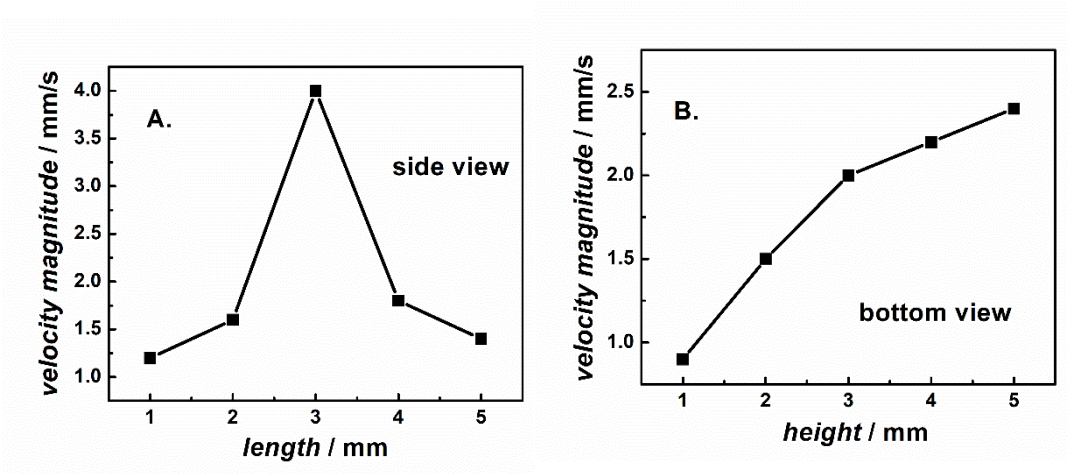

Figure 8.6.1.6 The velocity in Rotating Droplet system registered with PIV in five different cuts of each: A. Side view, and B. bottom view of the droplet.

Results obtained during PIV measurements and data analysis revealed that the velocity inside a Rotating Droplet system changes with height and depth of the droplet volume. The fastest movements can be observed in the middle part of the droplet, as seen in plot 8.6.1.6 (side view). The velocity of the Rotating Droplet system increases with increase of the height of the droplet, the closer to the rotating source (RRDE tip, placed at the top of the system) the faster the movement.

A limitation of my home-built system is the low frame rate of our camera that allows us to measure the flow in the droplet only at low rotation rates.

Knowledge obtained during experimental PIV gave me a handful of information which I could use while planning next set of calculations with COMSOL.

8.7 Results of COMSOL calculations on Rotating Droplet system

The previously shown results on Rotating Droplet velocity (Figure 8.5.2) made it clear that the computed model failed, because the velocity of the lower part of the droplet was too small. Even though I tried to simulate the system rotation with application of frictionless side walls, the droplet velocity was still too small. The next approach was based on idea that the side walls of the drop are being pushed, which, based on observation might be because the air around the droplet is also accelerated by the rotating top electrode. In COMSOL such a calculation can be implemented as two-phase fluid system, with both the air and the liquid being accurately simulated. Unfortunately, because of the axial motion of the system we could not calculate it in a cylindrically symmetric 2D model[11]. Application of the same reasoning to the 3D model was also not possible because of its high complexity (high computing power and long-term computations were needed)). For those reasons we decided to try to "cheat" the system to maintain the velocity of the droplet similar to the experimental data. Results of such simulation could be later used for simulation of the electrochemistry in the Rotating Droplet system. To achieve this goal I created an additional domain surrounding the droplet geometry. The domain outside the Rotating Droplet was rotating and its movement enforced movement of the system's walls, which significantly increased movement inside a droplet.

[11] COMSOL does not allow "swirl flows", i.e. motion in the phi-direction in 2D models, unless one purchases an additional module, the Computational Fluid Dynamics module.

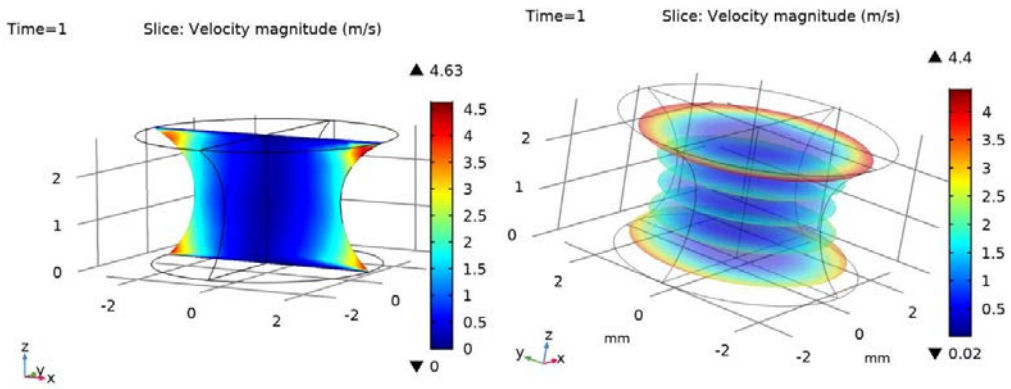

Figure 8.7.1 The graphical representation of the velocity inside a Rotating Droplet, simulation for 50 rpm in COMSOL, with application of surrounding domain.

Figure 8.7.1 shows the movement of the Rotating Droplet system under application of the movement in the surrounding domain. The central part of the droplet is characterized by the smallest velocity, but even there it is not equal to zero. The obtained results suggested that the flow profile was appropriate to the expected range of the velocities, and for that reason I used this data as a starting conditions for next step of calculation of the electrochemical phenomena within COMSOL Multiphysics.

For calculation of the electrochemical phenomena we applied the Interface called Transport of Diluted Species (later referred to as *tds*). I set the bottom wall of the droplet (the working electrode surface) as the surface where the electrochemical process occurs. The electrode reaction was described as fluxes in and out of the boundary. These fluxes were described by the Butler-Volmer equation for the reaction:

$$ox + ne^- \rightleftarrows red \qquad (Eq.\ 8.5.2,)$$

$$\phi_A = -k_f * red + k_b * red \qquad (Eq.\ 8.5.3)$$

$$\phi_B = k_f * red - k_b * ox \qquad (Eq.\ 8.5.4)$$

Where:

$$k_f = k_0 \exp[-\frac{\alpha_f nF\left(E-E^{\phi'}\right)}{RT}], \qquad (Eq.\ 8.5.5)$$

$$k_b = k_0 \exp[\frac{\alpha_b nF\left(E-E^{\phi'}\right)}{RT}], \qquad (Eq.\ 8.5.6),$$

ϕ_A and ϕ_B are fluxes in and out of the electrode, k_f and k_b are respectively forward and backward kinetic rates, k_0 is a standard kinetic rate constant, α is a charge transfer coefficient, *n* is a number

of electrons, F is the Faraday constant, E is the electrode potential, $E^{\phi'}$ is the equilibrium potential, R is the universal gas constant and T is the absolute temperature.

For the electrochemical simulation I chose parameters similar to the experimental parameters, which were: E^0 as 0.3 V, which is a standard potential for a certain reaction, range of the electrochemical window potential between 0 and 0.6 V, the scan rate 20 mV/s. I set the scan rate and time of the experiment to enable the two whole cycles of cyclic voltammetry with precision of 1s, which means that the solution of calculation were saved for each second. Last but not least the whole geometry was divided into subdomains with so called mesh. Mesh should be fine enough to give a decent solution but also not too fine to save the computation time.

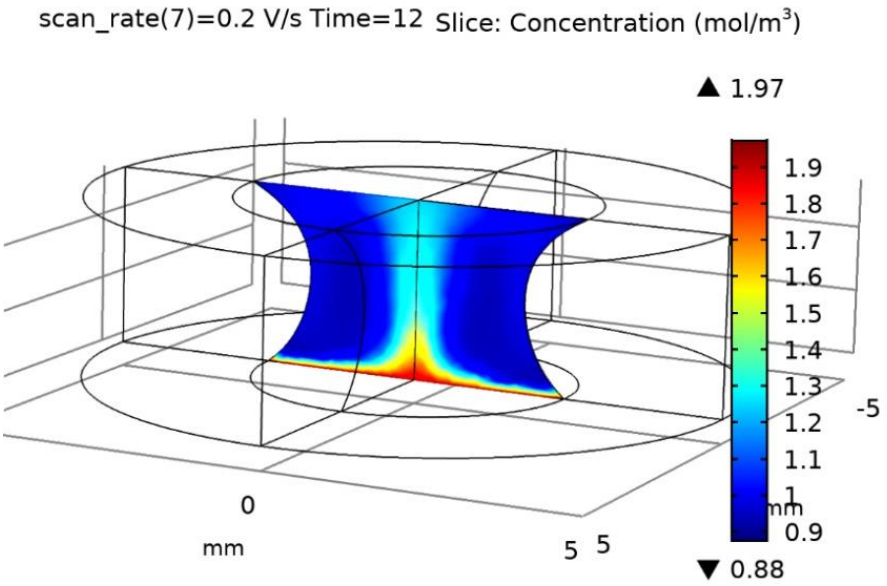

Figure 8.7.2 Result of COMSOL calculation of the cyclic voltammetry of a redox probe. The graph shows the distribution of product concentration at 0.6 V, when 50 rpm applied to the Rotating Droplet system.

The results visible in the figure 8.7.2 show the changes in the concentration of the product during the cyclic voltammetry measurement, at the first vertex potential (0.6 V). The initial concentration of the product in the reaction was set as 0 mM (0 mol/dm^3). At the bottom electrode where the flux of the reaction was set the substrate is consumed and the total concentration of the product is maximal. Moreover, the scaling in rainbow colors shows the depletion of the created product. The closer to the electrode surface, the more product species are present. The computation data shown in the figure 8.7.2 represents the Rotating Droplet experiments for a redox probe, with 50 rpm rotation rate applied. The results presented above suggest that the pattern of the electrochemical species flow from the electrode surface to the volume of the

droplet, which is similar to the behavior of electrochromic experiments for $ABTS^{2-}$ oxidation presented in Chapter 6 of this thesis.

Results presented in the fig. 8.7.3 show the graphical representation of the distribution of the reduced species of the redox probe which took part in the simulated cyclic voltammetry, first vertex potential. As it is visible at the electrode surface, the concentration of redox species which can be oxidized is equal to zero, whereas in the volume of the droplet approximately 0.5 mm above the electrode surface the supply of reduced redox species is equal to the initial 2 mM.

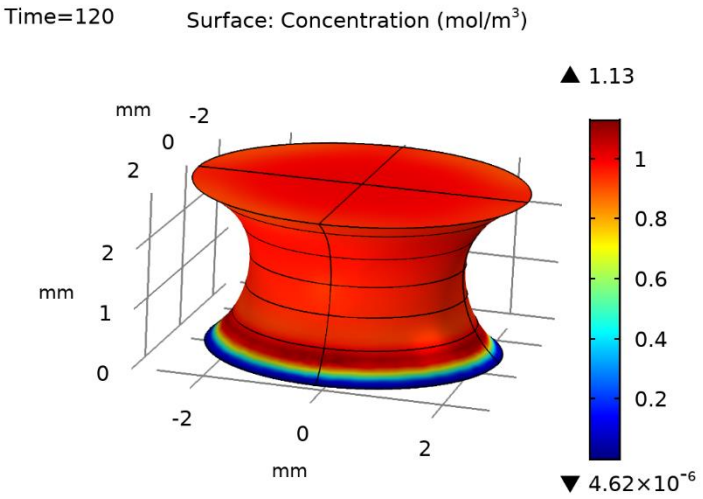

Figure 8.7.3 Result of COMSOL calculation of the cyclic voltammetry of a redox probe. The graph shows the distribution of substrate concentration at 0.6 V, when 0 rpm applied to the Rotating Droplet system.

The thickness of the layer of consumed substrates is proportional to the velocity of rotation. The higher the rotation speed, the higher the thickness of used redox species. The obtained results visible as a 3 D graphics of the redox species consumed on the working electrode surface were promising and I performed a series of simulations with different rotation velocities applied to the Rotating Droplet system.

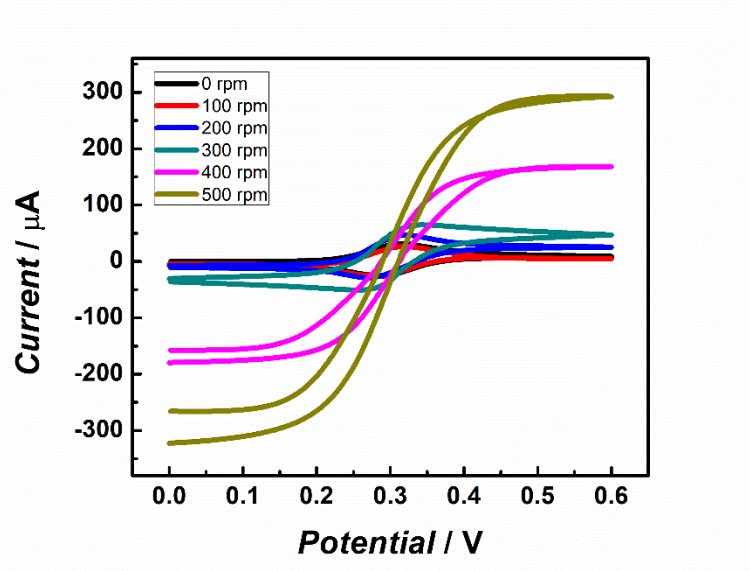

Figure 8.7.4 The Cyclic voltammogram obtained with COMSOL calculation of the transport of redox active species inside a Rotating Droplet system, various rotation rate applied.

The plot 8.7.4 shows the results of the COMSOL Multiphysics simulation of the electrochemical redox probe oxidation with cyclic voltammetry. In this simulation the parameter called standard rate constant was altered to higher values, to allow for faster charge transfer. The current increases with an increase of the rotation rate. The shape of the voltammograms for which the rotation rate was applied is sigmoidal which can indicate the hydrodynamically controlled mass transfer. Unfortunately, the reduction response is much bigger than in case of the experimental data. We have already seen this type of behavior in Fig. 5.4.2.3, but only for the highly porous surface when the ITO electrode surface was modified with the carbon nanoparticles with layer-by-layer method. Results of computations of the electrochemistry in the Rotating Droplet system do not fit to the experimental results, because we used incomplete definition of the velocity inside a droplet.

Calculation with COMSOL Multiphysics can be modulated by changing various parameters. The data presented in this section comes from the simulation of the velocity of Rotating Droplet based on swirling surrounding domain. Similar droplet velocity can be obtained with application of artificial internal pump which could pump the fluid inside a droplet. Use of the artificial internal pump imitates the convection measured inside a rotating drop. The next set of computation was performed with the use of internal pump and slip condition to the bottom wall (L=1 mm), instead of the previously used no-slip wall. It occurred to gave similar results to the experimental data. The data is presented in Fig. 8.7.5.

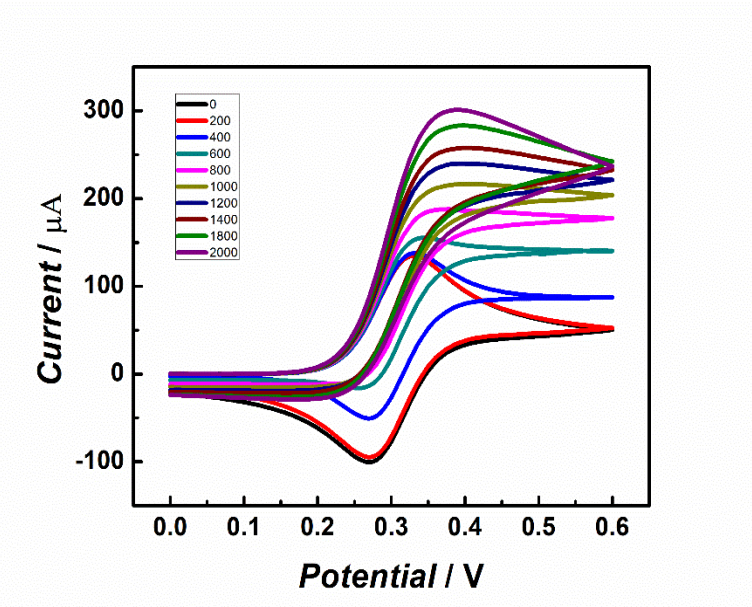

Figure 8.7.5 The Cyclic voltammogram obtained with COMSOL calculation of the transport of redox active species inside a Rotating Droplet system, various rotation rates applied, the specification of the bottom wall was changed from the no-slip to the slip wall, the length of the wall was 1 mm.

The results show that the current computed for a cyclic voltammetry calculation with COMSOL changes with rotation rate of the Rotating Droplet system. For lower velocities the obtained curves have a peak shape, whereas for higher rotation rate the response is sigmoidal. However, after reaching the 1200 rpm, the peak shape returns. The summary of the increase of the current value vs. the rotation rate is presented in the figure 8.7.6.

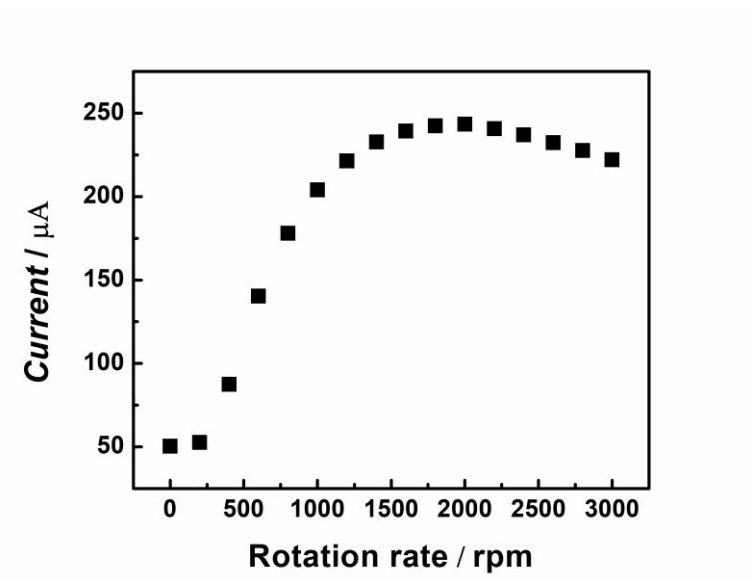

Figure 8.7.6 The current vs. rotation rate obtained with COMSOL Multiphysics 5.3 calculation of the transport of redox active species inside a Rotating Droplet system.

Figure 8.7.6 shows the correlation between oxidation current and the rotation rate applied to the Rotating Droplet system. For rotation rates below 1500 rpm the current increases with increase of the velocity. But for velocities higher than 1500 rpm the current decreases. All computation presented in this section comes from the models which were not perfect, but gave us an idea of how the system works. Result presented above can indicate that the model applied to the simulation did not fulfill all the conditions which govern the transport in a Rotating Droplet system, therefore further investigation is needed.

Conclusions

Information provided in Chapter 8 shows utility of theoretical methods dedicated to electrochemical measurements. Implementation of COMSOL Multiphysics into both projects "Calculation of the electrochemical depletion zone in a microfluidic channel" and "Calculation of the concentration profile and efficiency of the electrochemical reaction in posts based microchannel device" helped with creation of a better microchannel devices. The computation of the velocity and electrochemical measurements inside a Rotating Droplet system resulted in useful information about the flow profile in the system. COMSOL Multiphysics is a user-friendly system, which can easily answer basic questions. More complex and difficult problems need more specialized knowledge and operational time. Moreover, the failure with the calculation of the electrochemical measurement in a RD system forced me to use a complementary, empirical method for description of a flow profile inside a Rotating Droplet system. The results obtained with an application of the PIV method showed the velocity profile inside a RD system. The results from the PIV experiments inspired us to further develop the RD system with application of the computational methods. To overcome our computational limitations, we have already set up a collaboration with researchers with experience in computations of hydrodynamic systems (Konrad Sakowski from University of Warsaw) using an alternative program, ANSYS. The results that he obtained with ANSYS, together with the experimental PIV and the electrochemical data, gave us a basis for further collaboration using COMSOL Multiphysics (collaboration with Jane T. Stockmann from Memorial University of Newfoundland).

Bibliography

IV E. W. Nery, M. Kundys-Siedlecka, Y. Furuya, and M. Jönsson-Niedziółka, “Pencil lead as a material for microfluidic 3D-electrode assemblies,” *Sensors (Switzerland)*, vol. 18, no. 11, 2018.

[1] M. Raffel, A. Bauknecht, M. Ramasamy, G. K. Yamauchi, J. T. Heineck, and L. N. Jenkins, “Contributions of Particle Image Velocimetry to Helicopter Aerodynamics,” *AIAA J.*, vol. 55, no. 9, pp. 2859–2874, 2017.

[2] K. L. Pitts and M. Fenech, “Micro-particle image velocimetry for velocity profile measurements of micro blood flows,” *J. Vis. Exp.*, no. 74, p. e50314, 2013.

[3] C. (c) 2019 D. Brown, “Tracker,” 2019. [Online]. Available: https://physlets.org/tracker/.

Summary

The work behind this dissertation was devoted to detection of neurotransmitters in biological samples using a Rotating Droplet system. The Rotating Droplet (RD) is a new tool for electrochemical analysis is based on the principles of the standard Rotating Disc Electrode (RDE). The obvious similarities between these two methods inspired me to also look for differences between them and how they can be used. In this thesis I was looking for possibilities of applications of the Rotating Droplet for analytical purposes, especially for detection of neurotransmitters in presence of interferents.

Detection of neurotransmitters with using electrochemical methods requires employment of electrode materials, which allows for separation of the signals from the neurotransmitters and interferents present in a sample. Here, I used electrode modification with negatively charged carbon nanoparticles (CNPs(-)). CNPs(-) have electrocatalytic properties and their application allows for detection of dopamine and serotonin in presence of uric and ascorbic acids. Usually electrochemical analysis is done under stationary conditions. To lower the detection limit, hydrodynamic methods can be applied. In this thesis I have presented use of RD, a new hydrodynamic setup, for detection of neurotransmitters. However, before using the RD method for analytical purposes, it had to be characterized and optimized.

Data presented in this thesis show that with use of the RD it is possible to perform hydrodynamic electrochemical measurement in volumes as small as 70 μL. The RD exceeds the standard RDE method in the freedom of choice of working electrode surfaces. The RD system was optimized and tested for a number of electrode materials with application of different redox probes. The open side walls of the droplet facilitate oxygen transport from the surrounding atmosphere and therefore make the RD especially sensitive to the gaseous samples around it. The Rotating Droplet should thus be effective as a sensor for gaseous samples.

The Rotating Droplet has been used also for generation-collection experiments. The favorable geometry of the electrodes allowed for a significant increase of the collection efficiency over what was already achieved for conventional generation-collection setups. Using this mode the Rotating Droplet system was successfully used for detection of epinephrine. During the successive scans the signal from epinephrine (which is electrochemically reversible) was regenerated, while the signal from interferents oxidation (which was irreversible) was disappearing.

After these introductory studies I have managed to show that with use of the RD, multiple neurotransmitters (serotonin and dopamine) in presence of common interefernts (such as uric and ascorbic acid) can be detected. Moreover, I obtained a detection limit for serotonin as low as 10 nM and 100 nM for dopamine in buffer solution. The RD setup was then used for detection of serotonin in mice blood serum, where the small volume needed for analysis really is an advantage for the RD.

In the final chapter I have presented how computer simulations can be used to support electrochemical measurements. Application of COMSOL Multiphysics to the scientific projects related to microfluidic devices allowed us to understand different parameters which could help in creation of better versions of experimental setups. The computation for the Rotating Droplet revealed how complicated the system is. In the calculations the movement of the upper part of the droplet is not carried across to the whole droplet volume. As a result, the bottom part of the droplet, where the working electrode is placed, is almost stationary, which is contrary to experimental experience and provides insufficient transport of the analyte for the electrochemistry calculations. In order to understand the flow profile inside a Rotating Droplet I performed additional flow analysis with use of the PIV (Particle Image Velocimetry) method. The results from PIV, which are presented in the last chapter, helped with better definition of the Rotating Droplet system's parameters. These served as input for further refinement of the velocity computations in COMSOL. These computational velocities were used for calculation of the electrochemistry in the RD setup. The final results obtained using computer simulations are similar to the experimental data. However, to fully understand and to be able to predict the mechanisms and behavior inside a Rotating Droplet setup further computational research is needed.